HIGH PRECISION CALCULATION FOR THE DEVELOPMENT OF ATOMIC CLOCK AND THE SEARCH BEYOND THE STANDARD MODEL

by

Z. Zuhrianda

A dissertation submitted to the Faculty of the University of Delaware in partial fulfillment of the requirements for the degree of Doctor of Philosophy in Physics

Summer 2017

HIGH PRECISION CALCULATION FOR THE DEVELOPMENT OF ATOMIC CLOCK AND THE SEARCH BEYOND THE STANDARD MODEL

by

Z. Zuhrianda

Approved: _____

Edmund R. Nowak, Ph.D.
Chair of the Department of Physics and Astronomy

Approved: _____

George Watson, Ph.D.
Dean of the College of Art and Science

Approved: _____

Ann L. Ardis, Ph.D.
Interim Vice Provost for Graduate and Professional Education

I certify that I have read this dissertation and that in my opinion it meets the academic and professional standard required by the University as a dissertation for the degree of Doctor of Philosophy.

Signed: _____

Marianna Safronova, Ph.D.
Professor in charge of dissertation

I certify that I have read this dissertation and that in my opinion it meets the academic and professional standard required by the University as a dissertation for the degree of Doctor of Philosophy.

Signed: _____

Krzysztof Szalewicz, Ph.D.
Member of dissertation committee

I certify that I have read this dissertation and that in my opinion it meets the academic and professional standard required by the University as a dissertation for the degree of Doctor of Philosophy.

Signed: _____

Stephen Barr, Ph.D.
Member of dissertation committee

I certify that I have read this dissertation and that in my opinion it meets the academic and professional standard required by the University as a dissertation for the degree of Doctor of Philosophy.

Signed: _____

Doug Doren, Ph.D.
Member of dissertation committee

I certify that I have read this dissertation and that in my opinion it meets the academic and professional standard required by the University as a dissertation for the degree of Doctor of Philosophy.

Signed: _____

Matthew DeCamp, Ph.D.
Member of dissertation committee

I certify that I have read this dissertation and that in my opinion it meets the academic and professional standard required by the University as a dissertation for the degree of Doctor of Philosophy.

Signed: _____

John Gizis, Ph.D.
Member of dissertation committee

For my Parents and my Family...

TABLE OF CONTENTS

LIST OF TABLES

LIST OF FIGURES

ABSTRACT

The primary motivation of this work is the development of atomic clocks and the searches for new physics beyond the standard model. Optical clocks based on the forbidden transitions in an atom have been shown to be promising candidates for a better frequency standard. The search for new physics beyond the standard model can be done by looking for tiny deviations of atomic properties which is not expected by this model. Highly precise calculations for atomic systems are needed to provide further understanding in these studies.

The main formalisms that we use for the calculation on the atomic systems are all-order method, which is based on linear single double coupled cluster (LCCSD) method, and the combination of configuration interaction (CI) and all-order methods. These methods are suitable to study open-shell atomic systems and capable of calculating the electron correlations up to all order.

In this work, we carried out the following calculations. First, we proposed a new method of determining transition matrix elements using the measurement of magic wavelength in Sr lattice clock. Next, we calculated the blackbody radiation shift in Tl^+ and Hg, the magic wavelength in Hg, and the hyperfine quenching rate in Cd. Next, we developed a method to calculate the specific mass shift in the all-order formalism and apply it to Na, K, and Rb atoms. Next, we calculated Ra atomic properties for electric dipole moment (EDM) experiments, and parity non-conserving amplitude of Cs and Fr. Finally, we calculated the energies and transition matrix elements of highly charged Mo and Tc ions.

Chapter 1

INTRODUCTION

In this work, we applied high precision calculations using ab-initio methods in the study of the electron in atomic systems. The systems that we mainly discuss here are the particular cases of the open-shell atoms with one valence electron (monovalent) and two valence electrons (divalent). The primary methods that we use in this study are many-body perturbation theory (MBPT) [1] and all-order [2] methods for the monovalent system, and CI [3], CI+MBPT [4], and CI+all-order [5] methods for the divalent system. The primary motivation of this work is the ongoing developments of the atomic clock and the experimental searches for new phenomena beyond the standard model.

1.1 Development of the ab-initio calculation methods for atomic system.

The calculation of electronic structure in heavy atoms is a quantum many-body problem. In this type of calculation, the initial approximation is commonly carried out by the application of Dirac-Hartree-Fock (DHF) method [6]. We can solve the first few energy levels of the DHF wavefunction self-consistently in the central field approximation, i.e. using Hydrogen-like wavefunctions to describe the one-electron wavefunction with a spherically symmetric effective potential to account for the average repulsion from the other electrons. Using these initial wavefunctions, we form a full basis set using the B-spline interpolation [7].

Using the DHF basis set as the unperturbed wavefunctions (zeroth order), we can calculate the next order of corrections using the many-body perturbation theory (MBPT). This method has been developed and applied in the calculation of the electronic spectrum of the monovalent system up to the third order [1]. The number of

the correlation diagrams in MBPT method grows exponentially with increasing order of the perturbation. For this reason, MBPT method is no longer practical past the third order.

An alternative to MBPT method is the all-order method. In 1985, Lindgren developed this method based on the linked-diagram theorem to automatically generate higher order corrections from a set of iterative rules and carried out a non-relativistic treatment of the energies and hyperfine structures of Li [8]. He called this method all-order method since in principle it can calculate the perturbative effects to all orders by iteration. It can be shown that an equivalent method can be derived from the coupled cluster (CC) expansion [9]. A relativistic treatment of all-order method was developed by Blundell et al. to calculate the energies of He [10] and the energies and matrix elements of Li, and Be^+ [2]. Although all-order method had been quite successful for calculations in small systems, it was shown, by comparison with MBPT method, that this treatment is incomplete at the third order of energy. Blundell et al. improved this method to make it complete up to the third order of energy and calculated the energies and matrix elements of Cs [11]. Using all-order method, Safronova et al. calculated the energies and matrix elements of the rest of alkali atoms, Na, K, Rb, and Cs [12]. The all-order method has been shown to perform better than the third order MBPT for alkali atoms [12].

For calculations in monovalent systems, the MBPT and all-order methods are sufficient. To explore the system with more than one valence electron, a new approach needs to be developed. Configuration interaction method (CI) has been used since 1927 to study systems with few electrons [13, 3]. The main drawback of CI method is that the size of the configuration space increases exponentially with the number of electrons. Therefore, in practical CI calculations, the core-core and core-valence electron correlations are ignored. In 1996, Dzuba et al. proposed a way to combine CI and MBPT methods for atomic calculations [4]. In the CI+MBPT method, the core-core and core-valence electrons correlations are calculated first using the second order MBPT method, and then later on added as effective terms in the Hamiltonian. The

Hamiltonian is then used to build the configuration space for the CI calculations. The CI calculations will account for the valence-valence correlations. With this combined technique, it is possible to carry out calculations which include all electron correlations (core-core, core-valence, and valence-valence) in the system with more than one valence electron. Using similar method, Safronova et al. combined CI and all-order methods in 2009 [5]. In CI+all-order method, the effective correlation terms for the CI Hamiltonian are calculated using the all-order method. This method is currently the most precise method available for calculations of atomic systems.

We now discuss the motivations behind this work.

1.2 Extracting transition matrix elements from magic wavelengths

One of the most challenging problems in the experimental and theoretical atomic systems is the accurate determinations of the transition matrix elements. Theoretical errors has been showed to up to 0.2% [14] for alkali systems, but for more complicated systems it can be about 1% [15, 16, 17]. More importantly, on the experimental side, there is a lack of data available due to technical difficulties in conducting the experiments. In practice, the transition matrix elements are extracted from the measurements of the lifetimes which can be difficult to do if the branching ratios for the corresponding transitions are too small.

Here, we propose an alternative method for obtaining the transition matrix elements by utilizing the measurement of "magic zero" wavelengths. Magic zero wavelength is the wavelength in which the dynamic polarizability of the corresponding state turns to zero [17, 18]. Magic zero wavelengths have been measured before in Rb [19, 20], K [21] and metastable He [22], therefore experimental techniques for measuring them are readily available and well established.

In this work, we discuss the approach to obtain transition matrix elements of $5s5p\,^3P_0$ state in Sr atom. Sr is chosen as the best available benchmark for several reasons. First, the experimental techniques have been well developed due to its importance in atomic clock development [23] and studies of many-body effects in degenerate

quantum gasses [24, 25]. Next, the matrix element of Sr $5s5p\,^3P_0 - 5s4d\,^3D_1$ transition is known to 0.23% accuracy from the $5s4d\,^3D_1$ lifetime measurement [23]. Finally, in theory, Sr is one of the best understood system from the recent calculation of blackbody radiation (BBR) shift of $5s^2\,^1S_0 - 5s5p\,^3P_0$ clock transition [26].

1.3 Improving the accuracy of optical clocks

An ultra-precise clock is a critical component in the advances of fundamental sciences and practical technology. A better clock provides better measurements which can be used to probe phenomena predicted by theories beyond the standard model that are too small to observe using the current clock. Furthermore, it provides the technology for a better GPS system which is a crucial tool for the development of deep space probes.

It is shown in [27] that a higher transition frequency provides a better stability in the atomic clock. This work leads to active researches of optical clocks that operate at a higher frequency than that of the microwave clock. Currently, two types of optical clock schemes are being developed, the single ion in an ion trap scheme [28, 29, 30] and the neutral atoms in an optical lattice scheme [31, 32, 33]. Single ion clocks provide better precisions with the decrease in atomic interactions and Doppler effects; however, lattice clocks has the advantage of utilizing many atoms which result in better stability [34]. Currently, the most accurate atomic clock has been achieved with an accuracy of 8.6×10^{-18} in Al^+ single ion clock [30].

By definition, the current standard of a second is determined by the transition of the hyperfine ground state of Cs microwave clock operating at 0 K [35]. The Cs clock itself is still under ongoing development with the latest NIST-F2 clock achieving 10^{-16} level of accuracy [36].

When operating at the room temperature, the atomic clock is exposed to the electromagnetic field perturbation from the BBR. This radiation creates a shift in the energy level which in turn produces a systematic uncertainty in the transition frequency. The BBR shift is the leading factor in the uncertainty of atomic clocks; therefore its

precise determination is crucial for the development of atomic clocks. In this work, the BBR shifts for Tl^+ and Hg are calculated in the CI+all-order formalism.

Previous analysis has shown that the polarizabilities of $ns^2\ ^1S_0$ and $nsnp\ ^3P_0$ state are almost equal for B^+, Al^+ and In^+ ions [17]. These values result in an anomalously small BBR shifts in the $ns^2\ ^1S_0 - nsnp^3P_0$ transition of these ions. These ions belong to the same IIIB group, two other systems in this group, Ga, and Tl, have not been studied yet. Tl^+ based clock has been proposed in [37], therefore makes it an appealing system for the BBR shift study. Frequency standard based on the Tl^+ $6s^2\ ^1S_0\, m_F = 0 - 6s6p\ ^3P_0\, m_{F'} = 0$ transition has been proposed [37]. The radioactive isotope of ^{204}Tl has a half-life of 3.78 years, a spin of 2, and a small magnetic moment of 0.0908 nuclear magnetons making it an ideal object for a very high-resolution laser spectroscopy. Because of its small nuclear magnetic moment, the natural linewidth of the clock transition in $^{204}Tl^+$ is expected to be orders of magnitude smaller than the estimated value for stable Tl isotopes. Our calculation of BBR shift of Tl^+ has been published in [38].

Despite the difficulties of handling its operational wavelength in ultraviolet (UV) range, Hg is one of the promising candidates for an atom clock among the other neutral atom system. A recent study shows that its BBR shift ratio is smaller by at least an order of magnitude compared to the other neutral atom clock candidates, Sr and Yb [39]. Moreover, its large Z is convenient for the search of α variation since the clock transition is sensitive to Z, $\sim (\alpha Z)^2$. The experimental work on the Hg atomic clock is currently ongoing at RIKEN [33].

Other calculations that we also carried out in this work are the calculations of hyperfine quenching rates of ^{25}Mg, ^{87}Sr and ^{113}Cd clock transition in CI+all order formalism. The primary motivation for this is the development of Cd clock. We also calculate hyperfine quenching rates of ^{25}Mg and ^{87}Sr to compare the accuracy of our method with the available calculations [40, 41, 42]. Similar to Hg, Cd is also a promising candidate for optical lattice clock due to its possible small BBR shift, despite the difficulty of handling the operational range at UV frequency. Furthermore,

it has a variety of isotopes making it an excellent system for a variety of fundamental physics experiments. In atomic isotopes with half-integer I, the electronic state may mix with other states through hyperfine interactions. Thus, in this isotope, the $^3P_0$ state may contain small admixtures from the state with $J = 1$ which allows for the usually forbidden hyperfine quenched $E1$ decay.

1.4 Searches beyond the standard model in atoms

The standard model of particle physics is currently the best model which explains the particle interactions at the fundamental level (for a review of the standard model see for example [43]). The standard model contains 17 known fundamental particles which consist of six quarks, six leptons, and five bosons. This model fully describes the electromagnetic, weak and strong interactions among these particles.

The standard model was formulated during the early seventies as the combined model of the strong [44, 45] and electroweak [46, 47, 48] interactions. At the time, not all particles predicted by this model, namely the charm quark, W, Z and Higgs bosons have been discovered. The charm quark was discovered shortly after in 1974 as the constituent of J/Ψ meson [49, 50]. Next, The W and Z bosons were discovered in 1983 in the proton-antiproton scattering experiment [51, 52]. Finally, the Higgs boson was discovered in 2012 in the recent LHC experiment [53, 54, 55]. These discoveries have shown that the standard model is still a strong theory even decades after its formulation.

Despite its success, there are still lingering problems that the standard model can not explain. Neutrinos are predicted to be massless particles, yet observations have shown that their states oscillate among each other. This phenomenon means that these states are mixed which can only happen if they are massive. Next, the current matter-antimatter imbalance also does not have a satisfying explanation in the standard model. Furthermore, astronomical data suggests the existence of unknown matter called the dark matter. The particles in the standard model currently have no good candidates for this new matter. Finally, gravity as the fourth fundamental force

is still untouched in the standard model. Therefore, a new theory beyond the standard model is expected to answer this problem.

Experimental searches of new phenomena not predicted by the standard model are currently ongoing. If these phenomena are discovered, they could signal the existence of new physics not yet explained in the standard model. These experiments generally can be divided into two categories, the high energy, and the low energy test. In the high energy, the experiments are carried out by colliding high-energy particles to produce new particles outside of the standard model elements. In the low energy regime, the experiments carried out in atomic systems to search for unusual properties which are not predicted by the standard model. Indeed, these properties should be minuscule since so far no one has seen it yet, therefore high precision measurements, and theoretical calculations are paramount in these experiments.

In this work, the searches beyond standard model in atomic systems are studied. We confine our discussion in the search of permanent EDM in Ra, and PNC study in Cs and Fr.

1.4.1 The search of permanent EDM

The current matter-antimatter imbalance requires CP violating processes to occur in the early universe. The present standard model allows such operations through the Cabibbo-Kobayashi-Maskawa (CKM) matrix mixing, Pontecorvo-Maki-Nakagawa-Sakata (PMNS) matrix mixing and the Quantum Chromodynamics (QCD) θ term [56]. Interactions involving these terms at higher orders allow for processes that violate CP. However, these processes are too small to produce the currently observed result.

Theories beyond the standard model such as supersymmetry predict new particles which allow for new CP violating processes. The search for these new particles is still ongoing in high energy experiment. An alternative way to test these theories is by searching for non-zero atomic electric dipole moment (EDM) in the low energy regime. In the case of non-zero EDM, d_E, there will be an effective interaction between

particle spin $\vec{S}$ and electric field $\vec{E}$, $d_E\vec{S}\cdot\vec{E}$. Under parity and time reversal transformations, the operator $\vec{S}$ and $\vec{E}$ transform as $\vec{S} \xrightarrow{\mathcal{P}} \vec{S}, \vec{E} \xrightarrow{\mathcal{P}} -\vec{E}$ and $\vec{S} \xrightarrow{\mathcal{T}} -\vec{S}, \vec{E} \xrightarrow{\mathcal{T}} \vec{E}$. Therefore, the combination $\vec{S}\cdot\vec{E}$ violates both parity and time reversal transformation. Thus, assuming CPT conservation holds, the existence of non-zero EDM (d_E) violates the CP conservation. This nonzero EDM is predicted to be larger by several orders of magnitude in these new theories than the one predicted by the standard model.

Ra is a suitable system for the search of atomic EDM. It has been shown recently that the EDM in this system has an enhancement factor of up to 10^5 compared to other atoms [57]. The Ra EDM experiment is currently ongoing by the Argonne group [58]. In this work, we carried out a preliminary study of the lifetimes, polarizabilities and hyperfine constants of Ra using the CI+all order formalism which will be useful for the experiment.

1.4.2 The study of PNC

Parity is one of the fundamental transformation in physics. It was shown by C. S. Wu et al. in 1957 that the beta decay process in cobalt-60 violates parity [59]. This parity nonconservation (PNC) process is caused by the weak interaction which is mediated by W and Z bosons in the standard model.

In atomic systems, the PNC experiments have been carried out in Cs [60] and currently ongoing in Fr [61]. These experiments are carried out by measuring the highly forbidden transition from which PNC amplitude can be extracted. By combining the results from Cs PNC experiment and theory, Porsev et al. have managed to obtain the weak charge Q_W [62]. Their calculation of Q_W differs from the standard model prediction by 1.5σ. It was shown in [63] that highly excited-states might have a larger contribution to the uncertainty of the Q_W than previously expected. Apart from extracting the Q_W value, it also possible to evaluate the nuclear anapole moments and nuclear weak coupling constant from the PNC experiments. It is shown in [64] that the nuclear weak coupling constant extracted from the Cs PNC experiment is in disagreement with the other results obtained from nuclear parity violating experiments.

1.5 The calculations of isotope shift

Recent studies in quasar absorption spectra show a possible sign of a change in the fine structure constant α [65]. Indeed, extra dimensional theories such as the superstring theory predict variations in the fundamental constants [66]. Although extensive analyses have been done [65, 67, 68], it is not yet entirely known whether the change is real or caused by systematic errors. The possibility of different isotopic abundance in the early universe compared to its terrestrial value might be an alternative explanation for this change. This possibility can be tested if we know the values of the isotope shift of the corresponding atomic transition. However, for the time being, only a few of these are known experimentally. Therefore, precise calculations of these quantities are an important key to understand this problem.

An accurate determination of the isotope shift is also necessary for nuclear studies. By comparing the calculated and measured values of isotope shift, it is possible to determine atomic nuclei charge distribution [69].

Finally, an accurate isotope shift calculation is necessary for solving the problem of dark matter. It is possible that the mass deficit in the universe is due to the existence of little black holes [70]. These elementary black holes, formed in the early universe, might have electric charges which attract electrons and form black hole atoms. The electronic spectra of the black hole atoms will have an isotope shift compared to the corresponding atoms on earth.

The determination of the isotope shift requires the calculations of two-body matrix elements. Previous works in the calculations of isotope shift in Na, K, and Rb using third order MBPT have shown significant discrepancies between the theoretical and experimental results [71, 72]. One possible cause of these discrepancies is the exclusion of higher order corrections, therefore a logical approach to solving this problem is to extend this formalism into the all-order method. Calculation methods for the two-body matrix elements in the all-order formalism have not been developed yet. In this work, we show for the first time, the development of the calculation methods of general two-body matrix elements in all-order method and apply them to the calculations of

isotope shift in Na, K, and Rb.

1.6 The calculations of energies, matrix elements and lifetimes of highly charged Mo and Tc

A highly charged ion is an atom with multiple of its outermost electrons stripped. Several studies have shown that due to their smaller size compared to their neutral counterpart, highly charged ions are less sensitive to external perturbation. This feature results in a smaller fractional frequency shift, as a matter of fact, studies have shown that this shift can be less than 1×10^{-19} [15, 73]. This property makes them excellent candidates for optical clock and the search of the spatial α-variation.

Tc is a rare element which naturally occurs as a product of radioactive processes in heavy elements such as uranium or molybdenum. Only small amounts of this element are found in the Earth's crust. Due to this reason, there are currently little studies on this element. However, the stellar spectra of some star have shown abundant of Tc in them [74]. Since the half-life of Tc is far less than the age of the stars, then this element must have been created after the formation of these stars. Therefore, a better understanding of Tc can provide us with a better insight on the nucleosynthesis in stars.

In this work, we carried out a preliminary study of highly charged Mo V, Mo VI, Tc VI, and Tc VII. We carried out the calculations of energy spectra of the low lying level, transition matrix elements, and lifetimes in these ions. The electronic configurations of Mo and Tc differ by one electron, therefore apart from their nuclear structure, they are similar. Since experimental data are available for Mo but not for Tc, we use Mo as a testbed to test the accuracy of our calculations by comparing them with the available experimental measurements.

1.7 Thesis structure

We organize this work as follows.

In Chapter 2, the all-order and CI+all-order method are described. These methods are the methods mainly used for all the calculations in this work. The methods to calculate the transition matrix elements within these formalisms are also described in this chapter.

In Chapter 3, we proposed a new method for determining the transition matrix elements from the measurements of magic and magic zero wavelength in an atom.

In Chapter 4, we provided the optical clock related calculation. In this chapter, BBR shift of Tl^+ and Hg are calculated. Next, the magic wavelength of Hg is calculated. Finally, the hyperfine quenching rate of Cd is calculated.

In Chapter 5, we provide the calculation related to the searches for new physics beyond the standard model. In this section, we calculated the atomic properties of Ra. Next, we calculated the PNC amplitude of Cs and Fr.

In Chapter 6, we provided the calculation of the isotope shift of Na, K, and Rb.

In Chapter 7, we provided the calculation of the energies and matrix elements of highly charged Mo and Tc.

We concluded and summarized the whole work in chapter 8.

Chapter 2

CALCULATION METHODS

In this chapter, we describe the calculation method which will be used in this work. The methods used to calculate the monovalent system is discussed in sec. 2.1 and for the divalent system in sec. 2.2.

2.1 Methods for monovalent system

For this type of calculation, we use all-order method [8]. There are two variants of this approach, the single double (SD) and single double partial triple (SDpT).

2.1.1 The SD method

In SD all-order, a set of rules is defined to generate high order corrections iteratively. Originally, this method was derived from the linked-diagram theorem [8], later it was shown that it could be obtained equivalently from coupled cluster (CC) expansion [10]. In this work, we will follow the derivation of SD all-order method from coupled cluster (CC) expansion as given in [75].

The coupled cluster (CC) theory was first developed in [76] for the nuclear physics studies. According to CC theory, the exact single valence atomic wavefunction $|\Psi_v\rangle$ can be written as [11]

$$|\Psi_v\rangle = \exp(S)|\Phi_v\rangle, . \tag{2.1}$$

Where S is the cluster operator and $|\Phi_v\rangle$ is the zeroth order wavefunction. In CC method, the cluster operator can be written as $S = S_1 + S_2 + S_3 + ...$ where S_n is the n-th excitation term that describes the excitation of n electrons from the wavefunction $|\Phi_v\rangle$. Here, the zeroth order wavefunction is taken to be the frozen core Dirac Hartree

Fock (DHF) wavefunction $|\Phi_v\rangle = a_v^\dagger|0_C\rangle$ where $|0_C\rangle$ is a closed shell core electrons state.

If we expand the exponential from Eq. (2.1) and using the expansion of S, we obtain the CC expansion of the exact wavefunction

$$|\Psi_v\rangle = \left(1 + S_1 + S_2 + S_3 + \frac{1}{2}S_1^2 + \frac{1}{2}S_2^2 + S_1S_2 + \cdots\right)|\Phi_v\rangle. \tag{2.2}$$

In open shell systems, the non linear terms of Eq. (2.2) contributes to the energy corrections starting from the fourth order [9] and S_3 contributes partially to the third order energy [2]. The dominant contributions to the energy corrections in this system comes from the single and double excitation terms. In SD all-order approximation, only these terms are kept from Eq. (2.2), thus we obtain the SD wavefunction $|\Psi_v^{\rm SD}\rangle$

$$|\Psi_v^{\rm SD}\rangle = (1 + S_1 + S_2)\,|\Phi_v\rangle. \tag{2.3}$$

In the second quantization, Eq. (2.3) can be written as

$$\begin{aligned} |\Psi_v^{SD}\rangle \;=\; & \Bigg[1 + \sum_{ma}\rho_{ma}a_m^\dagger a_a + \sum_{m}\rho_{mv}a_m^\dagger a_v + \\ & \frac{1}{2}\sum_{\substack{mn\\ab}}\rho_{mnab}a_m^\dagger a_n^\dagger a_b a_a + \sum_{\substack{mn\\a}}\rho_{mnva}a_m^\dagger a_n^\dagger a_a a_v\Bigg]|\Phi_v\rangle, \end{aligned} \tag{2.4}$$

where we define $\rho_{ma}, \rho_{mv}, \rho_{mnab}$ and ρ_{mnva} as the single core, single valence, double core and double valence coefficients respectively. Furthermore, the labeling for the indices uses the following conventions

$a, b, c, d, ...$	core states,
$v, w, ...$	valence states,
$m, n, o, p, ...$	excited states (including valence states),
$i, j, k, l, ...$	other states.

Next we plug Eq. (2.4) to the Schrödinger equation

$$H|\Psi_v^{SD}\rangle = E|\Psi_v^{SD}\rangle. \tag{2.5}$$

Where we use DHF Hamiltonian in "no-pair" approximation [77]. In this approximation, contributions from the negative energy states (positron) are ignored. These states contribute to small energy corrections at the order of α^3 a.u. that can be treated separately with Quantum Electrodynamics (QED). We write the Hamiltonian as $H = H_0 + V_I$ with

$$H_0 = \sum_i \epsilon_i a_i^\dagger a_i, \tag{2.6}$$

$$V_I = \frac{1}{2}\sum_{ijkl} g_{ijkl} a_i^\dagger a_j^\dagger a_l a_k - \sum_{ij} U_{ij} a_i^\dagger a_j, \tag{2.7}$$

where ϵ_i is the one-electron DHF energy of state i, g_{ijkl} are the two-body Coloumb matrix elements

$$g_{ijkl} = \int d^3r \int d^3r' \psi_i^\dagger(\mathbf{r})\psi_j^\dagger(\mathbf{r}')\frac{1}{|\mathbf{r}-\mathbf{r}'|}\psi_k(\mathbf{r})\psi_l(\mathbf{r}'), \tag{2.8}$$

and U_{ij} is the core electron Hartree Fock potential

$$U_{ij} = (V_{HF})_{ij} = \sum_a (g_{iaja} - g_{iaaj}). \tag{2.9}$$

We can obtain the relations for the excitation coefficients ρ and energy E by identifying the following terms in the Schrödinger equation

$$\begin{aligned}
a_v^\dagger|0_C\rangle &\rightarrow E, \\
a_m^\dagger a_a a_v^\dagger|0_C\rangle &\rightarrow \rho_{ma}, \\
a_m^\dagger|0_C\rangle &\rightarrow \rho_{mv}, \\
a_m^\dagger a_n^\dagger a_a a_b a_v^\dagger|0_C\rangle &\rightarrow \rho_{mnab}, \\
a_m^\dagger a_n^\dagger a_a|0_C\rangle &\rightarrow \rho_{mnva},
\end{aligned}$$

so that we get a set of iterative relations for the excitation coefficients

$$(\epsilon_a - \epsilon_m)\rho_{ma} = \sum_{bn} \tilde{g}_{mban}\rho_{nb} + \sum_{bnr} g_{mbnr}\tilde{\rho}_{nrab} - \sum_{bcn} g_{bcan}\tilde{\rho}_{mnbc}, \tag{2.10}$$

$$(\epsilon_v - \epsilon_m + \delta E_v)\rho_{mv} = \sum_{bn} \tilde{g}_{mbvn}\rho_{nb} + \sum_{bnr} g_{mbnr}\tilde{\rho}_{nrvb} - \sum_{bcn} g_{bcvn}\tilde{\rho}_{mnbc}, \tag{2.11}$$

$$\begin{aligned}(\epsilon_{ab} - \epsilon_{mn})\rho_{mnab} &= g_{mnab} + \sum_{cd} g_{cdab}\rho_{mncd} + \sum_{rs} g_{gmnrs}\rho_{rsab} \\ &+ \left[\sum_r g_{mnrb}\rho_{ra} - \sum_c g_{cnab}\rho_{mc} + \sum_{rc} \tilde{g}_{cnrb}\tilde{\rho}_{mrac}\right] + \begin{bmatrix} a \leftrightarrow b \\ m \leftrightarrow n \end{bmatrix},\end{aligned} \tag{2.12}$$

$$\begin{aligned}(\epsilon_{vb} - \epsilon_{mn} + \delta E_v)\rho_{mnvb} &= g_{mnvb} + \sum_{cd} g_{cdvb}\rho_{mncd} + \sum_{rs} g_{mnrs}\rho_{rsvb} \\ &+ \left[\sum_r g_{mnrb}\rho_{rv} - \sum_c g_{cnvb}\rho_{mc} + \sum_{rc} \tilde{g}_{cnrb}\tilde{\rho}_{mrvc}\right] + \begin{bmatrix} v \leftrightarrow b \\ m \leftrightarrow n \end{bmatrix},\end{aligned} \tag{2.13}$$

and core (δE_C) and valence (δE_v) energies

$$\delta E = \delta E_C + \delta E_v, \tag{2.14}$$

$$\delta E_C = \frac{1}{2}\sum_{mnab} g_{abmn}\tilde{\rho}_{nmba}, \tag{2.15}$$

$$\delta E_v = \sum_{ma} \tilde{g}_{vavm}\rho_{ma} + \sum_{mab} g_{abvm}\rho_{mvab} + \sum_{mna} g_{vbmn}\tilde{\rho}_{mnvb}. \tag{2.16}$$

Throughout Eqs. (2.10)-(2.16) we use the following definition to simplify the equations

$$\tilde{g}_{ijkl} = g_{ijkl} - g_{ijlk}, \tag{2.17}$$

$$\tilde{\rho}_{ijkl} = \rho_{ijkl} - \rho_{ijlk}, \tag{2.18}$$

$$\epsilon_{ij} = \epsilon_i + \epsilon_j. \tag{2.19}$$

Eqs. (2.10)-(2.16) describes the SD all-order method. These equations are to be solved iteratively where every iteration is equivalent to adding the next order of

g_{ijkl} into the wavefunction $|\Psi_v\rangle$. Therefore, every iteration effectively includes the next order correlation function contributions to the wavefunction. Essentially we can iterate endlessly to obtain contributions of all order of perturbation or until the required accuracy has been achieved.

Finally, we would like to mention the symmetry of the double excitation coefficient ρ_{ijkl}. The Coulomb matrix element is symmetric under the interchange $i \leftrightarrow j$ and $k \leftrightarrow l$ (see Eq. (2.8))

$$g_{ijkl} = g_{jilk}, \tag{2.20}$$

therefore from Eqs. (2.12) and (2.13), this leads to the symmetric relation for the double excitation coefficient

$$\rho_{ijkl} = \rho_{jilk}. \tag{2.21}$$

2.1.2 The single double partial triple (SDpT) method.

A direct comparison between the energy terms obtained by the SD all-order method with third order MBPT [78] reveals that the SD energy terms are incomplete at the third order of perturbation. Two approaches have been devised to circumvent these problems, one by adding explicit third order terms [11] and another by including the partial triple excitation terms [12]. In this section, we will briefly describe both methods.

To show the incompleteness of the SD energy, we start by explicitly deriving the first two iterations of the SD excitation coefficients. In the first iteration, the excitation coefficients become

$$\rho_{ma} = 0, \tag{2.22}$$

$$\rho_{mv} = 0, \tag{2.23}$$

$$\rho_{mnab} = \frac{g_{mnab}}{(\epsilon_{ab} - \epsilon_{mn})}, \tag{2.24}$$

$$\rho_{mnvb} = \frac{g_{mnvb}}{(\epsilon_{vb} - \epsilon_{mn})}. \tag{2.25}$$

Therefore the valence energy becomes

$$\delta E_v = \sum_{mab} \frac{\tilde{g}_{abvm} g_{mvab}}{\epsilon_{ab} - \epsilon_{mv}} + \sum_{mnb} \frac{\tilde{g}_{vbmn} g_{mnvb}}{\epsilon_{vb} - \epsilon_{mn}}, \tag{2.26}$$

Which is exactly the second order MBPT valence energy.

In the second iteration, we have the following equations for the excitation coefficients

$$\rho_{ma} = \frac{1}{(\epsilon_a - \epsilon_m)} \left[\sum_{bnr} g_{mbnr} \tilde{g}_{nrab} - \sum_{bcn} g_{bcan} \tilde{g}_{mnbc} \right], \tag{2.27}$$

$$\rho_{mv} = \frac{1}{(\epsilon_v - \epsilon_m + \delta E_v)} \left[\sum_{bnr} g_{mbnr} \tilde{g}_{nrvb} - \sum_{bcn} g_{bcvn} \tilde{g}_{mnbc} \right], \tag{2.28}$$

$$\begin{aligned} \rho_{mnab} = \frac{1}{(\epsilon_{ab} - \epsilon_{mn})} \Bigg[& g_{mnab} + \sum_{cd} g_{cdab} g_{mncd} + \sum_{rs} g_{mnrs} g_{rsab} \\ & + \sum_{rc} \tilde{g}_{cnrb} \tilde{g}_{mrac} \Bigg] + \begin{bmatrix} a \leftrightarrow b \\ m \leftrightarrow n \end{bmatrix} + O(g^3), \end{aligned} \tag{2.29}$$

$$\begin{aligned} \rho_{mnvb} = \frac{1}{(\epsilon_{ab} - \epsilon_{mn} + \delta E_v)} \Bigg[& g_{mnvb} + \sum_{cd} g_{cdvb} g_{mncd} + \sum_{rs} g_{mnrs} g_{rsvb} \\ & + \sum_{rc} \tilde{g}_{cnrb} \tilde{g}_{mrvc} \Bigg] + \begin{bmatrix} v \leftrightarrow b \\ m \leftrightarrow n \end{bmatrix} + O(g^3), \end{aligned} \tag{2.30}$$

where $O(g^3)$ is the terms that contain the third order of g_{ijkl}. Using these, the valence energy will now include the energy in the second, third and fourth order of g. The

valence energy terms that contains the third order are given by

$$\begin{aligned}
\delta E_v^{(3)} &= \sum_{mabcd} \frac{\tilde{g}_{abvm} g_{cdab} g_{mvcd}}{(\epsilon_{ab} - \epsilon_{vm})(\epsilon_{cd} - \epsilon_{mv})} + \sum_{mabrs} \frac{\tilde{g}_{abvm} g_{mvrs} g_{rsab}}{(\epsilon_{ab} - \epsilon_{vm})(\epsilon_{ab} - \epsilon_{rs})} \\
&+ \sum_{mabcr} \frac{\tilde{g}_{abvm} \tilde{g}_{cvrb} \tilde{g}_{mrac}}{(\epsilon_{ab} - \epsilon_{vm})(\epsilon_{ac} - \epsilon_{mr})} + \sum_{mabcr} \frac{\tilde{g}_{abvm} \tilde{g}_{cmra} \tilde{g}_{vrbc}}{(\epsilon_{ab} - \epsilon_{vm})(\epsilon_{bc} - \epsilon_{vr})} \\
&+ \sum_{mabnr} \frac{\tilde{g}_{vavm} g_{mbnr} \tilde{g}_{nrab}}{(\epsilon_{a} - \epsilon_{m})(\epsilon_{ab} - \epsilon_{nr})} + \sum_{mabcn} \frac{\tilde{g}_{vavm} g_{bcan} \tilde{g}_{mnbc}}{(\epsilon_{a} - \epsilon_{m})(\epsilon_{bc} - \epsilon_{mn})} \\
&+ \sum_{mnbcd} \frac{\tilde{g}_{vbmn} g_{cdvb} g_{mncd}}{(\epsilon_{vb} - \epsilon_{mn})(\epsilon_{cd} - \epsilon_{mn})} + \sum_{mnbrs} \frac{\tilde{g}_{vbmn} g_{mnrs} g_{rsvb}}{(\epsilon_{vb} - \epsilon_{mn})(\epsilon_{vb} - \epsilon_{rs})} \\
&+ \sum_{mnbrc} \frac{\tilde{g}_{vbmn} \tilde{g}_{cnrb} \tilde{g}_{mrvc}}{(\epsilon_{vb} - \epsilon_{mn})(\epsilon_{vc} - \epsilon_{mr})} + \sum_{mnbrc} \frac{\tilde{g}_{vbmn} \tilde{g}_{cmrv} \tilde{g}_{nrbc}}{(\epsilon_{vb} - \epsilon_{mn})(\epsilon_{bc} - \epsilon_{nr})}.
\end{aligned} \tag{2.31}$$

Comparing these terms with the third order MBPT energy [11], we found that the following set of terms are missing from the SD all order third order energy

$$\begin{aligned}
\delta E_{v\,\mathrm{extra}}^{(3)} &= \sum_{mnabc} \frac{\tilde{g}_{abmn} \tilde{g}_{cmav} \tilde{g}_{nvbc}}{(\epsilon_{ab} - \epsilon_{mn})(\epsilon_{bc} - \epsilon_{nv})} + \sum_{mnabs} \frac{\tilde{g}_{abmn} \tilde{g}_{nvas} \tilde{g}_{msvb}}{(\epsilon_{ab} - \epsilon_{mn})(\epsilon_{vb} - \epsilon_{ms})} \\
&+ \sum_{mnabc} \frac{g_{abmn} \tilde{g}_{cvbv} \tilde{g}_{mnca}}{(\epsilon_{ab} - \epsilon_{mn})(\epsilon_{ca} - \epsilon_{mn})} + \sum_{mnabs} \frac{g_{abmn} \tilde{g}_{mvsv} \tilde{g}_{nsba}}{(\epsilon_{ab} - \epsilon_{mn})(\epsilon_{ab} - \epsilon_{ns})} \\
&+ \sum_{mnabc} \frac{g_{abmn} \tilde{g}_{cvbv} \tilde{g}_{mnca}}{(\epsilon_{ab} - \epsilon_{mn})(\epsilon_{ca} - \epsilon_{mn})} + \sum_{mnabs} \frac{g_{abmn} \tilde{g}_{mvsv} \tilde{g}_{nsba}}{(\epsilon_{ab} - \epsilon_{mn})(\epsilon_{ab} - \epsilon_{ns})} \\
&+ \sum_{mnabs} \frac{g_{abmn} \tilde{g}_{mnvs} g_{vsba}}{(\epsilon_{ab} - \epsilon_{mn})(\epsilon_{ab} - \epsilon_{vs})} + \sum_{mnabc} \frac{g_{abmn} \tilde{g}_{cvba} g_{mnvc}}{(\epsilon_{ab} - \epsilon_{mn})(\epsilon_{vc} - \epsilon_{mn})} \\
&+ \sum_{mnabc} \frac{g_{abmn} \tilde{g}_{cmab} \tilde{g}_{vnvc}}{(\epsilon_{ab} - \epsilon_{mn})(\epsilon_{c} - \epsilon_{n})} + \sum_{mnabs} \frac{g_{abmn} \tilde{g}_{mnas} \tilde{g}_{vsvb}}{(\epsilon_{ab} - \epsilon_{mn})(\epsilon_{b} - \epsilon_{s})},
\end{aligned} \tag{2.32}$$

Therefore the SD third order energy is not complete.

To make the energy from the SD all-order complete, we can manually add the missing terms from Eq. (2.32) to the total energy so that $\delta E_{SD}^{(3)} = \delta E_v^{(3)} + \delta E_{v\,\mathrm{extra}}^{(3)}$. An alternative way to solve this problem can be done by adding the triple excitation

terms to the wavefunction $|\Psi_v\rangle$

$$|\Psi_v\rangle = |\Psi_v^{SD}\rangle + \left[\frac{1}{6}\sum_{mnrab}\rho_{mnrvab}a_m^\dagger a_n^\dagger a_r^\dagger a_b a_a a_v + \frac{1}{18}\sum_{mnrabc}\rho_{mnrabc}a_m^\dagger a_n^\dagger a_r^\dagger a_c a_a b_a\right]|\Phi_v\rangle. \quad (2.33)$$

Inserting Eq. (2.33) to the Schrödinger equation using the same the Hamiltonian as we did in the previous section and then identify the following terms with the operators

$$a_m^\dagger a_n^\dagger a_r^\dagger a_a a_b a_c a_v^\dagger|0_C\rangle \rightarrow \rho_{mnrabc}, \quad (2.34)$$

$$a_m^\dagger a_n^\dagger a_m^\dagger a_a a_b|0_C\rangle \rightarrow \rho_{mnrvab}, \quad (2.35)$$

yields the iterative equations for the triple excitation coefficients

$$(\epsilon_a+\epsilon_b+\epsilon_c-\epsilon_m-\epsilon_n-\epsilon_r)\rho_{mnrabc} = \sum_{\substack{123=\{mnr\}\\1'2'3'=\{abc\}}}\frac{1}{2}\left(\frac{1}{2}g_{121'2'}\rho_{33'}-\sum_d g_{1d1'2'}\rho_{23d3'}+\sum_s g_{23s3'}\rho_{1s1'2'}\right) + O(\rho_{ijki'j'k'}) \quad (2.36)$$

$$(\epsilon_a+\epsilon_b+\epsilon_v-\epsilon_m-\epsilon_n-\epsilon_r+\delta E_v)\rho_{mnrvab} = \sum_{\substack{123=\{mnr\}\\1'2'3'=\{vab\}}}\frac{1}{2}\left(\frac{1}{2}g_{121'2'}\rho_{33'}-\sum_d g_{1c1'2'}\rho_{23c3'}+\sum_s g_{23s3'}\rho_{1s1'2'}\right) + O(\rho_{ijki'j'k'}) \quad (2.37)$$

where the second terms in both equations refer to the terms containing triple excitation terms ρ_{ijklmn}. The notation in the summation $123 = \{ijk\}$ means that the index 123 range over the permutation of index ijk with positive (negative) sign for even (odd) permutation. With the inclusion of triple excitation terms, the all-order equations

become

$$\delta E_v = (SD) + \sum_{mnab} g_{abmn}\rho_{mnvvab}, \tag{2.38}$$

$$(\epsilon_a - \epsilon_m)\rho_{ma} = (SD) + \sum_{nrbc} g_{bcnr}\rho_{mnrabc}, \tag{2.39}$$

$$(\epsilon_v - \epsilon_m + \delta E_v)\rho_{mv} = (SD) + \sum_{nrab} g_{abnr}\rho_{mnrvab}, \tag{2.40}$$

$$\begin{aligned}(\epsilon_a + \epsilon_b - \epsilon_m - \epsilon_n)\rho_{mnab} &= (SD) - \sum_{rcd} g_{cdar}\rho_{mnrbdc} - \sum_{rcd} g_{cdbr}\rho_{nmradc} \\ &\quad - \sum_{rsc} g_{cmrs}\rho_{snrbac} - \sum_{rsc} g_{cnrs}\rho_{smrabc},\end{aligned} \tag{2.41}$$

$$\begin{aligned}(\epsilon_a + \epsilon_v - \epsilon_m - \epsilon_n + \delta E_v)\rho_{mnva} &= (SD) + \sum_{rcb} g_{bcar}\rho_{mnrvcb} + \sum_{rc} g_{bcvr}\rho_{mnrabc} \\ &\quad + \sum_{rsb} g_{bmrs}\rho_{srnvba} + \sum_{rsb} g_{bnrs}\rho_{srmvab}.\end{aligned} \tag{2.42}$$

It has been shown in [12] that to include the whole third order terms, only the changes in δE_v and ρ_{mv} due to triple excitation addition are necessary. Thus, for the present work we ignore the changes in the other coefficients ρ_{ma}, ρ_{mnab} and ρ_{mnva}. Plugging the triple excitation terms from Eqs. (2.36) and (2.37) into Eqs. (2.38) and (2.40) and removing the relatively small terms with the power of g greater than three we obtain

$$\begin{aligned}\delta E_v \approx &\sum_{ma} \tilde{g}_{vavm}\rho_{ma} + \sum_{mab} g_{abvm}\tilde{\rho}_{mvab} + \sum_{mnb} g_{vbmn}\tilde{\rho}_{mnvb} \\ &+ \sum_{mnab} \frac{\tilde{g}_{abmn}}{\epsilon_{ab} - \epsilon_{mn}} \Bigg\{ \sum_{c} \tilde{g}_{cmav}\tilde{\rho}_{nvbc} + \sum_{s} \tilde{g}_{nvas}\tilde{\rho}_{msvb} + \sum_{c} \tilde{g}_{cvbv}\rho_{mnca} \\ &\qquad + \sum_{s} \tilde{g}_{mvsv}\rho_{nsba} + \sum_{c} g_{cmab}\tilde{\rho}_{vnvc} + \sum_{s} g_{mnas}\tilde{\rho}_{vsvb} \\ &\qquad + \sum_{s} g_{mnvs}\rho_{vsba} + \sum_{c} g_{cvba}\rho_{mnvc} \Bigg\},\end{aligned} \tag{2.43}$$

$$\begin{aligned}(\epsilon_v - \epsilon_m + \delta E_v)\rho_{mv} \approx &\sum_{bn} \tilde{g}_{mbvn}\rho_{nb} + \sum_{bmr} g_{mbnr}\tilde{\rho}_{nrvb} - \sum_{bcn} g_{bcvn}\tilde{\rho}_{mnbc} \\ &- \sum_{nrab} \frac{\tilde{g}_{abnr}}{\epsilon_{ab} - \epsilon_{nr}} \Bigg\{ \sum_{c} \tilde{g}_{ncva}\tilde{\rho}_{rmcb} - \sum_{s} \tilde{g}_{rmsa}\tilde{\rho}_{snvb} + \sum_{c} \tilde{g}_{mcva}\rho_{nrcb} \\ &\qquad - \sum_{s} \tilde{g}_{rmsv}\rho_{nsab} + \sum_{c} g_{ncab}\tilde{\rho}_{rmcv} - \sum_{s} g_{nrsa}\tilde{\rho}_{smvb}\end{aligned}$$

$$- \sum_{s} g_{nrsv}\rho_{msab} + \sum_{c} g_{mcab}\rho_{nrcv} \Bigg\}. \tag{2.44}$$

These are the single double partial triple (SDpT) equations. With these equations, the third order energy of the MBPT is recovered after one iteration.

2.1.3 Transition matrix element

In the second quantization formalism, the matrix elements are obtained using the one- and two-body operator applied to the wavefunction. The one-body operator is used to calculate most of the matrix elements such as the radiative transition matrix element, and the two-body operator is used to calculate the two-body part of the specific mass shift matrix element. The calculation method for one-body matrix elements in all-order formalism has been developed in [2]. In this work, we developed the calculation method for two-body matrix elements in all-order formalism for the first time.

In this section, we will derive the one- and two-body operators in the SD formalism. For simplicity, we only show the general form of the operators. The reduced forms after the angular reduction are given in Appendix B.

2.1.3.1 The one-body operator

In general, the one-body operator Z can be expressed using the ladder operator as

$$Z = \sum_{ij} z_{ij} : a_i^\dagger a_j :, \tag{2.45}$$

where z_{ij} is the matrix element of the corresponding Z operator between one particle wavefunction $z_{ij} = \langle j|Z|i\rangle$. The product of operators inside the two colons indicates the normal ordering of the operator [79].

Subsequently, the matrix element between SD wavefunction Ψ_v and Ψ_w is given by

$$Z_{wv} = \frac{\langle \Psi_w|Z|\Psi_v\rangle}{\sqrt{\langle \Psi_v|\Psi_v\rangle\langle \Psi_w|\Psi_w\rangle}}, \tag{2.46}$$

The terms inside the brackets in Eq. (2.46) can be simplified by using the Wick's theorem [79]. We group the terms in the brackets using the following designation

$$\langle \Psi_w | Z | \Psi_v \rangle = \delta_{wv} Z_0 + Z_{\rm val} + Z_{\rm ad}, \tag{2.47}$$

$$\langle \Psi_v | \Psi_v \rangle = 1 + N_C + N_v. \tag{2.48}$$

In Eqs. (2.47) and (2.48), N_C and Z_0 contain the core contribution terms; N_v and $Z_{\rm val}$ contain the valence contribution terms; $Z_{\rm ad}$ contains the additional terms. Those terms are given by

$$N_C = \sum_{ma} \rho^*_{ma}\rho_{ma} + \frac{1}{2}\sum_{mnab} \tilde{\rho}^*_{mnab}\rho_{nmba}, \tag{2.49}$$

$$\begin{aligned} N_v = & \sum_{m} \rho^*_{mv}\rho_{mv} - \sum_{a} \rho^*_{va}\rho_{va} + \sum_{ma} \rho^*_{ma}\tilde{\rho}_{vmva} \\ & + \sum_{ma} \tilde{\rho}^*_{vmva}\rho_{ma} + \sum_{mab} \rho^*_{vmab}\tilde{\rho}_{vmba} - \sum_{mna} \rho^*_{mnva}\tilde{\rho}_{nmva}, \end{aligned} \tag{2.50}$$

$$\begin{aligned} Z_0 = & \sum_{ma} z_{am}\rho_{ma} + \sum_{ma} z_{ma}\rho^*_{ma} + \sum_{mnabc} z_{ab}\rho^*_{mnbc}\tilde{\rho}_{nmac} - \sum_{mnrab} z_{mn}\rho^*_{rmab}\tilde{\rho}_{rnba} \\ & - \sum_{mab} z_{ab}\rho^*_{mb}\rho_{ma} + \sum_{mna} z_{mn}\rho^*_{ma}\rho_{na} - \sum_{mnab} z_{am}\rho^*_{nb}\tilde{\rho}_{nmab} - \sum_{mnab} z_{ma}\tilde{\rho}^*_{nmab}\rho_{nb}, \end{aligned} \tag{2.51}$$

$$Z_{ad} = z_{wv} \times N_C + \sum_{ma} z_{ma}\rho^*_{ma}\rho_{wv} + \sum_{ma} z_{am}\rho^*_{vw}\rho_{ma}, \tag{2.52}$$

$$Z_{\rm val} = z_{wv} + Z^{(a)} + \cdots + Z^{(t)}, \tag{2.53}$$

where

$$Z^{(a)} = \sum_{ma} z_{am}\tilde{\rho}_{wmva} + \sum_{ma} z_{ma}\tilde{\rho}^*_{vmwa}, \tag{2.54}$$

$$Z^{(b)} = -\sum_{a} z_{av}\rho_{wa} - \sum_{a} z_{wa}\rho^*_{va}, \tag{2.55}$$

$$Z^{(c)} = \sum_{m} z_{wm}\rho_{mv} + \sum_{m} z_{mv}\rho^*_{mw}, \tag{2.56}$$

$$Z^{(d)} = \sum_{mn} z_{mn}\rho^*_{mw}\rho_{nv}, \tag{2.57}$$

$$Z^{(e)} = \sum_{ab} z_{ab}\rho^*_{vb}\rho_{wa}, \tag{2.58}$$

$$
\begin{aligned}
Z^{(f)} &= -\sum_{ma} z_{av}\rho^*_{mw}\rho_{ma} - \sum_{ma} z_{wa}\rho^*_{ma}\rho_{mv}, && (2.59)\\
Z^{(g)} &= -\sum_{ma} z_{mv}\rho^*_{ma}\rho_{wa} - \sum_{ma} z_{wm}\rho^*_{va}\rho_{ma}, && (2.60)\\
Z^{(h)} &= \sum_{mna} z_{am}\rho^*_{nw}\tilde{\rho}_{nmva} + \sum_{mna} z_{ma}\tilde{\rho}^*_{nmwa}\rho_{nv}, && (2.61)\\
Z^{(i)} &= \sum_{mna} z_{mn}\rho^*_{ma}\tilde{\rho}_{wnva} + \sum_{mna} z_{mn}\tilde{\rho}^*_{vmwa}\rho_{na}, && (2.62)\\
Z^{(j)} &= -\sum_{mab} z_{ab}\rho^*_{mb}\tilde{\rho}_{wmva} - \sum_{mab} z_{ab}\tilde{\rho}^*_{vmwb}\rho_{ma}, && (2.63)\\
Z^{(k)} &= \sum_{mab} z_{am}\rho^*_{vb}\tilde{\rho}_{wmab} + \sum_{mab} z_{ma}\tilde{\rho}^*_{vmab}\rho_{wb}, && (2.64)\\
Z^{(l)} &= -\sum_{mab} z_{av}\rho^*_{mb}\tilde{\rho}_{wmab} - \sum_{mab} z_{wa}\tilde{\rho}^*_{vmab}\rho_{mb}, && (2.65)\\
Z^{(m)} &= -\sum_{mna} z_{mv}\tilde{\rho}^*_{nmwa}\rho_{na} - \sum_{mna} z_{wm}\rho^*_{na}\tilde{\rho}_{nmva}, && (2.66)\\
Z^{(n)} &= \sum_{mnab} z_{ab}\rho^*_{mnwb}\tilde{\rho}_{nmva}, && (2.67)\\
Z^{(o)} &= \sum_{mabc} z_{ab}\tilde{\rho}^*_{vmbc}\tilde{\rho}_{wmac}, && (2.68)\\
Z^{(p)} &= \sum_{mnra} z_{mn}\tilde{\rho}^*_{rmwa}\tilde{\rho}_{rnva}, && (2.69)\\
Z^{(q)} &= \sum_{mnab} z_{mn}\rho^*_{vmab}\tilde{\rho}_{wnba}, && (2.70)\\
Z^{(r)} &= -\sum_{mnab} z_{am}\tilde{\rho}^*_{vnwb}\tilde{\rho}_{nmab} - \sum_{mnab} z_{ma}\tilde{\rho}^*_{nmab}\tilde{\rho}_{wnvb}, && (2.71)\\
Z^{(s)} &= \sum_{mnab} z_{av}\rho^*_{mnwb}\tilde{\rho}_{nmab} + \sum_{mnab} z_{wa}\rho^*_{mnab}\tilde{\rho}_{nmvb}, && (2.72)\\
Z^{(t)} &= -\sum_{mnab} z_{mv}\rho^*_{nmab}\tilde{\rho}_{wnba} - \sum_{mnab} z_{wm}\rho^*_{vnab}\tilde{\rho}_{nmba}. && (2.73)
\end{aligned}
$$

Within this work, we are only interested in the nonscalar one-body operator. For such case of an operator, it has been shown [2] that the core contribution and disconnected diagrams vanish. Therefore the one-body operator reduces to

$$
Z_{wv} = \frac{z_{wv} + Z_{\mathrm{val}}}{\sqrt{(1+N_v)(1+N_w)}} \qquad (2.74)
$$

2.1.3.2 The two-body operator

In general, the two-body matrix element P can be expressed using the ladder operator as the sum of one-body operator S and two-body operator T

$$P = S + T, \tag{2.75}$$

where

$$S = \frac{1}{2}\sum_{ij} t_{ij} : a_i^\dagger a_j :, \tag{2.76}$$

$$T = \frac{1}{2}\sum_{ijkl} t_{ijkl} : a_i^\dagger a_j^\dagger a_l a_k : . \tag{2.77}$$

The treatment of the one-body part is the same as we have done in the previous section. The two-body operator will be used in this work to calculate the specific mass shift [80] term which is a diagonal matrix element. In the diagonal case, the matrix element for operator T is given by

$$\langle \Psi_v | T | \Psi_v \rangle = T_0 + T_{\text{val}}, \tag{2.78}$$

where we used similar designation as in the previous section for the terms on the right side. The T_0 contains the core contribution and T_{val} contains the valence contribution. After simplifying with the Wick's theorem [79] we have

$$T_0 = T_0^{(a)} + \cdots + T_0^{(e)} \tag{2.79}$$

$$T_{\text{val}} = T^{(a)} + \cdots + T^{(y)} \tag{2.80}$$

where

$$T_0^{(a)} = \tfrac{1}{2} t_{abmn} \tilde{\rho}_{nmba} + \tfrac{1}{2} t_{mnab} \tilde{\rho}^*_{nmba} \tag{2.81}$$

$$T_0^{(b)} = -\tfrac{1}{2} \tilde{t}_{abmc} \rho^*_{nc} \tilde{\rho}_{nmba} - \tfrac{1}{2} \tilde{t}_{mabc} \tilde{\rho}^*_{nmcb} \rho_{na} \tag{2.82}$$

$$T_0^{(c)} = \tfrac{1}{2} \tilde{t}_{manr} \rho^*_{mb} \tilde{\rho}_{rnab} + \tfrac{1}{2} \tilde{t}_{mnra} \tilde{\rho}^*_{nmab} \rho_{rb} \tag{2.83}$$

$$T_0^{(d)} = -\tfrac{1}{2} \tilde{t}_{manb} \rho^*_{mb} \rho_{na} + \tfrac{1}{2} t_{mnab} \tilde{\rho}^*_{nmba} \tag{2.84}$$

$$T_0^{(e)} = -\tfrac{1}{4} t_{abcd} \tilde{\rho}^*_{mndc} \tilde{\rho}_{nmba} - \tilde{t}_{manb} \tilde{\rho}^*_{rmbc} \tilde{\rho}_{rnac} \tag{2.85}$$

and

$$
\begin{aligned}
T^{(a)} &= 2\tilde{t}_{vavm}\rho_{ma} && (2.86)\\
T^{(b)} &= -2t_{abvm}\tilde{\rho}_{mvba} && (2.87)\\
T^{(c)} &= 2t_{avmn}\tilde{\rho}_{nmva} && (2.88)\\
T^{(d)} &= 2\tilde{t}_{vamb}\rho^{*}_{vb}\rho_{ma} && (2.89)\\
T^{(e)} &= 2\tilde{t}_{vmna}\rho^{*}_{ma}\rho_{nv} && (2.90)\\
T^{(f)} &= -\tilde{t}_{vavb}\rho^{*}_{mb}\rho_{ma} + \tilde{t}_{vmvn}\rho^{*}_{ma}\rho_{na} && (2.91)\\
T^{(g)} &= 2\tilde{t}_{mavn}\rho^{*}_{mb}\tilde{\rho}_{vnab} && (2.92)\\
T^{(h)} &= 2t_{abvc}\rho^{*}_{mc}\tilde{\rho}_{mvba} && (2.93)\\
T^{(i)} &= 2t_{abmc}\rho^{*}_{vc}\tilde{\rho}_{vmba} && (2.94)\\
T^{(j)} &= -2\tilde{t}_{vavm}\rho^{*}_{nb}\tilde{\rho}_{nmab} && (2.95)\\
T^{(k)} &= -2t_{vamn}\rho^{*}_{vb}\tilde{\rho}_{nmab} && (2.96)\\
T^{(l)} &= 2\tilde{t}_{vamb}\rho^{*}_{nb}\tilde{\rho}_{nmva} && (2.97)\\
T^{(m)} &= -2\tilde{t}_{manb}\rho^{*}_{mb}\tilde{\rho}_{vnva} && (2.98)\\
T^{(n)} &= 2t_{mvrn}\rho^{*}_{ma}\tilde{\rho}_{nrva} && (2.99)\\
T^{(o)} &= -2t_{vmab}\tilde{\rho}^{*}_{mnba}\rho_{nv} && (2.100)\\
T^{(p)} &= 2t_{amnr}\rho^{*}_{mv}\tilde{\rho}_{rnva} && (2.101)\\
T^{(q)} &= -2\tilde{t}_{vamb}\tilde{\rho}^{*}_{vnbc}\tilde{\rho}_{nmac} && (2.102)\\
T^{(r)} &= -2t_{vmnr}\rho^{*}_{vmab}\tilde{\rho}_{rnba} && (2.103)\\
T^{(s)} &= 2t_{vabc}\rho^{*}_{mncb}\tilde{\rho}_{nmva} && (2.104)\\
T^{(t)} &= -2t_{mabc}\tilde{\rho}^{*}_{nmcb}\tilde{\rho}_{vnva} && (2.105)\\
T^{(u)} &= 2\tilde{t}_{vmna}\tilde{\rho}^{*}_{rmab}\tilde{\rho}_{rnvb} && (2.106)\\
T^{(v)} &= 2t_{mnra}\tilde{\rho}^{*}_{nmab}\tilde{\rho}_{vrvb} && (2.107)\\
T^{(w)} &= \tilde{t}_{manb}\tilde{\rho}^{*}_{vmbc}\tilde{\rho}_{vnac} - \tilde{t}_{manb}\tilde{\rho}^{*}_{rmvb}\tilde{\rho}_{rnva} && (2.108)\\
T^{(x)} &= -\tfrac{1}{2}t_{abcd}\tilde{\rho}^{*}_{vmdc}\tilde{\rho}_{vmba} + \tfrac{1}{2}t_{mnrs}\tilde{\rho}^{*}_{nmva}\tilde{\rho}_{srva} +
\end{aligned}
$$

$$\frac{1}{2}\tilde{t}_{vavb}\tilde{\rho}^{*}_{mnbc}\tilde{\rho}_{nmac} \tag{2.109}$$

Eq. (2.86)-(2.109) are the complete two body terms of the SD all-order formalism.

2.2 Methods for divalent system

The SD and SDpT methods that we have described in the previous sections are only applicable for single valence electron systems. A method was developed in [4, 81] where the combination of configuration interaction (CI) [9] with MBPT is applied to calculate the energy of a multivalence system. In this method, the CI is used to account for the valence-valence electrons correlations while the MBPT is used to account for the core-core and core-valence electrons correlations. We will briefly describe the CI+MBPT method in this section.

2.2.1 CI+MBPT method

We assume that the electrons in the atom can be divided into two groups, the valence and core electrons. The number of electrons in the core, N_{core}, is chosen such that the valence and core electrons energies are well separated. For example, For Sr (38 electrons) we can choose $N_{\text{core}} = 36$ with two valence electrons. Next, we divide the atom many-electron Hilbert space into two subspaces, P and Q. The subspace P contains the states where all the core electron states are filled and the subspace Q contains the rest of the states. From the completeness relation we have

$$\mathcal{P} + \mathcal{Q} = 1, \tag{2.110}$$

where $\mathcal{P}$ and $\mathcal{Q}$ are the projection operator to the subspace P and Q respectively.

In general, the subspace P has infinite dimensions so using it in calculations is impractical. We can, however, approximate it by defining a large enough configuration I, which is a subset of P, such that most of the low-lying states of P are contained in I. In this approximation, the wavefunction of the system can be expressed as a linear combination of this configuration

$$\psi = \sum_{I \in P^{\text{CI}}} C_I |I\rangle. \tag{2.111}$$

Putting this wavefunction to the Schrödinger equation we obtain an eigenvalue problem

$$\sum_{J \in P^{\mathrm{CI}}} H_{IJ} C_J = E C_I. \tag{2.112}$$

Therefore the Hamiltonian of the configuration space H_{CI} is a crucial part in obtaining the energy matrix.

The configuration Hamiltonian can be obtained by projecting the exact Hamiltonian $\mathcal{H}$ onto the configuration subspace

$$\mathcal{H}^{\mathrm{CI}} = \mathcal{P}^{\mathrm{CI}} \mathcal{H} \mathcal{P}^{\mathrm{CI}}. \tag{2.113}$$

We now assume that the configuration I can be made such that the Schrödinger equation solution from it can be obtained within the required accuracy. Henceforth, we are not going to explicitly put the label "CI" so that $\mathcal{P}^{\mathrm{CI}}$ is now written as $\mathcal{P}$.

The projected Hamiltonian is given by

$$\mathcal{P}\mathcal{H}\mathcal{P} = E_{\mathrm{core}} + \sum_{i > N_{\mathrm{core}}} h_i^{\mathrm{CI}} + \sum_{j > i > N_{\mathrm{core}}} \frac{1}{r_{ij}} \tag{2.114}$$

where E_{core} is the core electrons energy which includes the kinetic energy, the nucleus-core Coulomb interactions, and the core-core Coulomb interactions. The h_i^{CI} is the one body operator for the valence electrons which includes the kinetic terms, the nucleus-valence Coulomb interactions, and the core-valence Coulomb interactions. The last term is the Coulomb interaction between the valence electrons.

From Eq. (2.110) we can write Eq. (2.113) as

$$\mathcal{H} = \mathcal{P}\mathcal{H}\mathcal{P} + \mathcal{P}\mathcal{H}\mathcal{Q} + \mathcal{Q}\mathcal{H}\mathcal{P} + \mathcal{Q}\mathcal{H}\mathcal{Q}, \tag{2.115}$$

and the exact wavefunction Ψ as

$$\Psi = P\Psi + Q\Psi = \Phi + \chi. \tag{2.116}$$

The Schrodinger equation

$$\mathcal{H}\Psi = E\Psi, \tag{2.117}$$

now becomes two equations of two functions Φ and χ

$$(\mathcal{PHP})\Phi + (\mathcal{PHQ})\chi = E\Phi, \tag{2.118}$$

$$(\mathcal{QHQ})\chi + (\mathcal{QHP})\Phi = E\chi. \tag{2.119}$$

Next, we define the Green function

$$\mathcal{R}_{\mathcal{Q}}(E) = (E - \mathcal{QHQ})^{-1}, \tag{2.120}$$

so that Eq. (2.119) can be written as

$$\chi = \mathcal{R}_{\mathcal{Q}}(E)(\mathcal{QHP})\Phi. \tag{2.121}$$

Using Eq. (2.121) we can then write Eq. (2.118) as

$$(\mathcal{PHP} + \Sigma(E))\Phi = E\Phi, \tag{2.122}$$

where

$$\Sigma(E) = (\mathcal{PHQ})\mathcal{R}_{\mathcal{Q}}(E)(\mathcal{QHP}). \tag{2.123}$$

Eq. (2.122) is the CI+MBPT equation. After the CI diagonalization, the first term of the equation will account for the valence-valence correlation (see Eq. (2.114)). The second term, $\Sigma(E)$, essentially connects the space $\mathcal{P}$ (all core electrons in ground state) and $\mathcal{Q}$ (at least one core electron is excited) thus it accounts for the core-valence and core-core correlations. In this formulation, the first term is considered as the unperturbed Hamiltonian, it is evaluated using CI while the second term is evaluated with MBPT. Finally, since $\Sigma(E)$ is a function of the energy, it is necessary to solve the equation by iteration.

We will now explicitly derive $\Sigma(E)$ using the perturbation formalism. The starting approximation will be the Dirac-Fock Hamiltonian as the unperturbed Hamiltonian. The number of electrons in the averaged potential used in the self-consistency procedure N_{DF} can be varied with the condition $N < N_{\mathrm{DF}} < N_{\mathrm{core}}$. In the simplest approximation, we can choose $N_{\mathrm{DF}} = N_{\mathrm{core}}$ which is the approximation used throughout this work.

We define the one-electron unperturbed Dirac-Fock Hamiltonian $h_{\rm DF}$

$$h_0 \equiv h_{\rm DF} = c\alpha \times \mathbf{p} + (\beta - 1)mc^2 - \frac{Z}{r} + V_{\rm DF}^N, \tag{2.124}$$

such that

$$h_{\rm DF} a_i^\dagger |0\rangle = \epsilon_i a_i^\dagger |0\rangle \tag{2.125}$$

where ϵ_i is the Dirac-Fock energy of orbital i. The potential $V_{\rm DF}^N$ is chosen to approximate the average repulsion from all the core electrons [6], it is solved self-consistently. The many-electron the Dirac-Fock Hamiltonian can be written as

$$\mathcal{H}_{\rm DF} = E_{\rm core} - \sum_a \epsilon_a a_a^\dagger a_a + \sum_m \epsilon_m a_m^\dagger a_m \equiv E_{\rm core} + \tilde{\mathcal{H}}_{\rm DF}, \tag{2.126}$$

where $E_{\rm core}$ is the matrix element of the exact energy of the core electrons

$$E_{\rm core} = \langle \Psi_{\rm core} | \mathcal{H} | \Psi_{\rm core} \rangle, \tag{2.127}$$

$$\Psi_{\rm core} = a_1^\dagger a_2^\dagger \cdots a_{N_{\rm core}}^\dagger |0\rangle. \tag{2.128}$$

From Eq. (2.126) we can see that the operator $\mathcal{H}_{\rm DF}$ commutes with both $\mathcal{P}$ and $\mathcal{Q}$ so that

$$\mathcal{P}\mathcal{H}_{\rm DF}\mathcal{Q} = \mathcal{Q}\mathcal{H}_{\rm DF}\mathcal{P} = 0. \tag{2.129}$$

We can now write Eq. (2.123) as

$$\begin{aligned} \Sigma(E) &= (\mathcal{P}(\mathcal{H} - \mathcal{H}_{\rm DF})\mathcal{Q})\mathcal{R}_{\mathcal{Q}}(\mathcal{E})(\mathcal{Q}(\mathcal{H} - \mathcal{H}_{\rm DF})\mathcal{P}) \\ &= (\mathcal{P}(V - V^{N_{\rm DF}})\mathcal{Q})\mathcal{R}_Q(E)(\mathcal{Q}(V - V^{N_{\rm DF}})\mathcal{P}), \end{aligned} \tag{2.130}$$

where V is the exact potential. Thus, $(V - V_{\rm DF}^N)$ is the residual potential that will be used as the perturbation. Using the usual MBPT technique we can write down Eq. (2.120) as

$$\begin{aligned} \mathcal{R}_{\mathcal{Q}}(E) &\equiv \mathcal{Q}(E - \mathcal{H})^{-1}\mathcal{Q} \\ &= \mathcal{Q}(E - \mathcal{H}_{\rm DF})^{-1}\mathcal{Q} \\ &\quad + \mathcal{Q}(E - \mathcal{H}_{\rm DF})^{-1}\mathcal{Q}(\mathcal{V} - \mathcal{V}^{N_{\rm DF}})\mathcal{Q}(E - \mathcal{H}_{\rm DF})^{-1}\mathcal{Q} + \cdots \end{aligned} \tag{2.131}$$

Putting the above equation back to Eq. (2.130) and writing them in the matrix element form we obtain

$$\begin{aligned}\Sigma_{IJ} &= \sum_{M\in Q}\frac{U_{IM}U_{MJ}}{E-E_M}+\sum_{M,L\in Q}\frac{U_{IM}U_{ML}U_{LJ}}{(E-E_M)(E-E_L)}+\cdots \\ &\equiv \Sigma^{(2)}+\Sigma^{(3)}+\cdots,\end{aligned} \tag{2.132}$$

where U is the residual potential $(V-V_{\rm DF}^N)$. If we only take the expansion of $\Sigma(E)$ to its lowest order then the Eq. (2.122) becomes

$$\sum_{J\in P^{\rm CI}}\left(H_{IJ}+\sum_{M\in Q}\frac{U_{IM}U_{MJ}}{E-E_M}\right)C_J=EC_I, \tag{2.133}$$

which is the CI+MBPT equation in the explicit matrix element form. Notice that the Eq. (2.133) corresponds to the Brillouin-Wigner variant of the MBPT [9]. The other alternative using the Rayleigh-Schrodinger approach has its disadvantages as it will make the matrix on the left-hand side of the above equation becomes nonsymmetric [82].

The complete evaluation of the second term in Eq. (2.133) is shown in [4]. Following the notation used in [83] we divide $\Sigma(E)$ into a one body operator $\Sigma_1(E)$ and a two body operator $\Sigma_2(E)$. The one body operator can be written as [5]

$$(\Sigma_1^{(2)})_{xy}=\sum_{mab}\frac{g_{myab}\tilde{g}_{mxab}}{\epsilon_{ab}-\epsilon_{xm}+\tilde{\epsilon}_y-\epsilon_y}+\sum_{mna}\frac{g_{mnxa}\tilde{g}_{mnva}}{\tilde{\epsilon}_y+\epsilon_a-\epsilon_{mn}}, \tag{2.134}$$

and the two body operator as

$$\begin{aligned}(\Sigma_2^{(2)})_{mnvw} &= \sum_{cd}\frac{g_{vwcd}g_{mncd}}{\epsilon_{cd}-\epsilon_{mn}+\tilde{\epsilon}_v-\epsilon_v+\tilde{\epsilon}_w-\epsilon_w} \\ &\quad+\left[\sum_{rc}\frac{\tilde{g}_{wrnc}\tilde{g}_{mrvc}}{\tilde{\epsilon}_v+\epsilon_c-\epsilon_{mr}+\tilde{\epsilon}_w-\epsilon_w}+\begin{pmatrix}m\leftrightarrow n\\ v\leftrightarrow w\end{pmatrix}\right],\end{aligned} \tag{2.135}$$

where $\tilde{\epsilon}$ is the trial energy from the subsequent iteration.

2.2.2 CI+all-order method

In the CI+all-order formulation, the perturbative effect from Σ_1 and Σ_2 are evaluated within the framework of all-order method [5]. To do this, first, we express the

excitation coefficient ρ in terms of the matrix element Σ. Furthermore, an additional all-order equation need to be made for coefficient ρ_{mnvw} which is the coefficient ρ_{mnvb} with the index b replaced by w.

The matrix element Σ can be expressed using the excitation coefficient ρ as following

$$\Sigma_{ma} = \rho_{ma}(\epsilon_a - \epsilon_m), \tag{2.136}$$

$$\Sigma_{mnab} = \rho_{mnab}(\epsilon_{ab} - \epsilon_{mn}), \tag{2.137}$$

$$\Sigma_{mnva} = \rho_{mnva}(\tilde{\epsilon}_v + \epsilon_a - \epsilon_{mn}), \tag{2.138}$$

$$\Sigma_{mv} \equiv (\Sigma_1)_{mv} = \rho_{mv}(\tilde{\epsilon}_v - \epsilon_m), \tag{2.139}$$

$$\Sigma_{mnvw} \equiv (\Sigma_2)_{mnvw} = \rho_{mnvw}(\tilde{\epsilon}_v + \tilde{\epsilon}_w - \epsilon_{mn}). \tag{2.140}$$

The terms Σ_1 and Σ_2 are essentially the coefficients ρ_{mv} and ρ_{mnvw} multiplied by the appropriate energy differences. In this method, the core excitation coefficients ρ_{ma} and ρ_{mnab} are not modified. The rest of the equations are obtained by rewriting Eq. (2.11) and (2.13) replacing ρ with Σ and removing the terms that are already accounted by the CI procedure

$$\begin{aligned}
\Sigma_{mv} \equiv (\Sigma_1)_{mv} &= \sum_{nb} \frac{\tilde{g}_{mbvn}\Sigma_{nb}}{\epsilon_b - \epsilon_n + \tilde{\epsilon}_v - \epsilon_v} - \sum_{bcn} \frac{\tilde{g}_{bcvn}\Sigma_{mnbc}}{\epsilon_{bc} - \epsilon_{mn} + \tilde{\epsilon}_v - \epsilon_v} \\
&+ \sum_{bnr} \frac{\tilde{g}_{mbnr}\Sigma_{nrvb}}{\tilde{\epsilon}_v + \epsilon_b - \epsilon_{nr}},
\end{aligned} \tag{2.141}$$

$$\begin{aligned}
\Sigma_{mnvb} &= g_{mnvb} + \sum_{cd} \frac{g_{cdvb}\Sigma_{mncd}}{\epsilon_{cd} - \epsilon_{mn} + \tilde{\epsilon}_v - \epsilon_v} + \sum_{rs} \frac{g_{mnrs}\Sigma_{rsvb}}{\tilde{\epsilon}_v + \epsilon_b - \epsilon_{rs}} \\
&- \sum_{c} \frac{g_{cnvb}\Sigma_{mc}}{\epsilon_c - \epsilon_m + \tilde{\epsilon}_v - \epsilon_v} + \sum_{r} \frac{g_{mnvr}\Sigma_{rb}}{\epsilon_b - \epsilon_r + \tilde{\epsilon}_v - \epsilon_v} \\
&- \sum_{c} \frac{g_{mcvb}\sum_{nc}}{\epsilon_c - \epsilon_n + \tilde{\epsilon}_v - \epsilon_v} + \sum_{cr} \frac{\tilde{g}_{cnrb}\Sigma_{mrvc}}{\tilde{\epsilon}_v + \epsilon_c - \epsilon_{mr}} \\
&- \sum_{cr} \frac{g_{cnrb}\Sigma_{rmvc}}{\tilde{\epsilon}_v + \epsilon_c - \epsilon_{mr}} - \sum_{cr} \frac{g_{mcrb}\Sigma_{rnvc}}{\tilde{\epsilon}_v + \epsilon_c - \epsilon_{nr}} \\
&+ \sum_{cr} \frac{\tilde{g}_{mcvr}\Sigma_{rncb}}{\epsilon_{cb} - \epsilon_{nr} + \tilde{\epsilon}_v - \epsilon_v} - \sum_{cr} \frac{g_{mcvr}\Sigma_{ncrb}}{\epsilon_{cb} - \epsilon_{nr} + \tilde{\epsilon}_v - \epsilon_v} \\
&- \sum_{cr} \frac{g_{cnvr}\Sigma_{mrcb}}{\epsilon_{cb} - \epsilon_{mr} + \tilde{\epsilon}_v - \epsilon_v},
\end{aligned} \tag{2.142}$$

$$
\begin{aligned}
\Sigma_{mnvw} &\equiv (\Sigma_2)_{mnvw} \\
&= \sum_{cd} \frac{g_{cdvw}\Sigma_{mncd}}{\epsilon_{cd} - \epsilon_{mn} + \tilde{\epsilon}_v - \epsilon_v + \tilde{\epsilon}_w - \epsilon_w} - \sum_{c} \frac{g_{cnvw}\Sigma_{mc}}{\epsilon_c - \epsilon_m + \tilde{\epsilon}_v - \epsilon_v + \tilde{\epsilon}_w - \epsilon_w} \\
&\quad - \sum_{c} \frac{g_{mcvw}\Sigma_{nc}}{\epsilon_c - \epsilon_n + \tilde{\epsilon}_v - \epsilon_v + \tilde{\epsilon}_w - \epsilon_w} + \sum_{cr} \frac{\tilde{g}_{cnrw}\Sigma_{mrvc}}{\tilde{\epsilon}_v + \epsilon_c - \epsilon_{mr} + \tilde{\epsilon}_w - \epsilon_w} \\
&\quad - \sum_{cr} \frac{g_{cnrw}\Sigma_{rmvc}}{\tilde{\epsilon}_v + \epsilon_c - \epsilon_{mr} + \tilde{\epsilon}_w - \epsilon_w} - \sum_{cr} \frac{g_{mcrw}\Sigma_{rnvc}}{\tilde{\epsilon}_v + \epsilon_c - \epsilon_{nr} + \tilde{\epsilon}_w - \epsilon_w} \\
&\quad + \sum_{cr} \frac{\tilde{g}_{mcvr}\Sigma_{rncw}}{\epsilon_c + \tilde{\epsilon}_w - \epsilon_{nr} + \tilde{\epsilon}_v - \epsilon_v} - \sum_{cr} \frac{g_{mcvr}\Sigma_{rnwc}}{\epsilon_c + \tilde{\epsilon}_w - \epsilon_{nr} + \tilde{\epsilon}_v - \epsilon_v} \\
&\quad - \sum_{cr} \frac{g_{cnvr}\Sigma_{rmwc}}{\epsilon_c + \tilde{\epsilon}_w - \epsilon_{mr} + \tilde{\epsilon}_v - \epsilon_v},
\end{aligned}
\tag{2.143}
$$

these are the CI+All-order equations. These equations reduce to Eqs. (2.11) and (2.13) when $\tilde{\epsilon}_v = \epsilon_v$. The term containing ρ_{rv} in Eq. (2.11) corresponds to valence excitations which is accounted in CI procedure, thus it does not appear in Eqs. (2.142) and (2.143). The first, third and fifth term of Eq. (2.142) also correspond to valence excitation in the case of $b = w$, therefore, they are omitted. Furthermore, Eq. (2.143) does not contain Σ_{mnvw} on the right-hand side, so it is not an iterative equation. Therefore Σ_{mnvw} can be calculated last, once the other coefficients have converged.

2.2.3 Remarks on the Hamiltonian Diagonalization

The size of the Hamiltonian matrix formed in the CI+MBPT and CI+All order methods depends on the size of the configuration space. In practice, this space can be too large so that diagonalizing the whole matrix will be unrealistic. For such case, we can diagonalize a subset of the whole matrix using mathematical procedures, in our code, this is implemented by using Davidson diagonalization method [84]. This way, it is possible to obtain the wavefunction of the first few levels and their energies.

2.2.4 The transition matrix element.

Currently, the calculation of the transition matrix elements in the CI+MBPT and CI+All order methods have been developed to include the second order and the

random phase approximation [9] (RPA) terms. This calculation is done by first calculating the "bare" matrix element terms and then using the obtained radial integrals to calculate the second order and RPA terms. Finally, the bare terms are replaced with the effective "dressed" terms which include higher order corrections. In this section, we will briefly discuss the calculation method of the matrix element.

Consider many-electron states $|JM\rangle$ where J is the total angular momentum, and M is its projection. The matrix element of the spherical component of operator a rank L operator T, T^L_q, is given by

$$\langle J'M'|T^L_q|JM\rangle = \mathrm{Tr}\rho_{nljm,n'l'j'm'}\langle n'l'j'm'|T^L_q|nljm\rangle, \tag{2.144}$$

where $|nljm\rangle$ is the one electron state and "Tr" means the summation over all quantum numbers $nljm, n'l'j'm'$. In Eq. (2.144), $\rho_{nljm,n'l'j'm'}$ is the transition matrix element given by

$$\rho_{nljm,n'l'j'm'} = \langle J'M'|a^\dagger_{n'l'j'm'}a_{nljm}|JM\rangle. \tag{2.145}$$

We can obtain the reduced matrix element by using the Wigner-Eckart theorem. Summing over the magnetic quantum number m, the reduced transition matrix element of rank L is given by

$$\rho^L_{nlj,n'l'j'} = (-1)^{J'-M'}\begin{pmatrix} J' & L & J \\ -M' & q & M \end{pmatrix}^{-1}\sum_{mm'}(-1)^{j'-m'}\begin{pmatrix} j' & L & j \\ -m' & q & m \end{pmatrix}\rho^L_{nljm,n'l'j'm'}, \tag{2.146}$$

therefore

$$\langle J'||T^L||J\rangle = \mathrm{Tr}\rho^L_{nlj,n'l'j'}\langle n'l'j'||T^L||nlj\rangle.. \tag{2.147}$$

Using Eq. (2.147) we can obtain individual transition matrix element given the diagonal wave vectors.

Since we can only have several diagonalized wave vectors, there are only limited transition matrix elements than can be calculated. For some cases, it is required to

calculate the summation of transition matrix elements over the whole basis set. For example, the static E1 polarizability is given by [39]

$$\alpha_0^v(0) = \frac{-2}{3(2J_v+1)} \sum_n \frac{|\langle vJ_v||D||nJ_n\rangle|^2}{E_n - E_v}, \tag{2.148}$$

where D is the electric dipole operator. For this case, we calculate the matrix elements using an inhomogeneous equation [85, 86] which will be discussed next.

Suppose we solve the inhomogenous equation

$$(E_v - H)|X_{v,M'}\rangle = D_q|v, J_v, M_v\rangle, \tag{2.149}$$

where $q = 0, \pm 1$ and $M' = M_v + q$. The inhomogeneous function $X_{v,M'}$ in general can be decomposed in terms that correspond to a particular angular momentum J'

$$X_{v,M'} = \sum_{J'=J_v,J_v\pm1} X_{v,J',M'} \tag{2.150}$$

If we revert the reduced matrix element from Eq. (2.148)

$$\alpha_0^v(0) = \frac{-2}{3(2J_n+1)} \sum_n (-1)^{-J_v+M_v} \begin{pmatrix} J_v & 1 & J_n \\ -M_v & q & M_n \end{pmatrix}^{-2} \frac{|\langle vJ_vM_v|D_q|nJ_nM_n\rangle|^2}{E_v - E_n}, \tag{2.151}$$

the last term can be expressed in terms of the inhomogeneous function $X_{v,J',M'}$

$$\begin{aligned} \frac{|\langle vJ_vM_v|D_q|nJ_nM_n\rangle|^2}{E_v - E_n} &= \frac{\langle vJ_vM_v|D_{-q}|nJ_nM_n\rangle\langle nJ_nM_n|D_q|vJ_vM_v\rangle}{E_v - E_n} \\ &= \sum_{J'} \frac{\langle vJ_vM_v|D_{-q}|nJ_nM_n\rangle\langle nJ_nM_n|(E_v - H)|X_{v,J',M'}\rangle}{E_v - E_n} \\ &= \sum_{J'} \langle vJ_vM_v|D_{-q}|nJ_nM_n\rangle\langle nJ_nM_n|X_{v,J',M'}\rangle. \end{aligned} \tag{2.152}$$

In the third step, the Hamiltonian is operated to the left to cancel the denominator. If we plug Eq. (2.152) to Eq. (2.151) and carry the summation over n we obtain

$$\alpha_0^v(0) = \frac{2}{3(2J_v+1)} \sum_{J'} (-1)^{-J_v+M_v} \begin{pmatrix} J_v & 1 & J' \\ -M_v & q & M' \end{pmatrix} \langle v, J_v, M_v|D_{-q}|X_{v,J',M'}\rangle. \tag{2.153}$$

Therefore the summation over the transition matrix elements can be obtained if we solve the inhomogeneous function $X_{v,J',M'}$ from Eq. (2.149). Note that the $3J$ symbol on the right-hand side of Eq. (2.153) is not always non zero, in the case of zero $3J$ symbols, the equation is no longer valid, so it is necessary to do the calculation with $q = \pm 1$.

2.3 One electron reduced matrix elements

In this work, a lot of our calculations utilize the one-electron reduced electric dipole matrix element $\langle a||D||b\rangle$ and the one-electron reduced matrix element of tensor operator $T^{(1)}$ of rank 1 $\langle a||T^{(1)}||a\rangle$. In this section, we will list the formulas for these matrix elements.

The one-electron reduced electric dipole matrix element $\langle k||D||v\rangle$ is calculated using the following formula [6]

$$\langle a||D||b\rangle = \begin{cases} -\sqrt{l_a}\int_0^\infty dr\, f_b\left(\frac{d}{dr} + \frac{l_a}{r}\right) f_a, \text{for } l_b = l_a - 1 \\ \sqrt{l_a+1}\int_0^\infty dr\, f_b\left(\frac{d}{dr} - \frac{l_a+1}{r}\right) f_a, \text{for } l_b = l_a + 1 \end{cases}, \tag{2.154}$$

where f is the large component of the Dirac wavefunction and l is the orbital quantum number. The one-electron reduced matrix element of tensor operator $T^{(1)}$ of rank 1 $\langle a||T^{(1)}||a\rangle$ is given by [6]

$$\langle a||T^{(1)}||a\rangle = -\frac{2\kappa_a}{2(j_a+1)}\int_0^\infty \frac{dr}{r^2} 2 f_a g_a, \tag{2.155}$$

where κ is the total relativistic angular quantum number and g_a is the small component of the Dirac wavefunction.

2.4 Basis states

Unless otherwise noted, the basis set used in this work is constructed using B-spline technique [6] with principal quantum number $n = 35$ for each partial waves with $l \leq 5$. This set is formed in a spherical cavity with radius 60 a.u.

Chapter 3

EXTRACTING TRANSITION RATES FROM ZERO POLARIZABILITY SPECTROSOPY

In this chapter, we discuss the method to extract the transition matrix element via measurement of magic wavelength [87]. We choose Sr as the currently best system available for this study. First, we provide a brief review of the magic wavelength and magic zero wavelength theories.

3.1 Method

An atom inside an oscillating electric field will form an induced electric dipole moment which oscillates with the driving frequency ω. The induced dipole moment $\mathbf{p}$ will interact with the electric field $\mathbf{E}$ and create an effective potential [88]

$$U_{\text{dip}} = \frac{1}{2}\langle \mathbf{pE} \rangle = \frac{1}{2\epsilon_0 c}\Re(\alpha)I, \tag{3.1}$$

where ϵ_0, c, α and I are the vacuum permittivity, speed of light, dynamic polarizability and electric field intensity respectively. In the previous equation we have used the relation between the dipole moment amplitude $\tilde{p}$ and the electric field amplitude $\tilde{E}$, $\tilde{p} = \alpha\tilde{E}$. Atomic optical trap is created by using two counterpropagating laser beams that formed a standing wave of an electric field. This standing wave effectively creates a periodical potential well with a depth given by Eq. (3.1).

The dynamic polarizability that determines the depth of the optical trap depends on the electronic properties of the atom. In practice, a lattice clock utilizes two electronic states, $|A\rangle$ and $|B\rangle$, as the primary clock transition. By changing the laser wavelength, we can change how the atoms interact with the optical lattice. There are two important types of the wavelength that we will consider, the magic and magic zero wavelengths.

The magic wavelength ω_{magic} is defined as the wavelength when both the polarizabilities of the state $|A\rangle$ and $|B\rangle$ are equal ($\alpha^{|A\rangle}(\omega_{\text{magic}}) = \alpha^{|B\rangle}(\omega_{\text{magic}})$) at the leading order of multipole expansion (electric dipole). When this condition happens the lattice depth for both states $|A\rangle$ and $|B\rangle$ are equal. This condition enables the transition between both states with a transition frequency which, at the leading order, is independent of the electric field intensity [31]. Neutral atom lattice clocks operates at the magic wavelength.

The magic zero wavelength ω_{zero} is defined as the wavelength when one of the polarizabilities of the state $|A\rangle$ and $|B\rangle$ is zero ($\alpha^{|A\rangle}(\omega_{\text{zero}}) = 0$ or $\alpha^{|B\rangle}(\omega_{\text{zero}}) = 0$) at the leading order of multipole expansion. When operating at this wavelength, the optical lattice interacts exclusively to one of the states. The determination of this wavelength enables the use of multiple laser beams operating at different magic zero wavelengths to create lattices for various purposes (e.g. to create "storing" and "transporting" lattices in quantum computer [89]).

Measurements of the magic and magic zero wavelengths enable us to precisely determine $E1$ transition matrix elements. Because by knowing the magic wavelength, we can determine the dynamic polarizability which is given by [39]

$$\alpha_0^v(\omega) = \frac{2}{3(2J+1)} \sum_k \frac{\langle k||D||v\rangle^2 (E_k - E_v)}{(E_k - E_v)^2 - \omega^2}, \tag{3.2}$$

where J and D are the total angular quantum number and electric dipole operator respectively. From Eq. (3.2) we can extract the transition matrix element.

Note that the contribution of the virtual state k to the total polarizability depends on the vicinity of the driving frequency ω to the corresponding resonance frequency $E_k - E_v$. In other words, some contributions will have an enhancement factor depending on how close the measured wavelength to the corresponding resonance.

3.2 Results

Using CI+all order formalism, we evaluate the magic and magic zero wavelength of Sr. To increase the accuracy of our calculation we replace several transition

energies with their experimental values and the transition matrix elements with their recommended values.

We replace the first ten $5s5p\,^3P_0$ and the first four $5s^2\,^1S_0$ transitional energies with their experimental values taken from [90]. In the current CI+all order code, the transition matrix elements are evaluated with the second order and RPA terms. Higher order terms of the Sr transition matrix element has been shown to contribute to 0.4-1.7% of the total values [26]. Recommended values for the first few matrix elements has been extracted in [26] from $5s5p\,^1P^o_1$ lifetime [91], $5s^2\,^1S_0 - 5s5p\,^3P_0$ transition stark shift [92] and 814 nm magic wavelength [93]. The recommended values for $5s5p\,^3P_0 - 5s4d\,^3D_1$ transition matrix element has been extracted from the recent Sr clock BBR shift measurement [23] and the $5s5p\,^1P_1 - 5s^2\,^1S_0$ from the $5s5p\,^1P^o_1$ lifetime [91]. The summary of all the replacements made in the calculation is shown in Table 3.1.

We calculate the dynamic polarizability of the $5s^2\,^1S_0$ and $5s5p\,^3P_0$ state and plot their result. For clarity we made two plots of dynamic polarizability (a.u.) vs wavelength (nm) in different range, $350 < \lambda < 460$ nm and $460 < \lambda < 840$ nm. These plots are shown in Figures 3.1 and 3.2. The $5s^2\,^1S_0$ and $5s5p\,^3P_0$ polarizabilities are shown by the red and blue lines respectively. The magic wavelengths are shown at the crossing between the blue and red lines as red circles and the magic zero wavelengths are shown at the crossing between the polarizability lines with the horizontal axis. Note that the 813.4 nm magic wavelength is shown on the right side of Figure 3.2. The $5s5p\,^3P_0$ transition resonances are shown as dashed black lines.

We list the CI+all-order and recommended values of the magic and magic zero wavelengths in Table 3.2. The recommended values are obtained after the energies and matrix elements replacements as explained previously. We have found five additional magic wavelengths apart from the 813.4 nm. There are eight $5s5p\,^3P_0$ and one $5s^2\,^1S_0$ magic zero wavelengths. The $5s^2\,^1S_0$ magic zero wavelength agrees with the results of the previous works [89, 94]. The $5s5p\,^3P_0$ magic zero wavelength at 632(2) nm is 5 nm longer than the result in [89] which gives 627 nm.

Table 3.1: The resonance wavelengths λ and reduced dipole matrix elements D in Sr. Vacuum wavelength values are given in nm. The calculated and recommended matrix elements are given in a.u.

Transition			Wavelength		Matrix elements D	
			CI+all	Expt.	CI+all	Recomm. [26]
$5s5p\ ^3P_0$	-	$5s4d\ ^3D_1$	2642.4	2603.1	2.714	2.6707(62)[a]
$5s5p\ ^3P_0$	-	$5s6s\ ^3S_1$	682.0	679.3	1.972	1.962(10)[b]
$5s5p\ ^3P_0$	-	$5s5d\ ^3D_1$	484.2	483.3	2.458	2.450(24)[b]
$5s5p\ ^3P_0$	-	$5p^2\ ^3P_1$	471.5	474.3	2.627	2.605(26)[b]
$5s5p\ ^3P_0$	-	$5s7s\ ^3S_1$	433.3	432.8	0.522	0.516(8)[b]
$5s5p\ ^3P_0$	-	$5s6d\ ^3D_1$	394.3	394.2	1.175	1.161(17)[b]
$5s5p\ ^3P_0$	-	$5s8s\ ^3S_1$	377.1	378.2	0.302	
$5s5p\ ^3P_0$	-	$5s7d\ ^3D_1$	361.4	363.0	0.822	
$5s5p\ ^3P_0$	-	$5s9s\ ^3S_1$	348.4	355.4	0.270	
$5s5p\ ^3P_0$	-	$5s8d\ ^3D_1$	336.7	334.8	0.820	
$5s5p\ ^3P_1$	-	$5s^2\ ^1S_0$	678.7	689.5	0.158	
$5s5p\ ^1P_1$	-	$5s^2\ ^1S_0$	458.3	460.9	5.272	5.248(2)[c]
$5s6p\ ^3P_1$	-	$5s^2\ ^1S_0$	293.6	295.3	0.035	
$5s6p\ ^1P_1$	-	$5s^2\ ^1S_0$	291.5	293.3	0.283	

[a]Ref. [23].
[b]Ref. [26].
[b]Ref. [91].

Figure 3.1: The plot of dynamic polarizability (a.u.) vs wavelength (nm) in the range $350 < \lambda < 460$ nm. The polarizabilities of $5s5p\,^3P_0$ and $5s^2\,^1S_0$ are shown by the blue and red lines respectively. The intersects between the blue, and red lines are the magic wavelengths shown by red circles. The intersects between the lines and the horizontal axis are the magic-zero wavelengths shown by blue circles. The resonances between the $5s5p\,^3P_0$ and the corresponding states are shown by black dashed lines.

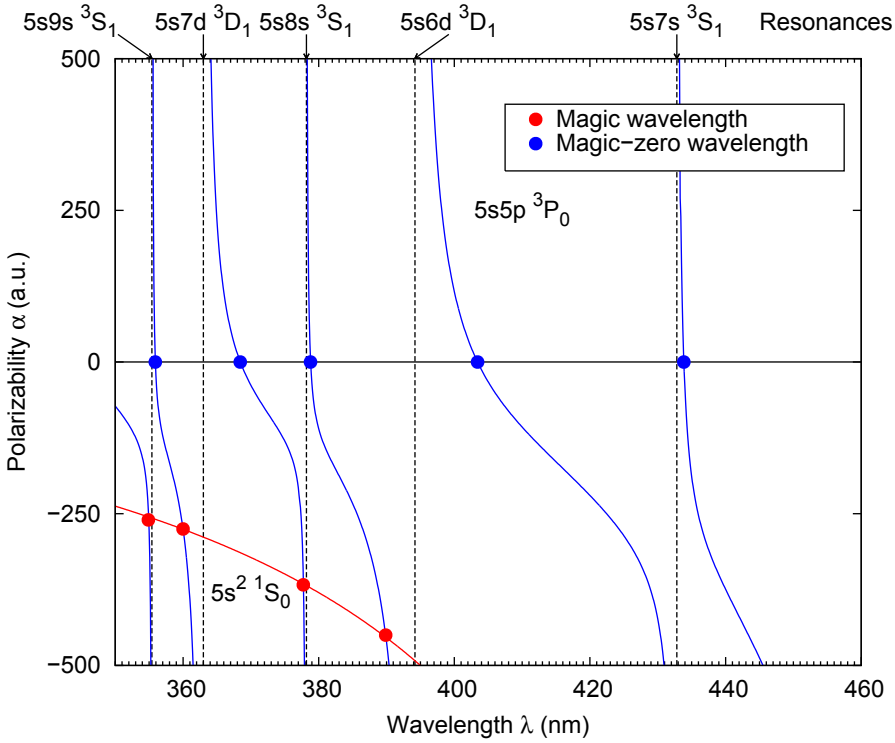

Figure 3.2: Plot of dynamic polarizability (a.u.) vs wavelength (nm) in the range $460 < \lambda < 840$ nm. Polarizability of $5s5p\,^3P_0$ and $5s^2\,^1S_0$ are shown by the blue and red lines respectively. The intersects between the blue and red lines are the magic wavelength shown by the red circle. The intersects between the lines and the x axis are the magic-zero wavelengths shown by the blue circle. The resonances between the $5s5p\,^3P_0$ and the corresponding states are shown by the black dashed lines.

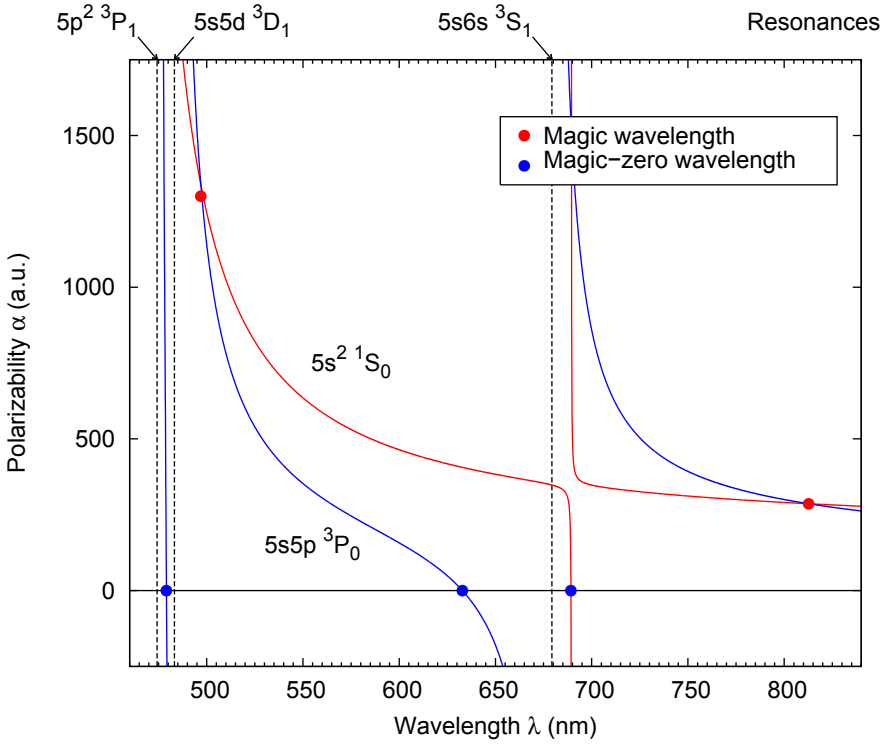

Table 3.2: Magic-zero λ_{zero} and magic λ_{magic} wavelengths. See text for the explanation of the recommended value calculations.

λ_{zero}		λ_{magic}	
CI+all-order	Recomm.	CI+all-order	Recomm.
$5s5p\ ^3P_0$		$5s^2\ ^1S_0 - 5s5p\ ^3P_0$	
	355.92		354.9
367.0	368.45	358.5	360.0
377.8	378.81	376.8	377.75
403.35	403.428	390.1	389.9
434.35	433.85		497.0
478.35	479.126		
634.7	632.83		
1672.9	1666.6		
$5s^2\ ^1S_0$			
679.55	689.20		

Tables 3.3 and 3.4 show the contributions from the ten lowest transitions to the total polarizabilities of $5s5p\,^3P_0$ state at the magic zero wavelengths. The contribution to total polarizability from the transition is calculated using Eq. (3.2) and given in a.u. The dominant contributions at the corresponding magic zero wavelength are shown in bold. The total polarizability is calculated by solving the inhomogeneous equation as explained in Sec. 2.2.4. The "other" contribution is obtained by subtracting the ten contributions from the total polarizability. The total polarizability is zero within the numerical accuracy.

In theory, a global fit can be done to extract the transition matrix elements if all the magic zero wavelengths have been measured. We propose a second simpler method to extract the transition matrix elements from the magic zero wavelength measurement. First, the transition matrix elements from the first and second contributions of Tables 3.3 and 3.4 have been critically evaluated. The $5s5p\ ^3P_0 - 5s4d\ ^3D_1$ matrix element is known to 0.5% accuracy from the $5s4d\,^3D_1$ lifetime measurement [23] and the $5s5p\ ^3P_0 - 5s6s\ ^3S_1$ matrix element to 1% accuracy from the BBR shift measurement

Table 3.3: The breakdown by the transition of the contributions (in a.u.) to the dynamic polarizability of $5s5p\,^3P_0$ state, at the eight magic-zero wavelengths. The first ten rows give the contributions from the transitions, and all other contributions are grouped together in row "Other". The chain of dominant contributions relevant to the extraction of matrix elements (see text for a discussion) is highlighted in bold.

Contribution	1666.6 nm	632.84 nm	479.127 nm	433.85 nm
$5s5p\,^3P_0$ - $5s4d\,^3D_1$	**-188.7**	-17.1	-9.5	-7.8
$5s5p\,^3P_0$ - $5s6s\,^3S_1$	**45.9**	**-251.4**	-37.9	-26.4
$5s5p\,^3P_0$ - $5s5d\,^3D_1$	**46.3**	**101.9**	**-2404**	-176.0
$5s5p\,^3P_0$ - $5p^2\,^3P_1$	**51.2**	**107.5**	**2361**	-241.2
$5s5p\,^3P_0$ - $5s7s\,^3S_1$	1.8	3.2	9.2	**337.9**
$5s5p\,^3P_0$ - $5s6d\,^3D_1$	8.2	12.7	24.1	44.6
$5s5p\,^3P_0$ - $5s8s\,^3S_1$	0.5	0.8	1.3	2.1
$5s5p\,^3P_0$ - $5s7d\,^3D_1$	3.8	5.4	8.4	12.0
$5s5p\,^3P_0$ - $5s9s\,^3S_1$	0.4	0.6	0.8	1.2
$5s5p\,^3P_0$ - $5s8d\,^3D_1$	3.4	4.6	6.4	8.1
Other	27.1	32.0	39.2	44.8
Total	0.0	0.0	-0.3	-0.7
Uncertainty in α	11.6	8.7	10.5	6.6
Uncertainty in λ_{zero}	0.1 nm	0.2 nm	0.05 nm	0.25 nm

Table 3.4: The breakdown by the transition of the contributions (in a.u.) to the dynamic polarizability of $5s5p\,^3P_0$ state, at the eight magic-zero wavelengths. The first ten rows give the contributions from the transitions indicated, and all other contributions are grouped together in row "Other". The chain of dominant contributions relevant to the extraction of matrix elements (see text for a discussion) is highlighted in bold.

Contribution	403.429 nm	378.81 nm	368.45 nm	355.92 nm
$5s5p\,^3P_0$ - $5s4d\,^3D_1$	-6.7	-5.9	-5.6	-5.2
$5s5p\,^3P_0$ - $5s6s\,^3S_1$	-20.8	-17.3	-15.9	-14.5
$5s5p\,^3P_0$ - $5s5d\,^3D_1$	-97.5	-67.6	-58.9	-50.3
$5s5p\,^3P_0$ - $5p^2\,^3P_1$	-123.2	-82.9	-71.7	-60.7
$5s5p\,^3P_0$ - $5s7s\,^3S_1$	-11.2	-5.5	-4.4	-3.5
$5s5p\,^3P_0$ - $5s6d\,^3D_1$	**171.7**	-93.8	-53.8	-34.3
$5s5p\,^3P_0$ - $5s8s\,^3S_1$	4.2	**147.2**	-9.5	-3.9
$5s5p\,^3P_0$ - $5s7d\,^3D_1$	18.9	44.0	**122.7**	-89.1
$5s5p\,^3P_0$ - $5s9s\,^3S_1$	1.7	3.2	5.5	**142.7**
$5s5p\,^3P_0$ - $5s8d\,^3D_1$	10.6	15.1	18.9	28.6
Other	52.3	64.0	72.7	90.6
Total	0.0	0.4	0.0	0.4
Uncertainty in α	12	67	4.3	2.2
Uncertainty in λ_{zero}	0.05 nm	0.1 nm	0.6 nm	6 nm

[26]. The measurements of the magic zero wavelengths at 1666, 632 and 479 nm should let us determine the matrix elements from the first four contributions as well as the accuracy of the "other" contribution. Note that the third and fourth contributions are very dominant at the 479 nm magic zero wavelength. From the measurement of this magic zero wavelength, we should be able to determine these contributions. Therefore, magic zero wavelength measurement at 479 nm should be the priority.

Once the first four matrix element is determined, we can go to the next measurement, the magic zero wavelength at 433 nm. The dominant contribution at this magic wavelength comes from the fifth transition. Therefore, measurement of this magic zero wavelength should let us determine the transition matrix element from the fifth contribution. We can keep repeating the same procedure for the rest of the magic zero measurements until we obtain all the possible transition matrix elements.

Chapter 4

CALCULATIONS FOR THE DEVELOPMENT OF OPTICAL ATOMIC CLOCKS

In this chapter we calculate the BBR shift of Tl^+, magic wavelengths and BBR shift of Hg, and hyperfine quenching rates of ^{113}Cd.

4.1 BBR shift in $6s^2\,{}^1S_0 - 6s6p\,{}^3P_0$ clock transition of Tl^+

In this section, we calculate the BBR shift of Tl^+ as done in [38]. First, we briefly discuss the theory of BBR shift. The derivation of the BBR shift formula was first done in [95], later on, a generalized multipolar formula was derived in [96]. Previous calculations for BBR shift have been done for singly-charged ions [17, 97, 98] and neutral atoms [96].

BBR shift can be found by integrating the perturbation due to the radiation over the whole BBR spectrum. The BBR energy density spectrum $u_\omega(T)$ in atomic units is given by the Planck's law

$$u_\omega(T) = \frac{\alpha^3}{\pi^2}\frac{\omega^3}{e^{\omega/k_BT}-1}, \tag{4.1}$$

where α is the fine structure constant, ω the BBR frequency and k_B the Boltzmann constant.

Assuming the time evolution of excited state amplitudes adiabatically follow the reference state v, the BBR shift is given by (for complete derivation see [95] and [96])

$$\delta E_v^{\mathrm{BBR}} = -\frac{(\alpha k_BT)^3}{2J_v+1}\sum_n |\langle v||D||n\rangle|^2 F(y_n) \tag{4.2}$$

where J_v is the total angular momentum of state v, D is the E1 transition operator, and $y_n = (E_n - E_g)/k_BT$. The summation runs over the intermediate states n. Function

$F(y_n)$ is the function that corresponds to the integration of the electric fields from BBR over its whole spectrum [95]

$$F(y) = \int_0^\infty \left(\frac{1}{y+x} + \frac{1}{y-x}\right) \frac{x^2 dx}{e^x - 1}. \tag{4.3}$$

It should be noted that Eq. (4.2) is obtained by using the multipole expansion of the electromagnetic coupling taking only the E1 leading term into consideration. The next to leading term (M1) is not required at the current accuracy level. However, it is required at 10^{-18} accuracy level [96].

In our system, the energy difference between the states is far greater than the ambient temperature at 300 K ($(E_n - E_v) \gg k_B T$). In this limit, the function $F(y)$ can be expanded as [96]

$$F(y) \approx \frac{4\pi^3}{45y} + \frac{32\pi^5}{189y^3} + \frac{32\pi^7}{45y^5} + \frac{512\pi^9}{99y^7}. \tag{4.4}$$

Using this expansion and the formula of the E1 polarizability

$$\alpha_0^v(\omega) = \frac{2}{3(2J_n+1)} \sum_n \frac{(E_n - E_v)|\langle v||D||n\rangle|^2}{\omega_{nv}^2 - \omega^2}, \tag{4.5}$$

we can express the BBR shift in Eq. (4.2) in term of static E1 polarizability $\alpha_0^v(0)$

$$\delta E_v^{\mathrm{BBR}} = -\frac{2}{15}(\alpha\pi)^3 (k_B T)^4 \alpha_0^v(0)(1+\eta). \tag{4.6}$$

In the Eq. (4.6), we have separated the contribution to the BBR shift into the static (the first term) and dynamic (the second term) contributions. In our system, the static contribution dominates over the dynamic contribution. From Eqs. (4.2)-(4.5), it is straightforward to see that the dynamic term η in Eq. (4.6) is given by

$$\eta = \eta_1 + \eta_2 + \eta_3 = \frac{80}{63(2J_v+1)} \frac{\pi^2}{\alpha_0^v(0) k_B T} \sum_n \frac{|\langle n||D||v\rangle|^2}{y_n^3} \left(1 + \frac{21\pi^2}{5y_n^2} + \frac{336\pi^4}{11y_n^4}\right). \tag{4.7}$$

Previous analysis has shown that the polarizabilities of $ns^2\ ^1S_0$ and $nsnp\ ^3P_0$ state are almost equal for B^+, Al^+ and In^+ ions [17]. These polarizabilities result in anomalously small BBR shifts in the $ns^2\,^1S_0 - nsnp^3P_0$ transition for these ions. These ions belong to the same IIIB group, two other atoms in this group, Ga and

Tl, have not been studied yet. Frequency standard based on the Tl^+ $6s^2\,{}^1S_0\,m_F = 0 - 6s6p\,{}^3P_0\,m_{F'} = 0$ transition has been proposed [37]. The radioactive isotope of ^{204}Tl has a half-life of 3.78 years, a spin of 2, and a tiny magnetic moment of 0.0908 nuclear magnetons making it an ideal object for a very high-resolution laser spectroscopy. Because of its small nuclear magnetic moment, the natural linewidth of the clock transition in $^{204}Tl^+$ is expected to be orders of magnitude smaller than estimated for stable Tl isotopes.

To test our precision, we first calculated the energy of Tl^+ for several low-lying states. These energies are shown in Table 4.1 along with their comparison with experimental values obtained from [90]. The two electron binding energies are given in the first row, and the other energies are counted from the ground state. We used four different methods to calculate the energies, pure CI, CI+MBPT, CI+all-order and CI+all-order with Breit interaction [99] included. Breit interaction is the leading QED effect which is not accounted in our "no-pair" approximation. We show that compared to the experimental values, the best result was obtained by the CI+all-order method with an error of less than 1.7%.

Comparisons between the experimental and CI+all-order transition energies are given in Table 4.2. As can be seen, compared to the theoretical energies relative to the ground state, the transition energies has significantly better precision with an error of less than 0.35%.

Next, we calculated the polarizabilities of the states $6s^2\,{}^1S_0$ and $6s6p\,{}^3P_0$. We separated the contributions from the core and valence states. Furthermore, the core polarizability is divided into two parts, $\alpha_{\rm C}$ and $\alpha_{\rm VC}$. $\alpha_{\rm VC}$ is the small counter term that accounts for the part of α_C that contains the forbidden excitation from core state to the occupied valence state. For this system, we approximate the value of $\alpha_{\rm VC}$ to be the sum of its value for single valence system. Therefore, for we use $6s^2$ state $\alpha_{\rm VC}(6s^2) = 2\alpha_{\rm VC}(6s)$ and for $6s6p$ state $\alpha_{\rm VC}(6s6p) = \alpha_{\rm VC}(6s) + \alpha_{\rm VC}(6p)$. Both these contributions are calculated with RPA (see section 2.2.4).

Table 4.1: Comparisons between the experimental and theoretical values of energy levels in cm^{-1} for the first few even and odd configuration states. The energies are given in cm^{-1} in column Expt. and CI+all respectively for the experimental and theoretical values obtained using CI+all-order method. The first entry is the values of two-electron binding energy. The remaining entries are the difference between the corresponding energy and the ground state ($6s^2\ ^1S_0$). Differences in percent with the experimental values are given for other calculation methods. CI+all$^{\rm B}$ refers to the values from the CI+all-order method with Breit interaction [99] included.

State	Expt.	CI+all	Differences (%)			
			CI	CI+MBPT	CI+all	CI+all$^{\rm B}$
$6s^2\ ^1S_0$	405365	407125	-7.22	1.8	0.43	0.63
$6s7s\ ^3S_1$	105229	106028	-11.67	2.66	0.76	1.03
$6s7s\ ^1S_0$	108000	108904	-10.83	2.63	0.84	1.11
$6s6d\ ^1D_2$	115166	116194	-12.09	3.05	0.89	1.18
$6s6d\ ^3D_1$	116152	116857	-11.04	2.45	0.61	0.89
$6s6d\ ^3D_2$	116436	117284	-11.06	2.49	0.73	1.00
$6s6d\ ^3D_3$	116831	117758	-11.06	2.45	0.79	1.06
$6p^2\ ^3P_0$	117408	118450	-7.59	2.95	0.89	1.17
$6p^2\ ^3P_1$	125338	126440	-8.28	3.24	0.88	1.19
$6p^2\ ^3P_2$	128817	129839	-8.61	3.06	0.79	1.09
$6s8s\ ^3S_1$	133568	134187	-10.05	2.1	0.46	0.71
$6s8s\ ^1S_0$	134292	134950	-9.83	2.11	0.49	0.73
$6s6p\ ^3P_0$	49451	50288	-15.64	5.8	1.69	2.01
$6s6p\ ^3P_1$	52394	53060	-14.6	5.19	1.27	1.60
$6s6p\ ^3P_2$	61728	62669	-14.37	5.37	1.53	1.89
$6s6p\ ^1P_1$	75663	76145	-6.73	1.59	0.64	0.92
$6s7p\ ^3P_0$	119361	120155	-10.64	2.46	0.67	0.92
$6s7p\ ^3P_1$	119576	120472	-10.44	2.53	0.75	1.01
$6s7p\ ^3P_2$	122209	122675	-10.65	2.33	0.53	0.79
$6s7p\ ^1P_1$	122379	124019	-9.17	2.97	1.34	1.60
$6s5f\ ^3F_2$	136216	136600	-10.28	1.95	0.27	0.52
$6s5f\ ^3F_3$	136115	136577	-10.2	2.02	0.35	0.61
$6s5f\ ^3F_4$	136230	136595	-10.24	1.94	0.27	0.53
$6s5f\ ^1F_3$	136263	136756	-10.23	2.01	0.36	0.62

Table 4.2: Comparison of transition energies between the experimental [90] and the CI+all-order values in cm^{-1}. The last column gives the relative differences in percent

Transition	Expt.	CI+all-order	Difference (%)
6s6p $^3P_0$ - 6s7s $^3S_1$	55778	55739	0.07
6s6p $^3P_0$ - 6s6d $^3D_1$	66701	66569	0.20
6s6p $^3P_0$ - 6p^2 $^3P_1$	75887	76152	-0.35
6s6p $^3P_0$ - 6s8s $^3S_1$	84117	83899	0.26

The breakdown contributions for the polarizability is given in Table 4.3. The polarizability is given in a_0^3 with the few dominant contributions shown, these are obtained using the corresponding dipole matrix elements from Table 4.4. The "Other" contributions is obtained by subtracting the dominant α_C and α_{VC} contributions from the the total polarizability. To evaluate the uncertainty due to the correlation corrections, we carried out the calculation with CI, CI+MBPT, CI+all-order and CI+all-order with Breit interaction (CI+all^B) method. Furthermore, we also calculated the polarizability with CI+all-order method using the experimental energy (CI+all^C) to evaluate uncertainties due to the energy. We showed that using the experimental energy, the polarizability changes by 0.5% for $^3P_1$ and $^1P_1$ transition and by 0.07% for $^3S_1$ and $^3D_1$ transition. These uncertainties agree with the energy uncertainties shown before in Table 4.1 and 4.2.

In Table 4.5 we demonstrate the calculation of the dynamic term η to BBR shift defined in Eq. (4.7). In our calculation, only the dominant terms from the nearest transitions are considered. It can be seen that η is small and the difference $\Delta\eta = \eta(6s^2) - \eta(6s6p) \simeq .00001$ which is $\ll 1$. Therefore, we can safely say that the dynamic factor only gives small contributions to the total BBR shift.

The final result of the Tl^+ BBR shift for all different calculation methods are given in Table 4.6. We calculated the absolute ratio between the BBR shifts with the $6s^2\,^1S_0 - 6s6p\,^3P_0$ transition frequency $\nu_0 = 1.483 \times 10^{-15}$ Hz.

Table 4.3: Contributions for $6s^2\ ^1S_0$ and $6s6p\ ^3P_0$ polarizabilities in a_0^3. The values given in CI+All$^{\mathrm{C}}$ are calculated using CI+All order method with experimental energies. The leading contributions from the valence electron are listed for each state, the remaining valence contribution is given in "Other". The contribution from the core and its correction due to the presence of valence electron is given by α_C and α_{VC} respectively.

State	Contr.	α_0				
		CI	CI+MBPT	CI+all	CI+all$^{\mathrm{B}}$	CI+all$^{\mathrm{C}}$
$6s^2\ ^1S_0$	$6s^2\ ^1S_0 - 6s6p\ ^3P_1$	0.589	1.149	0.984	0.985	0.997
	$6s^2\ ^1S_0 - 6s6p\ ^1P_1$	16.131	13.057	13.450	13.351	13.535
	Other	0.269	0.143	0.383	0.155	0.155
	α_C	4.983	4.983	4.983	4.983	4.983
	α_{VC}	-0.071	-0.071	-0.071	-0.071	-0.071
	Total	21.901	19.261	19.501	19.402	19.599
$6s6p\ ^3P_0$	$6s6p\ ^3P_0 - 6s7s\ ^3S_1$	3.113	2.499	2.519	2.504	2.517
	$6s6p\ ^3P_0 - 6s6d\ ^3D_1$	9.563	7.86	7.912	7.857	7.897
	$6s6p\ ^3P_0 - 6s8s\ ^3S_1$	5.219	4.603	4.69	4.657	4.706
	Other	1.782	1.63	1.66	1.652	1.660
	α_C	4.983	4.983	4.983	4.983	4.983
	α_{VC}	-0.338	-0.338	-0.338	-0.338	-0.338
	Total	24.322	21.236	21.426	21.316	21.425
$\Delta\alpha_0(^1S_0 - ^3P_0)$		2.421	1.975	1.925	1.914	1.826

Table 4.4: The dipole matrix elements used to calculate the dominant contribution to total polarizability in a.u. The values obtained from CI, CI+MBPT, CI+all and CI+all$^{\mathrm{B}}$ are given.

Transition	D			
	CI	CI+MBPT	CI+all	CI+all$^{\mathrm{B}}$
$6s^2\ ^1S_0 - 6s6p\ ^3P_1$	0.424	0.658	0.597	0.599
$6s^2\ ^1S_0 - 6s6p\ ^1P_1$	2.789	2.619	2.646	2.640
$6s6p\ ^3P_0 - 6s7s\ ^3S_1$	1.044	0.975	0.980	2.504
$6s6p\ ^3P_0 - 6s6d\ ^3D_1$	2.007	1.893	1.897	7.857
$6s6p\ ^3P_0 - 6s8s\ ^3S_1$	1.616	1.557	1.562	4.657

Table 4.5: Detailed calculation of the dynamic factor η using CI+all order method. The corresponding E1 transition matrix elements in a.u. are given in column D. Only the leading contributions from the first few dominant transitions to η are considered.

State	Contr.	D	η_{pg}
$6s^2\ ^1S_0$	$6s^2\ ^1S_0 - 6s6p\ ^3P_1$	0.597	0.000014661
	$6s^2\ ^1S_0 - 6s6p\ ^1P_1$	2.646	0.000097255
$\eta(6s^2)$			**0.00011191**
$6s6p\ ^3P_0$	$6s6p\ ^3P_0 - 6s7s\ ^3S_1$	0.980	0.000030947
	$6s6p\ ^3P_0 - 6s6d\ ^3D_1$	1.897	0.000068140
	$6s6p\ ^3P_0 - 6s8s\ ^3S_1$	1.562	0.000023075
$\eta(6s6p)$			**0.00012216**

Table 4.6: The values of blackbody radiation shift frequency for each method. $\Delta\alpha_0$ is the polarizability difference between the $6s^2\,{}^1S_0$ and $6s6p\,{}^3P_0$ state in cm^{-1}. The correction η for each $6s^2$ and 6s6p state are given in their corresponding column. The blackbody radiation shift frequency is given in column labeled $\Delta\nu_{\rm BBR}$ in Hz, and the last column gives its absolute ratio compared to the absolute transition frequency ν_0 which, for Tl^+, is given by $\nu_0 = 1.483 \times 10^{-15}$ Hz.

Method	$\Delta\alpha_0$	$\eta(6s^2)$	$\eta(6s6p)$	$\Delta\nu_{\rm BBR}$ (Hz)	$\mid \Delta\nu_{\rm BBR}/\nu_0 \mid$
CI	2.421	0.000132	0.000151	-0.02084	1.406×10^{-17}
CI+MBPT	1.975	0.000109	0.000112	-0.01700	1.147×10^{-17}
CI+all	1.925	0.000112	0.000122	-0.01657	1.118×10^{-17}
CI+all$^{\rm B}$	1.914	0.000111	0.000121	-0.01648	1.111×10^{-17}
CI+all$^{\rm C}$	1.826	0.000114	0.000130	-0.01572	1.061×10^{-17}

Taking the CI+all$^{\rm C}$ value as our final result, we estimated the uncertainty by evaluating the difference between the total polarizability difference calculated by all methods. The BBR shift differs by 5% between CI+all and CI+all$^{\rm C}$ and by 2% between CI+all and CI+MBPT. Also, note that the inclusion of Breit interaction only changes the total polarizability difference by 0.5%. By considering these differences, we can safely assume that the total uncertainty of the BBR shift should not exceed 10%. Therefore we arrive at our final result of the BBR shift $\Delta\upsilon_{\rm BBR} = 0.0157(16)$ Hz.

In Table 4.7 we give the comparison between the calculated BBR shift of Tl^+ and the other previously estimated ions B^+, Al^+ and In^+ [17]. It can be seen that Tl^+, with the exception of Al^+, has the smallest BBR shift among these ions.

4.2 Magic Wavelengths and BBR shift of $6s\,{}^1S_0 - 6s6p\,{}^3P_0$ clock transition of Hg

In this section, we evaluated the BBR shift, magic wavelength and magic zero wavelength of Hg using CI+all-order method. We also use CI+MBPT and experimental energies to evaluate the uncertainties of our result.

Table 4.7: Comparison of the BBR shift calculation in group IIIB ions. The results for B^+, Al^+ and In^+ are taken from [17]. Polarizability differences in a.u., BBR shift, transition frequency, fractional BBR shift, and uncertainty are given.

Ion	$\Delta\alpha_0$	$\Delta\nu_{\rm BBR}$ (Hz)	ν_0 (Hz)	$\lvert\Delta\nu_{\rm BBR}/\nu_0\rvert$	Uncertainty
B^+	-1.85(19)	-0.0159(16)	1.119×10^{15}	1.42×10^{-17}	1×10^{-18}
Al^+	0.495(50)	-0.00426(43)	1.121×10^{15}	3.8×10^{-18}	4×10^{-19}
In^+	2.01(20)	-0.0173(17)	1.267×10^{15}	1.36×10^{-17}	1×10^{-18}
Tl^+	1.83(18)	-0.0157(16)	1.483×10^{15}	1.06×10^{-17}	1×10^{-18}

For this calculation we use four different approaches to estimate the total uncertainty: (1) CI+all order with theoretical energy (AO-th), (2) CI+all order with experimental energy (AO-exp), (3) CI+MBPT with theoretical energy (MBPT-th) and (4) CI+MBPT with experimental energy (MBPT-exp). The energy replacements were done for the first four transitions of $6s\,^1S_0$ state and the first eight transitions of $6s6p\,^3P_0$ state.

In Table 4.8 we give the energies and transition matrix elements of $6s\,^1S_0$ and $6s6p\,^3P_0$ transitions. The values for the first four $6s\,^1S_0$ and the first eight $6s6p\,^3P_0$ transitions are given. We show the experimental energies as well as the theoretical energies obtained using CI+all-order and CI+MBPT. Theoretical values of the transition matrix elements obtained using CI+all-order and CI+MBPT are also given. As can be seen for the given transition energies, the CI+all-order results differ by 0.6-4.6% from the experiment while the CI+MBPT results differ by 1.5-6.1% from the experiment. Note that the theoretical $6s^2\,^1S_0 - 6s6p\,^3P_1$ transition energy differs from the experimental energies by twice as much compared to the other $6s^2\,^1S_0$ transition. In particular, the energy from CI+MBPT differs by 6.1%, and the CI+all-order differs by 1.6% when compared with the experiment which shows that the higher order correlation for this transition accounts for about 4.6%. Also, note that the $6s6p\,^3P_0 - 6s8d\,^3D_1$ energy differs by 4.6% for CI+all-order and 5.0% for CI+MBPT when compared with the

Table 4.8: Transition energies and transition matrix elements for the first four $6s\,^1S_0$ transitions and the first eight $6s6p\,^3P_0$ transitions of Hg. Theoretical energies obtained using CI+all order and CI+MBPT are given in $\Delta E_{\rm AO}$ and $\Delta E_{\rm MBPT}$ respectively. Experimental energies taken from [90] are given in $\Delta E_{\rm exp}$. Electric dipole transition matrix elements obtained using CI+all order and CI+MBPT are given in $D_{\rm AO}$ and $D_{\rm MBPT}$ respectively.

State	Contribution	$\Delta E_{\rm AO}$	$\Delta E_{\rm MBPT}$	$\Delta E_{\rm exp}$	$D_{\rm AO}$	$D_{\rm MBPT}$
$6s^2\,^1S_0$	$6s^2\,^1S_0 - 6s6p\,^3P_1$	40029	41893	39412	0.517	0.573
	$6s^2\,^1S_0 - 6s6p\,^1P_1$	54478	55457	54069	2.940	2.913
	$6s^2\,^1S_0 - 6s7p\,^3P_1$	70087	71689	69662	0.033	0.041
	$6s^2\,^1S_0 - 6s7p\,^1P_1$	71873	73364	71295	0.654	0.629
$6s6p\,^3P_0$	$6s6p\,^3P_0 - 6s7s\,^3S_1$	24396	24152	24705	1.357	1.367
	$6s6p\,^3P_0 - 6s6d\,^3D_1$	33269	33153	33691	1.903	1.896
	$6s6p\,^3P_0 - 6s8s\,^3S_1$	35864	35721	36316	0.419	0.418
	$6s6p\,^3P_0 - 6s7d\,^3D_1$	38994	38856	39439	0.942	0.942
	$6s6p\,^3P_0 - 6s8d\,^3D_1$	40130	39970	42034	0.239	0.237
	$6s6p\,^3P_0 - 6s10s\,^3S_1$	41612	41475	42623	0.631	0.626
	$6s6p\,^3P_0 - 6s9d\,^3D_1$	42396	42239	43426	0.189	0.180
	$6s6p\,^3P_0 - 6s10d\,^3D_1$	43599	43465	44259	0.614	0.616

experimental values. These differences are particularly significant when compared with the other $6s6p\,^3P_0$ transition energies. The CI+all-order and CI+MBPT transition matrix elements mostly agree with up to 4.9% difference except for the $6s^2\,^1S_0 - 6s7p\,^3P_1$ transition matrix elements which differ by 21.6%.

Contributions to the static polarizability in all four approaches along with their comparison with other results are given in Table 4.9. We show the contributions of the first four $6s^2\,^1S_0$ transitions and the first eight $6s6p\,^3P_0$ calculated using sum over states are given. Total polarizability is obtained by solving the inhomogeneous equation (see chapter 2). Other contributions are obtained by subtracting the dominant contributions from the total polarizability. Contributions from the core electrons are accounted by the Core and VC terms. Taking the result from AO-th as our final

value, we approximate the numerical error by evaluating its difference with the results from the other three approaches. Thus, our final values of the static polarizability are $\alpha_0(0) = 33.326(1.014)$ a.u. for $6s^2\,{}^1S_0$ and $\alpha_0(0) = 55.284(442)$ a.u. for $6s6p\,{}^3P_0$. Our results are in good agreement with the previous CI+MBPT results from [32].

The breakdown of the dynamic contribution to the BBR shift is given in Table 4.10. We calculate the term η used in Eq. 4.6, this term accounts for the dynamic part of the BBR spectrum. As can be seen from the table, the final dynamic BBR shift $\Delta\nu^{\rm dyn}_{\rm BBR} \ll 1$ thus its effect is insignificant in the current precision limit. Using Eq. 4.6 we calculate the total BBR shift of Hg $6s^2\,{}^1S_0 - 6s6p\,{}^3P_0$ transition and obtain the final value of $\Delta\nu_{\rm BBR} = -0.189(11)$ Hz. With the $6s^2\,{}^1S_0 - 6s6p\,{}^3P_0$ clock transition frequency $\nu_0 = 1.1286 \times 10^{15}$ Hz we have the final value of the ratio of the BBR shift to clock transition $\Delta\nu_{\rm BBR}/\nu_0 = -1.68(9) \times 10^{-16}$.

We plot the dynamic polarizability around the magic wavelength at 368 nm in Figure 4.1. Similar to the BBR shift calculation, the AO-exp is taken as the final value, and the other results are used to evaluate the uncertainty. We found that for Hg $6s^2\,{}^1S_0 - 6s6p\,{}^3P_0$ transition our final value for the magic wavelength is $\lambda_{\rm magic} = 367.7(1.7)$ nm with $\alpha_{\rm magic} = 41.90(64)$ a.u. Our result differs by 4-8 nm from other works $\lambda_{\rm magic} = 363$ nm [101] and $\lambda_{\rm magic} = 360$ nm [32]. $6s6p\,{}^3P_0$ state dynamic polarizability around the magic zero wavelength 384 nm is plotted in Figure 4.2. For the magic zero wavelength of $6s6p\,{}^3P_0$ state; our final value is given by $\lambda_{\rm magic-zero} = 383.9(5.1)$ nm.

4.3 Hyperfine quenching rates of ^{113}Cd $5s^2\,{}^1S_0 - 5s5p\,{}^3P_0$ transition

In this section, we carried out an original derivation of the formula for the hyperfine quenching rate in the special case where the total initial and final angular momentum equal to zero. In the case of non-zero nuclear spin I, the radiative transition from state a to b in atomic units is given by [104]

$$A_{a\to b} = \frac{4\alpha\omega^3_{ab}}{3}\frac{1}{[J_a][I]}\sum_{F_aF_b}|\langle\gamma_bJ_bIF_b||D||\gamma_aJ_aIF_a\rangle|^2, \tag{4.8}$$

Table 4.9: Contributions to the static polarizability calculated using AO-th, AO-exp, MBPT-th and MBPT-exp. Contributions from the four dominant $6s^2\,{}^1S_0$ transitions and the eight dominant $6s6p\,{}^3P_0$ transitions are given. The other terms provided in "Other" are obtained by subtracting the dominant contributions from the total polarizability. The core and VC terms calculated with the second order MBPT + RPA are shown in Core and VC respectively. Other theoretical and experimental results are shown for comparison.

State	Contribution	$\alpha_0^{\mathrm{AO-th}}$	$\alpha_0^{\mathrm{MBPT-th}}$	$\alpha_0^{\mathrm{AO-exp}}$	$\alpha_0^{\mathrm{MBPT-exp}}$
$6s^2\,{}^1S_0$	$6s^2\,{}^1S_0 - 6s6p\,{}^3P_1$	0.978	1.145	0.993	1.218
	$6s^2\,{}^1S_0 - 6s6p\,{}^1P_1$	23.218	22.386	23.393	22.961
	$6s^2\,{}^1S_0 - 6s7p\,{}^3P_1$	0.002	0.003	0.002	0.004
	$6s^2\,{}^1S_0 - 6s7p\,{}^1P_1$	0.871	0.790	0.879	0.813
	Other	0.763	0.691	0.763	0.691
	Core	7.376	7.376	7.376	7.376
	VC	-0.080	-0.080	-0.080	-0.080
	Total	33.128	32.312	33.326	32.982
	Theory [100]	34.036			
	Theory [101]	31.32			
	Theory [32]	33.6			
	Expt. [102]	33.91(34)			
	Expt. [103]	33.75			
$6s6p\,{}^3P_0$	$6s6p\,{}^3P_0 - 6s7s\,{}^3S_1$	11.093	11.309	10.903	11.056
	$6s6p\,{}^3P_0 - 6s6d\,{}^3D_1$	15.965	15.874	15.719	15.620
	$6s6p\,{}^3P_0 - 6s8s\,{}^3S_1$	0.718	0.712	0.707	0.700
	$6s6p\,{}^3P_0 - 6s7d\,{}^3D_1$	3.331	3.342	3.291	3.293
	$6s6p\,{}^3P_0 - 6s8d\,{}^3D_1$	0.209	0.206	0.199	0.196
	$6s6p\,{}^3P_0 - 6s10s\,{}^3S_1$	1.398	1.383	1.365	0.112
	$6s6p\,{}^3P_0 - 6s9d\,{}^3D_1$	0.124	0.112	0.121	0.109
	$6s6p\,{}^3P_0 - 6s10d\,{}^3D_1$	1.266	1.278	1.247	1.255
	Other	14.789	14.387	14.789	14.387
	Core	7.376	7.376	7.376	7.376
	VC	-0.496	-0.496	-0.496	-0.496
	Total	55.669	55.483	55.284	54.842
	Theory [101]	55.32			
	Theory [32]	54.6			

Table 4.10: The breakdown of the dynamic contribution η to the BBR shift frequency in Hz. All-order dipole matrix elements and experimental energies are used for the calculation.

	η	$\alpha_0^v(0)$	$\Delta\nu_{\rm BBR}^{\rm dyn}$
$6s^2\,{}^1S_0 - 6s6p\,{}^3P_1$	0.000196		
$6s^2\,{}^1S_0 - 6s6p\,{}^1P_1$	0.000016		
$6s^2\,{}^1S_0 - 6s7p\,{}^3P_1$	0.000000		
$6s^2\,{}^1S_0 - 6s7p\,{}^1P_1$	0.000000		
Total($6s^2\,{}^1S_0$)	0.000216	33.326	-6.21×10^{-5}
$6s6p\,{}^3P_0 - 6s7s\,{}^3S_1$	0.000266		
$6s6p\,{}^3P_0 - 6s6d\,{}^3D_1$	0.000206		
$6s6p\,{}^3P_0 - 6s8s\,{}^3S_1$	0.000008		
$6s6p\,{}^3P_0 - 6s7d\,{}^3D_1$	0.000031		
$6s6p\,{}^3P_0 - 6s8d\,{}^3D_1$	0.000002		
$6s6p\,{}^3P_0 - 6s10s\,{}^3S_1$	0.000011		
$6s6p\,{}^3P_0 - 6s9d\,{}^3D_1$	0.000001		
$6s6p\,{}^3P_0 - 6s10d\,{}^3D_1$	0.000009		
Total($6s6p\,{}^3P_0$)	0.000534	55.284	-2.54×10^{-4}
Final $\Delta\nu_{\rm BBR}^{\rm dyn}(6s^2\,{}^1S_0 - 6s6p\,{}^3P_0)$			-1.92×10^{-4}

Figure 4.1: Dynamic polarizabilities of $6s^2\,{}^1S_0$ and $6s6p\,{}^3P_0$ states of Hg in different approximation for the wavelength region of $\lambda = 360 - 372$ nm. Wavelength is given in nm and polarizability in a.u. Results obtained using AO-th, MBPT-th, AO-exp and MBPT-exp approximation are shown in red, light red, dark blue and light blue color respectively. Magic wavelengths are shown at the intersections between $6s^2\,{}^1S_0$ and $6s6p\,{}^3P_0$ lines.

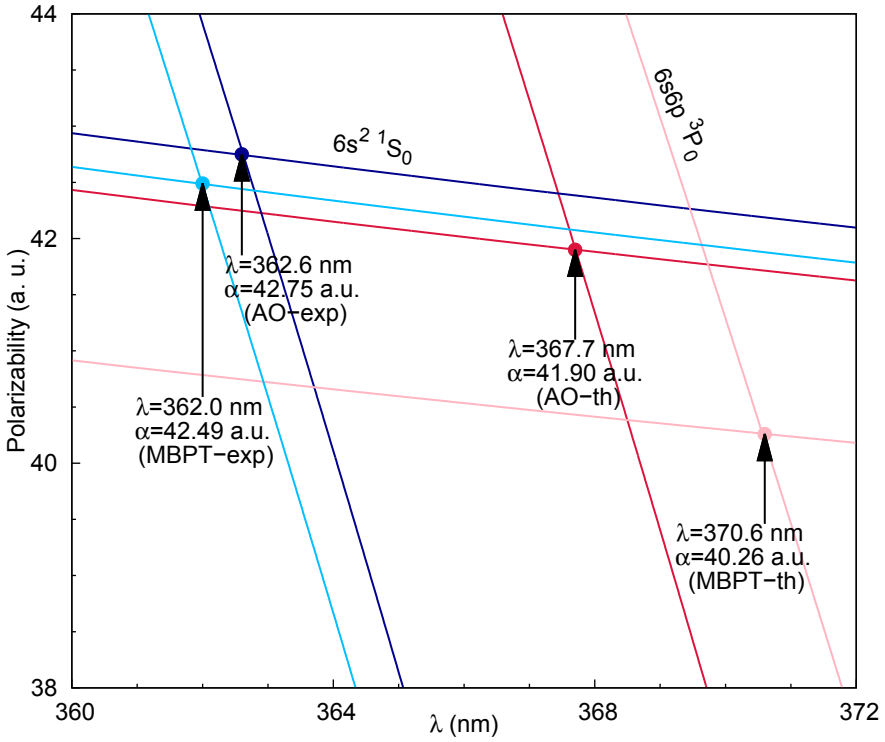

Figure 4.2: Dynamic polarizabilities of $6s6p\,^3P_0$ state of Hg in different approximations for the wavelength region of $\lambda = 375 - 390$ nm. Wavelength is given in nm and polarizability in a.u. Results obtained using AO-th, MBPT-th, AO-exp and MBPT-exp approximation are shown in red, light red, dark blue and light blue color respectively. Tuneout wavelengths are shown at the intersections between $6s6p\,^3P_0$ line and $\alpha = 0$ axis.

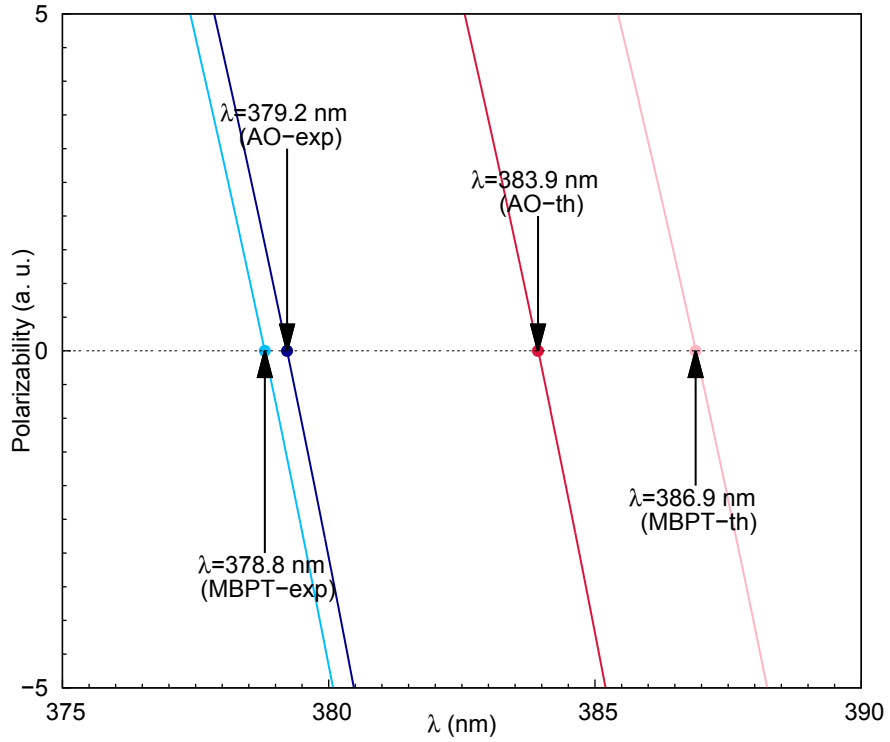

where J is the total electron angular momentum, F is the total angular quantum number $\mathbf{F} = \mathbf{I} + \mathbf{J}$, γ contains the rest of the other quantum numbers, and D is the dipole operator. The number in the square bracket is defined as $[A] = 2A + 1$.

The presence of a nuclear magnetic moment creates small shifts in the electron spectrum. These shifts can be represented as a state mixing due to the hyperfine interaction. Therefore, given a hyperfine interaction operator $H_{\rm hfs}$, the mixing of the state can be introduced via the perturbation expansion of the state $|\gamma IJFM_F\rangle$

$$|\gamma IJFM_F\rangle = |\gamma IJFM_F\rangle^{(0)} + \sum_{\gamma_n J_n} |\gamma_n IJ_nFM_F\rangle^{(0)} \frac{\langle \gamma_n IJ_nF_nM_{F_n}|^{(0)} H_{\rm hfs} |\gamma IJFM_F\rangle^{(0)}}{E(\gamma_n J_n) - E(\gamma J)}. \tag{4.9}$$

The hyperfine interaction is given as a series of the product between the multipole nuclear moment $M^{(k)}$ and even-parity electronic coupling $T^{(k)}$ [9]

$$H_{\rm hfs} = \sum_k M^{(k)} T^{(k)}, \tag{4.10}$$

In the current work we only consider the monopole contribution ($k = 1$) of the hyperfine operator. In this case, the nuclear moment is given by [9]

$$\langle I||M^{(1)}||I\rangle = \sqrt{\frac{(2I+1)(I+1)}{I}} \frac{\mu}{\mu_N}. \tag{4.11}$$

Furthermore, since $H_{\rm hfs}$ is a scalar operator it conserves the quantum numbers M and F. Taking this into consideration, we can write Eq. (4.9) in the reduced form

$$|\gamma IJF\rangle = |\gamma IJF\rangle^{(0)} + \sum_{\gamma_n J_n} |\gamma_n IJ_nF\rangle^{(0)} \frac{\langle \gamma_n IJ_nF||^{(0)} H_{\rm hfs} ||\gamma IJF\rangle^{(0)}}{E(\gamma_n J_n) - E(\gamma J)}. \tag{4.12}$$

With the expansion in (4.12), the dipole matrix element in Eq. (4.8) becomes

$$\begin{aligned}
\langle \gamma_b J_b IF_b||D||\gamma_a J_a IF_a\rangle &= \langle \gamma_b J_b IF_b||D||\gamma_a J_a IF_a\rangle^{(0)} \\
&\quad + \sum_{\gamma_n J_n} \langle \gamma_b J_b IF_b||D||\gamma_n J_n IF_a\rangle \frac{\langle \gamma_n J_n IF_a||H_{\rm hfs}||\gamma_a J_a IF_a\rangle}{E_n - E_{\gamma_a J_a}} \\
&\quad + \sum_{\gamma_n J_n} \frac{\langle \gamma_b J_b IF_b||H_{\rm hfs}||\gamma_n J_n IF_b\rangle}{E_n - E_{\gamma_b J_b}} \langle \gamma_n J_n IF_b||D||\gamma_a J_a IF_a\rangle \\
&= M^0_{ab} + M^1_{ab} + M^2_{ab}.
\end{aligned} \tag{4.13}$$

So in addition to the unperturbed dipole matrix element M^0_{ab}, we have two extra terms M^1_{ab} and M^2_{ab}. These terms will produce a small shift in the dipole transition rate called the hyperfine quenching rate. We will now derive the formulation of the hyperfine quenching rate.

4.3.1 Derivation of the Hyperfine Quenching Rate

The dipole and hyperfine matrix elements can be written in the reduced form by using the Wigner 6-j symbol

$$\langle \gamma' J' I F || H_{\rm hfs} || \gamma J I F \rangle = (-1)^{I+J'+F} \sum_k \begin{Bmatrix} I & I & k \\ J & J' & F \end{Bmatrix} \langle I || M^{(k)} || I \rangle \langle \gamma' J' || T^{(k)} || \gamma J \rangle, \tag{4.14}$$

$$\langle \gamma' J' I F || D || \gamma J I F \rangle = (-1)^{J'+I+F+1} \sqrt{[F][F']} \begin{Bmatrix} J' & F' & I \\ F & J & 1 \end{Bmatrix} \langle \gamma' J' || D || \gamma J \rangle. \tag{4.15}$$

We now evaluate each terms in $\sum_{F_a F_b} |\langle \gamma_b J_b I F_b || D || \gamma_a J_a I F_a \rangle|^2$ for the special case $J_a = J_b = 0$.

4.3.1.1 The Direct Terms

The first term $\sum_{F_a F_b} |M^0_{ab}|^2$ is given by

$$\begin{aligned} \sum_{F_a F_b} |M^0_{ab}|^2 &= \sum_{F_a F_b} [F_a][F_b] \begin{Bmatrix} J_b & F_b & I \\ F_a & J_a & 1 \end{Bmatrix} \begin{Bmatrix} J_b & F_b & I \\ F_a & J_a & 1 \end{Bmatrix} \langle \gamma_b J_b || D || \gamma_a J_a \rangle^2 \\ &= \sum_{F_a} \frac{[F_a]}{[J_a]} \{J_b J_a 1\} \{F_b F_a 1\} \langle \gamma_b J_b || D || \gamma_a J_a \rangle^2 \end{aligned} \tag{4.16}$$

Where we have used the orthogonality condition of the 6-j symbol

$$\sum_{F_b} [F_b] \begin{Bmatrix} J_b & F_b & I \\ F_a & J_a & 1 \end{Bmatrix}^2 = \frac{1}{[J_a]} \{J_b J_a 1\} \{F_b F_a 1\}. \tag{4.17}$$

Since

$$\sum_F [F] = [J][I], \tag{4.18}$$

The first term simplifies to

$$\sum_{F_a F_b} |M^0_{ab}|^2 = [I]\langle \gamma_b J_b||D||\gamma_a J_a\rangle^2. \tag{4.19}$$

The second term $\sum_{F_a F_b} |M^1_{ab}|^2$ is given by

$$\begin{aligned}\sum_{F_a F_b} |M^1_{ab}|^2 &= \sum_{\substack{\gamma_n J_n \\ \gamma_{n'} J_{n'}}} \sum_{\substack{k \\ F_a F_b}} [F_a][F_b]\langle I||M^{(k)}||I\rangle^2 \langle \gamma_b J_b||D||\gamma_n J_n\rangle\langle \gamma_{n'} J_{n'}||D^*||\gamma_a J_a\rangle \times \\ &\quad \frac{\langle \gamma_a J_a||T^{(k)*}||\gamma_{n'} J_{n'}\rangle}{E_{n'} - E_{\gamma_a J_a}} \frac{\langle \gamma_n J_n||T^{(k)}||\gamma_b J_b\rangle}{E_n - E_{\gamma_b J_b}} \begin{Bmatrix} J_b & F_b & I \\ F_a & J_n & 1 \end{Bmatrix} \begin{Bmatrix} J_{n'} & F_a & I \\ F_b & J_b & 1 \end{Bmatrix} \times \\ &\quad \begin{Bmatrix} I & I & k \\ J_{n'} & J_b & F_a \end{Bmatrix} \begin{Bmatrix} I & I & k \\ J_a & J_n & F_a \end{Bmatrix}. \end{aligned} \tag{4.20}$$

In the case of $J_a = J_b = 0$ the 6-j symbols reduce to

$$\begin{Bmatrix} 0 & F_b & I \\ F_a & J_n & 1 \end{Bmatrix} = \begin{Bmatrix} F_a & J_n & I \\ 0 & F_b & 1 \end{Bmatrix} = \frac{\delta_{J_n 1}\delta_{F_b I}}{\sqrt{3[I]}}, \tag{4.21}$$

$$\begin{Bmatrix} J_{n'} & F_a & I \\ F_b & 0 & 1 \end{Bmatrix} = \frac{\delta_{J_{n'} 1}\delta_{F_b I}}{\sqrt{3[I]}} \tag{4.22}$$

After summing over J_n and $J_{n'}$ we applied the condition $J_n = J_{n'} = 1$ so that

$$\begin{Bmatrix} I & I & k \\ 1 & 0 & F_a \end{Bmatrix} \begin{Bmatrix} I & I & k \\ 0 & 1 & F_a \end{Bmatrix} = \frac{\delta_{k1}\delta_{F_a I}}{3[I]}. \tag{4.23}$$

Thus, the second direct term simplifies to

$$\sum_{F_a F_b} |M^1_{ab}|^2 = \frac{\langle I||M^{(1)}||I\rangle^2}{9} \left| \sum_{\gamma_n} \langle \gamma_b 0||D||\gamma_n 1\rangle \frac{\langle \gamma_n 1||T^{(1)}||\gamma_a 0\rangle}{E_n - E_{\gamma_a 0}} \right|^2. \tag{4.24}$$

Following a similar procedure the third direct term $\sum_{F_a F_b} |M^2_{ab}|^2$ is given by

$$\sum_{F_a F_b} |M^2_{ab}|^2 = \frac{\langle I||M^{(1)}||I\rangle^2}{9} \left| \sum_{\gamma_n} \frac{\langle \gamma_b 0||T^{(1)}||\gamma_n 1\rangle}{E_n - E_{\gamma_b 0}} \langle \gamma_n 1||D||\gamma_a 0\rangle \right|^2. \tag{4.25}$$

4.3.1.2 The Interference Terms

The first interference terms $\sum_{F_aF_b} M^{0*}_{ab}M^{1}_{ab} + h.c.$ are given by

$$\begin{aligned}\sum_{F_aF_b} M^{0*}_{ab}M^{1}_{ab} + \sum_{F_aF_b} M^{1*}_{ab}M^{0}_{ab} &= \sum_{F_aF_b}\sum_{\substack{\gamma_n J_n \\ k}} (-1)^{J_a+J_b+J_n+2F_a+F_b+3I}[F_a][F_b]\langle I||M^{(k)}||I\rangle^2 \times \\ &\langle\gamma_a J_a||D^*||\gamma_b J_b\rangle\langle\gamma_b J_b||D||\gamma_n J_n\rangle\frac{\langle\gamma_n J_n||T^{(k)}||\gamma_a J_a\rangle}{E_n - E_{\gamma_a J_a}} \times \\ &\begin{Bmatrix} J_a & F_a & I \\ F_b & J_b & 1 \end{Bmatrix}\begin{Bmatrix} J_b & F_b & I \\ F_a & J_n & 1 \end{Bmatrix}\begin{Bmatrix} I & I & k \\ J_a & J_n & F_a \end{Bmatrix} + [a \leftrightarrow b],\end{aligned} \tag{4.26}$$

where the second term in the previous equation refers to the term similar to the first term with index a and b interchanged. These terms are non zero in general, however when $J_a = J_b = 0$, the first 6-j symbol in Eq. (4.26) does not satisfy the triangular inequality $\{J_aJ_b1\}$ so these terms are zero. Similarly, the second interference terms $\sum_{F_aF_b} M^{0*}_{ab}M^{2}_{ab} + h.c.$ for the case where initial and final total angular momentum are zero also vanish

$$\sum_{F_aF_b} M^{0*}_{ab}M^{2}_{ab} + \sum_{F_aF_b} M^{2*}_{ab}M^{0}_{ab} = 0. \tag{4.27}$$

The third interference terms $\sum_{F_aF_b} M^{1*}_{ab}M^{2}_{ab} + h.c.$ are given by

$$\begin{aligned}\sum_{F_aF_b} M^{1*}_{ab}M^{2}_{ab} + \sum_{F_aF_b} M^{2*}_{ab}M^{1}_{ab} &= \sum_{F_aF_b}\sum_{\substack{\gamma_n J_n \\ \gamma_{n'} J_{n'} \\ k}} (-1)^{J_a+J_b+J_n+J_{n'}+2F_a+2F_b}[F_a][F_b]\langle I||M^{(k)}||I\rangle^2 \times \\ &\frac{\langle\gamma_a J_a||T^{(k)*}||\gamma_n J_n\rangle}{E_n - E_{\gamma_a J_a}}\langle\gamma_n J_n||D^*||\gamma_b J_b\rangle\frac{\langle\gamma_b J_b||T^{(k)}||\gamma_{n'} J_{n'}\rangle}{E_{n'} - E_{\gamma_b J_b}} \times \\ &\begin{Bmatrix} I & I & k \\ J_n & J_a & F_a \end{Bmatrix}\begin{Bmatrix} J_n & F_n & I \\ F_b & J_b & 1 \end{Bmatrix}\begin{Bmatrix} I & I & k \\ J_{n'} & J_b & F_b \end{Bmatrix}\begin{Bmatrix} J_{n'} & F_{n'} & I \\ F_a & J_a & 1 \end{Bmatrix} + [a \leftrightarrow b]\end{aligned} \tag{4.28}$$

The second term in the previous equation is equal to the first one since it is symmetric under the interchange of $a \leftrightarrow b$. Next, if $J_a = J_b = 0$ the 6-j symbols reduce to

$$\begin{Bmatrix} I & I & k \\ J_n & 0 & F_a \end{Bmatrix} \begin{Bmatrix} J_n & F_n & I \\ F_b & 0 & 1 \end{Bmatrix} \begin{Bmatrix} I & I & k \\ J_{n'} & 0 & F_b \end{Bmatrix} \begin{Bmatrix} J_{n'} & F_{n'} & I \\ F_a & 0 & 1 \end{Bmatrix}$$
$$= \frac{\delta_{F_a I}\delta_{J_n k}}{\sqrt{[I][k]}} \frac{\delta_{F_b I}\delta_{J_n 1}}{\sqrt{[I][J_n]}} \frac{\delta_{F_b I}\delta_{J_{n'} k}}{\sqrt{[I][k]}} \frac{\delta_{F_a I}\delta_{J_{n'} 1}}{\sqrt{[I][J_{n'}]}}$$
$$= \frac{1}{9[I]^2}\delta_{F_a I}\delta_{J_n k}\delta_{F_b I}\delta_{J_n 1}\delta_{F_b I}\delta_{J_{n'} k}\delta_{F_a I}\delta_{J_{n'} 1}. \qquad (4.29)$$

Therefore after summation over the quantum numbers the interference terms reduce to

$$\sum_{F_a F_b} M^{1*}_{ab} M^{2}_{ab} + \sum_{F_a F_b} M^{2*}_{ab} M^{1}_{ab} = \frac{2\langle I||M^{(1)}||I\rangle^2}{9} \sum_{\gamma_n \gamma_{n'}} \frac{\langle \gamma_a 0||T^{(1)*}||\gamma_n 1\rangle}{E_n - E_{\gamma_a 0}} \langle \gamma_n 1||D^*||\gamma_b 0\rangle \times$$
$$\frac{\langle \gamma_b 0||T^{(1)}||\gamma_{n'} 1\rangle}{E_{n'} - E_{\gamma_b 0}} \langle \gamma_{n'} 1||D||\gamma_a 0\rangle. \qquad (4.30)$$

With all the non zero terms taken care of, the transition rate is now given by

$$A_{a\to b} = \frac{4\alpha^3}{3}\omega^3_{ab}\frac{1}{[J_a][I]} \sum_{F_a F_b} \left(|M^0_{ab}|^2 + |M^1_{ab}|^2 + |M^2_{ab}|^2 + 2M^{1*}_{ab}M^2_{ab}\right), \qquad (4.31)$$

To check the quality of our method, we first calculate the hyperfine constant A of ^{25}Mg, ^{87}Sr and ^{113}Cd. The monopole nuclear moment matrix element is given in Table 4.11 and the hyperfine constant A in Table 4.12. Our result differs by 0.2-7.4% from the experimental measurements; these differences are more prominent in the heavier atoms. The results in [40] agree slightly better with the experiment with only 0.5-1% difference. In [40], CI+MBPT is used with theoretical energies semiempirically shifted toward the experimental spectrum.

We give the breakdown of the hyperfine quenching terms M^1_{ab} and M^2_{ab} in Table 4.13 and 4.14 respectively. The initial and final state, $|\gamma_a 0\rangle$ and $|\gamma_b 0\rangle$, are the states that correspond to the clock transition of each atom. They are $3s^2\,{}^1S_0 - 3s3p\,{}^3P_0$ for Mg, $5s^2\,{}^1S_0 - 5s5p\,{}^3P_0$ for Sr and $5s^2\,{}^1S_0 - 5s5p\,{}^3P_0$ for Cd. For our calculation, we only consider the first three to four dominant contributions to the hyperfine quenching rate.

Table 4.11: The values of the monopole nuclear moment matrix element for ^{25}Mg, ^{87}Sr and ^{113}Cd. These values are calculated using Eq. (4.11) with the given nuclear spin I and nuclear magnetic moment in the unit of nuclear magneton μ/μ_N taken from [90].

Isotope	I	μ/μ_N	$\langle I\|\|M^{(1)}\|\|I\rangle$
^{25}Mg	5/2	-0.85546	-2.479
^{87}Sr	9/2	-1.093	-3.821
^{113}Cd	1/2	-0.6217	-1.523

Table 4.12: The values of diagonal even parity matrix elements , the hyperfine constants A and their comparison with other theoretical and experimental results are given in MHz.

state	$\langle\gamma J\|T^{(1)}\|\gamma J\rangle$ (MHz)	A (MHz)	th. [40][a] (MHz)	exp. (MHz)
		^{25}Mg		
3s3p $^3P_0$	421.25	-144.15	-146.1	-144.977(5) [105]
3s3p $^3P_3$	374.75	-128.23	-129.7	-128.445(5) [105]
		^{87}Sr		
5s5p $^3P_0$	1111.40	-269.95	-258.7	-260.083(5) [106]
5s5p $^3P_3$	920.48	-223.57	-211.4	-212.765(1) [106]
		^{113}Cd		
5s5p $^3P_0$	3226.10	-4011.33	-	-4123.813(1) [107]
5s5p $^3P_3$	2572.20	-3198.27	-	-3444.634(2) [107]

Table 4.13: Contributions of the excited states $|\gamma_n 1\rangle$ to M^1_{ab} hyperfine quenching term of Mg, Sr and Cd. $|\gamma_a 0\rangle$ and $|\gamma_b 0\rangle$ refer to the initial and final states respectively. The dipole matrix element is given in a.u., even parity electronic coupling operator in Mhz and energy difference in Mhz. The final term that contributes to the hyperfine quenching term M^1_{ab} is given in the last column.

$\|\gamma_n 1\rangle$	$\langle\gamma_b 0\|\|D\|\|\gamma_n 1\rangle$ (a.u.)	$\langle\gamma_n 1\|\|T^{(1)}\|\|\gamma_a 0\rangle$ (MHz)	$E_n - E_{\gamma_a 0}$ (MHz)	$\langle\gamma_b 0\|\|D\|\|\gamma_n 1\rangle \frac{\langle\gamma_n 1\|\|T^{(1)}\|\|\gamma_a 0\rangle}{E_n - E_{\gamma_a 0}}$ (a.u.)
		Mg		
$3s3p\,^3P_1$	-0.006	-828	6.452×10^5	7.760×10^{-6}
$3s3p\,^1P_1$	-4.029	-654	3.958×10^8	6.661×10^{-6}
$3s4p\,^3P_1$	0.001	-108	7.789×10^8	-8.693×10^{-11}
$3s4p\,^1P_1$	0.842	70	8.240×10^8	7.129×10^{-8}
		Sr		
$5s5p\,^3P_1$	-0.158	2059	5.653×10^6	5.741×10^{-5}
$5s5p\,^1P_1$	-5.272	-1451	2.182×10^8	3.506×10^{-5}
$5p^2\,^3P_1$	0.035	-414	5.852×10^8	-2.470×10^{-8}
$4d5p\,^3P_1$	-0.283	111	5.924×10^8	-5.304×10^{-8}
		Cd		
$5s5p\,^3P_1$	-0.159	6045	1.598×10^7	-5.998×10^{-5}
$5s5p\,^1P_1$	-3.440	-4260	3.978×10^8	-3.684×10^{-5}
$5s6p\,^3P_1$	0.013	-563	8.422×10^8	8.611×10^{-9}
$5s7p\,^3P_1$	-0.688	517	8.853×10^8	-4.013×10^{-7}

Table 4.14: Contributions of the excited states $|\gamma_n 1\rangle$ to M^2_{ab} hyperfine quenching term of Mg, Sr and Cd. $|\gamma_a 0\rangle$ and $|\gamma_b 0\rangle$ refer to the initial and final states respectively. The dipole matrix element is given in a.u., even parity electronic coupling operator in Mhz and energy difference in Mhz. The final term that contributes to the hyperfine quenching term M^1_{ab} is given in the last column.

$\|\gamma_n 1\rangle$	$\langle\gamma_b 0\|\|T^{(1)}\|\|\gamma_n 1\rangle$ (MHz)	$\langle\gamma_n 1\|\|D\|\|\gamma_a 0\rangle$ (a.u.)	$E_n - E_{\gamma_b 0}$ (MHz)	$\langle\gamma_a 0\|\|D\|\|\gamma_n 1\rangle \frac{\langle\gamma_n 1\|\|T^{(1)}\|\|\gamma_b 0\rangle}{E_n - E_{\gamma_b 0}}$ (a.u.)
		Mg		
$3s4s\,^3S_1$	-805	-1.531	1.235×10^9	9.979×10^{-7}
$3s3d\,^3D_1$	-3	-2.802	1.437×10^9	5.614×10^{-9}
$3s5s\,^3S_1$	426	-0.418	1.555×10^9	1.144×10^{-7}
		Sr		
$5s4d\,^3D_1$	-183	2.713	5.494×10^8	-9.050×10^{-7}
$5s6s\,^3S_1$	2088	-1.970	8.759×10^8	-4.697×10^{-6}
$5s5d\,^3D_1$	56	2.460	1.055×10^8	1.300×10^{-7}
		Cd		
$5s6s\,^3S_1$	-4610	-1.491	1.546×10^9	4.445×10^{-6}
$5s5d\,^3D_1$	-3	-2.316	1.784×10^9	3.798×10^{-9}
$5s7s\,^3S_1$	-2419	-0.433	1.876×10^9	5.582×10^{-7}
$5s6d\,^3D_1$	-2	-1.061	1.960×10^9	9.769×10^{10}

Table 4.15: Hyperfine quenching rate of ^{25}Mg, ^{87}Sr and ^{113}Cd in s^{-1}. The results from other works are given as comparison.

Isotope	$A^{\mathrm{hq}}_{a\to b}$	Other work
^{25}Mg	4.30×10^{-4}	4.44×10^{-4} [40]
		4.2×10^{-4} [42]
^{87}Sr	9.70×10^{-3}	7.58×10^{-3} [40]
		6.3×10^{-3} [41]
^{113}Cd	7.70×10^{-2}	

Note that in general M^1_{ab} term is larger by at least an order of magnitude compared to M^2_{ab} since M^2_{ab} has a greater suppression factor from the energy denominator.

Our final values of the hyperfine quenching rate values of ^{25}Mg, ^{87}Sr and ^{113}Mg are given in Table 4.15. Comparing with previously calculated results, our results for ^{25}Mg are in good agreement with only 2-3% difference. However, the results for ^{87}Sr differs by 24-43%. Note that even though the calculation in [40] omitted the M^2_{ab} term, the calculation was done by solving an inhomogeneous equation similar to the method explained in chapter 2 thus they include the contribution from all possible excited states. This additional contribution might be more significant in heavier atoms. Our final value of ^{113}Cd hyperfine quenching rate is 7.70×10^{-2} s^{-1}.

Chapter 5

CALCULATION FOR THE SEARCH OF NEW PHYSICS BEYOND THE STANDARD MODEL

In this chapter we carry out the calculation of the atomic properties of Ra and the parity non-conserving (PNC) amplitude of Cs and Fr. Ra is currently being used as the system to test the possibility of non zero electric dipole moment (EDM). The PNC amplitude is used to study the weak interaction and nuclear anapole moment in atoms.

5.1 Atomic properties of Ra for future EDM measurement

In this section we briefly review and provide the formulas for the lifetime, polarizability and the hyperfine constant.

5.1.1 Lifetime

The lifetime is calculated as an inverse of the total transition rate A_{ab} from state a to all possible lower states b

$$\tau_a = \frac{1}{\sum_{b \geq a} A_{ab}}. \tag{5.1}$$

For our calculation we only consider $E1$ transition, in this case the transition rate is given by [6]

$$A_{ab} = \frac{4\alpha}{3}\omega_{ab}^3 \frac{1}{(2J_a+1)} |\langle a||D||b\rangle|^2 = \frac{2.02613 \times 10^{18}}{\lambda^3} \frac{|\langle a||D||b\rangle|1^2}{(2J_a+1)} s^{-1}, \tag{5.2}$$

where $\omega_{ab} = E_a - E_b$, J_a is total angular momentum of state $|a\rangle$, D is the electric dipole operator and λ is the transition wavelength in Å.

5.1.2 Scalar and tensor polarizability

An atomic system immersed in an electric field will have its energy corrected by the Stark shift. The shift can be calculated using the perturbation theory assuming the electric field E as the the perturbation. The first order of perturbation to energy vanishes due to parity conservation while the second order energy correction of state $|J_v, M_{J_v}\rangle$ is given by [108]

$$\Delta W_{J_v M_{J_v}} = -\frac{1}{2} e^2 E^2 \left[\alpha_v^{(0)} + \frac{3M_{J_v}^2 - J_v(J_v+1)}{J_v(2J_v-1)} \alpha_v^{(2)} \right], \tag{5.3}$$

where e is the electron charge, J_v the total angular momentum and its projection M_{J_v}. We define the scalar and tensor polarizability, $\alpha_v^{(0)}$ and $\alpha_v^{(2)}$, as

$$\alpha_v^{(0)} = \frac{2}{3(2J_v+1)} \sum_{v \neq n} \frac{|\langle v||D||n\rangle|^2}{E_n - E_v}, \tag{5.4}$$

$$\alpha_v^{(2)} = \sqrt{\frac{40J_v(2J_v-1)}{3(2J_v+3)(J_v+1)(2J_v+1)}} \sum_{v \neq n} (-1)^{J_v+J_n} \begin{Bmatrix} J_v & 1 & J_n \\ 1 & J_v & 2 \end{Bmatrix} \frac{|\langle v||D||n\rangle|^2}{E_n - E_v}. \tag{5.5}$$

In general, the transition matrix element used in the polarizability is a position matrix element $\langle J_v||\vec{r}||J_n\rangle$. In our calculation, we use the multipole expansion of the operator $\vec{r}$ and take its leading term which is an $E1$ operator.

5.1.3 Hyperfine constant

The hyperfine correction is a small correction in the atomic spectrum due to the interactions between the electrons and the nucleus electric and magnetic moments. The two dominant terms for this correction are due to the electric dipole and the magnetic quadrupole moments. Assuming an atomic angular momentum state $|J, M_J\rangle$ and nuclear angular momentum state $|I, M_I\rangle$ so that the total angular momentum is $\mathbf{F} = \mathbf{I} + \mathbf{J}$, the hyperfine correction to the energy is given by [6, 109]

$$W_F = \frac{1}{2} KA + \frac{1}{2} \frac{3K(K+1) - 4J(J+1)I(I+1)}{2I(2I-1)2J(2J-1)} B, \tag{5.6}$$

Table 5.1: The theoretical and experimental energies of the Ra states in cm^{-1} measured from the ground state. The theoretical energy calculated using CI+all-order is given in column "CI+all" and the experimental energy taken from [90] is given in column "Expt."

State	CI+all	Expt.	State	CI+all	Expt.	State	CI+all	Expt.
$7s^2\,^1S_0$	0	0	$7s7d\,^3D_2$	32332	31993	$6d7p\,^1F_3$	34854	
$6d7s\,^3D_1$	14015	13716	$7s7d\,^3D_3$	32504	32197	$6d7p\,^3P_2$	35033	34383
$6d7s\,^3D_2$	14306	13994	$7s9s\,^1S_0$	34518		$7s8p\,^3P_0$	31163	31563
$6d7s\,^3D_3$	15047	14707	$7s9s\,^3S_1$	34712	34475	$7s8p\,^3P_1$	31396	31086
$6d7s\,^1D_2$	17531	17081	$7s7p\,^3P_0$	13440	13078	$7s8p\,^1F_3$	32232	31874
$7s8s\,^3S_1$	27021	26754	$7s7p\,^3P_1$	14338	13999	$7s8p\,^3P_2$	32652	32857
$7s8s\,^1S_0$	28204		$7s7p\,^3P_2$	17077	16689	$7s5f\,^3F_2$	35476	35256
$6d^2\,^3F_2$	30101		$7s7p\,^1P_1$	20971	20716	$7s5f\,^3F_3$	35484	35268
$6d^2\,^3P_0$	30459		$6d7p\,^3F_2$	28764	28038	$7s5f\,^3F_4$	35511	35294
$6d^2\,^3F_3$	30885		$6d7p\,^3F_3$	30913	30118	$7s5f\,^1F_3$	36513	
$6d^2\,^1D_2$	31429		$6d7p\,^1D_2$	31553	30918	$7s9p\,^1P_1$	36351	
$6d^2\,^3F_4$	31654		$6d7p\,^3D_1$	31942	32230	$7s6f\,^3F_2$	38154	
$6d^2\,^1S_0$	35737		$6d7p\,^3D_2$	33110	32507	$7s6f\,^3F_3$	38157	37922
$7p^2\,^3P_1$	31972	31249	$6d7p\,^3F_4$	33822	32368	$7s6f\,^3F_4$	38162	37930
$7p^2\,^1D_2$	32664	32215	$6d7p\,^3D_3$	34396	33197	$7s7f\,^3F_2$	39722	
$7p^2\,^3P_2$	33670	32941	$6d7p\,^3P_0$	34396	33782	$7s7f\,^3F_3$	39726	39361
$7s7d\,^3D_1$	32312	32001	$6d7p\,^3P_1$	34406	33824	$7s7f\,^3F_4$	39732	39367

where $K = F(F+1) - I(I+1) - J(J+1)$ and the constants A and B are given by

$$A = \frac{\mu}{IJ}\langle JJ|T_0^1|JJ\rangle, \tag{5.7}$$

$$B = 2Q\langle JJ|T_0^2|JJ\rangle. \tag{5.8}$$

Here, T_q^k is an irreducible tensor of rank k, μ is the nuclear magnetic moment and Q is the nuclear quadrupole moment.

The calculations are carried out in the CI+all-order formalism. The calculated energies and their comparison with the experimental values are given in Table 5.1 in cm^{-1}. These energies are measured from the ground state $7s^2\,^1S_0$. Compared to the currently known experimental values, our theoretical results differ by 1-4%.

Table 5.2: Lifetimes of Ra states.

State	Lifetime	State	Lifetime	State	Lifetime	State	Lifetime
$7s7p\,^3P_1$	392 ns	$6d^2\,^3F_4$	0.76 s	$7s5f\,^3F_3$	20.8 ns	$7s10s\,^3S_1$	91.2 ns
$7s7p\,^3P_2$	5.45 μs	$6d^2\,^1D_2$	167 ns	$7s5f\,^3F_4$	18.2 ns	$7s10s\,^3S_0$	77.0 ns
$7s7p\,^1P_1$	5.61 ns	$6d^2\,^3P_0$	20.1 ns	$7s5f\,^1F_3$	30.0 ns	$7s10p\,^1P_1$	21.1 ns
$7s6d\,^3D_1$	651 μs	$6d^2\,^1G_4$	6.56 μs	$7s6f\,^3F_3$	36.6 ns	$7s10p\,^3P_0$	652 ns
$7s6d\,^1D_2$	505 μs	$6d^2\,^1S_0$	159 ns	$7s6f\,^3F_4$	34.6 ns	$7s10p\,^3P_1$	275 ns
$7s8s\,^3S_1$	18.1 ns	$7s8p\,^3P_0$	74.2 ns	$7s6f\,^3F_2$	35.5 ns	$7s10p\,^3P_2$	287 ns
$7s8s\,^1S_0$	61.0 ns	$7s8p\,^3P_1$	30.7 ns	$7s6f\,^1F_3$	35.1 ns	$7s9d\,^1D_2$	109 ns
$6d7p\,^3F_2$	30.8 ns	$7s8p\,^3P_2$	49.4 ns	$7s7f\,^3F_3$	43.6 ns	$7s9d\,^3D_1$	57.3 ns
$6d7p\,^3F_3$	26.6 ns	$7s8p\,^1P_1$	16.3 ns	$7s7f\,^3F_4$	41.3 ns	$7s9d\,^3D_2$	72.4 ns
$6d7p\,^3F_4$	23.5 ns	$7p^2\,^3P_0$	5.48 ns	$7s7f\,^3F_2$	41.6 ns	$7s9d\,^3D_3$	66.0 ns
$6d7p\,^1D_2$	19.8 ns	$7p^2\,^3P_1$	27.9 ns	$7s8f\,^3F_2$	372 ns	$7s10d\,^3D_3$	65.3 ns
$6d7p\,^3D_1$	29.6 ns	$7p^2\,^3P_2$	46.2 ns	$7s8f\,^3F_4$	17.7 ns	$7s10d\,^3D_1$	5.15 ns
$6d7p\,^3D_2$	12.8 ns	$7p^2\,^1D_2$	29.2 ns	$7s9p\,^1P_1$	44.5 ns	$7s10d\,^3D_2$	54.2 ns
$6d7p\,^3D_3$	24.7 ns	$7p^2\,^3P_1$	33.0 ns	$7s9p\,^3P_0$	179 ns		
$6d7p\,^3P_0$	10.2 ns	$7s7d\,^3D_1$	18.9 ns	$7s9p\,^3P_1$	152 ns		
$6d7p\,^3P_1$	10.3 ns	$7s7d\,^3D_2$	18.7 ns	$7s9p\,^3P_2$	115 ns		
$6d7p\,^3P_2$	10.6 ns	$7s7d\,^3D_3$	20.9 ns	$7s8d\,^1D_2$	46.2 ns		
$6d7p\,^1F_3$	19.0 ns	$7s7d\,^3D_1$	48.2 ns	$7s8d\,^3D_1$	34.7 ns		
$6d^2\,^3F_2$	1.52 μs	$7s7d\,^3D_1$	29.3 ns	$7s8d\,^3D_2$	49.8 ns		
$6d^2\,^3F_3$	40.7 μs	$7s5f\,^3F_2$	21.7 ns	$7s8d\,^3D_3$	38.8 ns		

We give the the lifetimes and the polarizabilities in Tables 5.2 and 5.3 respectively. Currently the latest Ra lifetime measurements show 422 ± 20 ns for the $7s7p\,^3P_1$ state [110] and 385 ± 45 μs for the $7s6d\,^1D_2$ state [111]. Comparing these measurements with our calculated values we got 7% difference $7s7p\,^3P_1$ lifetime and 27% difference for for $7s6d\,^1D_2$ lifetime. We note that the $E1$ operator in the matrix element used to calculate the lifetimes contains only the second order and random phase approximation (RPA) term so we can expect some uncertainty coming from higher order terms. As for the polarizability, there is currently no known experimental measurement or other theoretical calculation for comparison.

The hyperfine structure constants for ^{223}Ra isotope are given in Table 5.4. These

Table 5.3: Scalar and tensor polarizabilities of Ra few low-lying states in a_0^3. The scalar polarizabilities are given in column $\alpha_v^{(0)}$ and tensor polarizabilities in $\alpha_v^{(2)}$.

State	$\alpha_v^{(0)}$	$\alpha_v^{(2)}$	State	$\alpha_v^{(0)}$	$\alpha_v^{(2)}$
$7s^2\,{}^1S_0$	246.37		$7s6d\,{}^3D_1$	651.7	1229
$7s7p\,{}^3P_0$	2233		$7s6d\,{}^3D_2$	102000	-101711
$7s7p\,{}^3P_1$	-170600	16421	$7s6d\,{}^1D_2$	241.7	-21.95
$7s7p\,{}^3P_2$	-346	-5.75	$7s6d\,{}^3D_3$	625.7	-438.4
$7s^2\,{}^1P_1$	241	-88.3			

values are calculated using the total nuclear spin $I = 3/2$ and nuclear gyromagnetic ratio $\mu = 0.713$ [112]. Both the electric dipole constant A and the magnetic quadrupole constant B are given along with previously measured values taken from [113]. We can see that our theoretical results differ by 7-16% when compared to the experimental measurements. By similar argument as before, these differences might result from the higher order terms of the matrix element operator.

As a summary, we have briefly reviewed the theory of lifetime, atomic polarizabilities, and hyperfine structure. The calculation of these properties is carried out for ^{223}Ra using the CI+all-order formalism. These results will be helpful for the development of Ra EDM search experiment.

5.2 Parity violations in Cs and Fr

The parity violating effects in atomic transitions come from the weak interactions between the quarks in nucleons and the electron or between the electron and other electrons. The latter effect is small and will not be discussed in this work. The weak interaction is based on the vector-axial vector (V-A) interaction. Therefore, for nucleon-electron interaction, there can be two types of terms in general, nucleon vector current term with electron axial vector current or electron vector current with nucleon axial vector current term. The main difference between these two types of terms is

Table 5.4: Hyperfine constants of ^{223}Ra few low lying states in MHz with $I = 3/2$ and $\mu = 0.713$ [112]. The hyperfine constants A and B are given in their corresponding column, known measurement from experiment [113] are given in column "Expt.".

Level	A	Expt.	B	Expt.
$7s6d\,^3D_1$	-654		119	
$7s6d\,^3D_2$	399		206	
$7s6d\,^3D_3$	441		327	
$7s6d\,^1D_2$	-188		429	
$7s7p\,^3P_1$	1346	1202.1	-431	-470.2
$7s7p\,^3P_2$	799	699.9	643	688.5
$7s7p\,^1P_1$	-404	-344.5	471	421.5

their dependency on the nuclear spin. For this reason, the first type of term is called the (nuclear) spin-independent term and the second type of term is called the (nuclear) spin-dependent term.

The spin independent Hamiltonian is given by [114, 115]

$$H^{\text{si}} = \frac{G}{2\sqrt{2}}\gamma_5 Q_W \rho_N(r), \tag{5.9}$$

where G is the Fermi coupling constant, Q_W weak charge, and $\rho_N(r)$ neutron density. γ_5 is defined by $\gamma_5 = i\gamma_0\gamma_1\gamma_2\gamma_3\gamma_4$ where γ_μ is the Dirac matrices. In the standard model, the weak charge is given by

$$Q_W = -N + Z(1 - 4s^2) \approx -N, \tag{5.10}$$

where $s^2 = \sin^2\theta_W \approx 1/4$ with θ_W the weak mixing angle.

There are three contributions to the spin dependent PNC hamiltonian. The first contribution comes from the nucleon, this arises when the nucleus has one unpaired nucleon. For this interaction, the hamiltonian is given by [114, 115]

$$H^{\text{sd}}_{(1)} = -\frac{G}{\sqrt{2}}\kappa_n \alpha \cdot \mathbf{I}\rho_N(r), \tag{5.11}$$

with a coupling constant κ_n. This coupling constant has been calculated in the extreme shell model [116] which give $\kappa_n(^{133}\mathrm{Cs}) = 0.0151$ and $\kappa_n(^{133}\mathrm{Cs}) = 0.0124$. The second contribution comes from the anapole moment, this is a toroidal moment that exist due to the weak interaction in nuclei first predicted in [117, 118]. The spin dependent hamiltonian due to anapole moment is given by [114, 115]

$$H^{\mathrm{sd}}_{(2)} = \frac{G}{\sqrt{2}}\kappa_a \alpha \cdot \mathbf{I}\rho_N(r), \tag{5.12}$$

where the anapole coupling constant κ_a depends on the weak processes in the nucleus [119]. The theoretical estimate of the anapole moment coupling constant gives $\kappa_n(^{133}\mathrm{Cs}) = 0.063 - 0.084$ while the experimental measurement gives $\kappa_n(^{133}\mathrm{Cs}) = 0.09(2)$ [120, 64].The third source of the spin dependent term arises from the perturbation of hyperfine nuclear interaction to the spin independent term, this term is given by [114, 115]

$$H^{\mathrm{sd}}_{(3)} = \frac{G}{\sqrt{2}}\kappa_{\mathrm{hi}} \alpha \cdot \mathbf{I}\rho_N(r). \tag{5.13}$$

The coupling constant κ_{hi} has been calculated in [121], the result for ^{133}Cs and ^{205}Tl are $\kappa_{\mathrm{hi}}(^{133}\mathrm{Cs})$=0.0078 and $\kappa_{\mathrm{hi}}(^{205}\mathrm{Tl})$=0.044. Combining all the three sources, the total spin dependent hamiltonian is given by

$$H^{(\mathrm{sd})} = \frac{G}{\sqrt{2}}\kappa \alpha \cdot \mathbf{I}\rho_N(r), \tag{5.14}$$

where

$$\kappa = \kappa_n + \kappa_a + \kappa_{\mathrm{hi}} \tag{5.15}$$

As a summary, evaluation of the spin independent term enable a precise determination of weak charge Q_W and evaluation of the spin dependent term enable an accurate determination of constant κ from which weak nuclear forces can be derived.

5.2.1 PNC amplitude

In the PNC atomic experiment, the ratio of highly forbidden dipole transition $E1_{\mathrm{PNC}}$ to its tensor transition probability β, $\mathrm{Im}(E1_{\mathrm{PNC}})/\beta$, is measured for two different total angular momentum $\mathbf{F} = \mathbf{I} + \mathbf{J}$. By knowing the transition probability β, the

different contributions from the spin-independent amplitude and the spin dependent amplitude can then be extracted from the two results. The spin-independent amplitude is extracted by taking the average of the two ratios, and the spin dependent amplitude is extracted from their difference. To illustrate this, in the Cs PNC experiment the Boulder group has measured $\mathrm{Im}(E1_{\mathrm{PNC}})/\beta = -1.6349(80)$ mV/cm for $6s_{F=4}$ to $7s_{F=3}$ and $\mathrm{Im}(E1_{\mathrm{PNC}})/\beta = -1.5576(77)$ mV/cm for $6s_{F=4}$ to $7s_{F=3}$ [60]. From these results, the difference is 0.077(11) mV/cm, and the average is 1.5935(56) mV/cm. Comparing the average of these results with the theoretical spin independent amplitude, Porsev et al. [62] extracted the weak charge and obtained $Q_W = -73.16(29)_{\mathrm{exp}}(20)_{\mathrm{th}}$ which is in perfect agreement with the result from the standard model.

We now discuss the calculation of the PNC spin independent and spin dependent amplitude.

5.2.1.1 Spin independent amplitude

The transition matrix element from Eq. (5.9) is given by

$$\langle a|H^{\mathrm{si}}|b\rangle = -i\frac{G}{\sqrt{8}}Q_W\delta_{-\kappa_a,\kappa_b}\delta_{m_a,m_b}\int_0^\infty dr\rho(r)(-g_af_b + f_ag_b), \tag{5.16}$$

where f and g are the large and small components or the radial Dirac wavefunction respectively. Note that the violation of parity is imposed by the Kronecker delta.

The spin independent PNC amplitude is given by

$$E^{\mathrm{si}}_{\mathrm{PNC}} = \langle n's|D|ns\rangle. \tag{5.17}$$

The state $|ns\rangle$ and $|n's\rangle$ can mix with other states through the weak interaction which results in nonzero amplitude for this transition. Using sum over states method, the spin independent amplitude can be written as [114, 115]

$$E^{\mathrm{si}}_{\mathrm{PNC}} = \sum_m \frac{\langle n's|D|mp_{1/2}\rangle\langle mp_{1/2}|H^{\mathrm{si}}|ns\rangle}{E_{ns} - E_{mp_{1/2}}} + \sum_m \frac{\langle n's|H^{\mathrm{si}}|mp_{1/2}\rangle\langle mp_{1/2}|D|ns\rangle}{E_{n's} - E_{mp_{1/2}}}, \tag{5.18}$$

or using the reduced matrix element (see appendix A for a review on the angular momentum diagram)

$$E_{\rm PNC}^{\rm si} = \; - \begin{array}{c} j'm'_j \\ \uparrow \\ \hline \\ jm_j \end{array} 10 \sum_m \left\{ \frac{\langle n's||D||mp_{1/2}\rangle\langle mp_{1/2}||H^{\rm si}||ns\rangle}{E_{ns} - E_{mp_{1/2}}} + \frac{\langle n's||H^{\rm si}||mp_{1/2}\rangle\langle mp_{1/2}||D||ns\rangle}{E_{n's} - E_{mp_{1/2}}} \right\}, \tag{5.19}$$

the initial and final total angular momentum is $j = j' = \frac{1}{2}$ and by convention the PNC amplitude is defined with $m_j = m_{j'} = \frac{1}{2}$ which gives

$$E_{\rm PNC}^{\rm si} = \frac{1}{\sqrt{6}} \sum_m \left\{ \frac{\langle n's||D||mp_{1/2}\rangle\langle mp_{1/2}||H^{\rm si}||ns\rangle}{E_{ns} - E_{mp_{1/2}}} + \frac{\langle n's||H^{\rm si}||mp_{1/2}\rangle\langle mp_{1/2}||D||ns\rangle}{E_{n's} - E_{mp_{1/2}}} \right\}. \tag{5.20}$$

5.2.1.2 Spin dependent amplitude

In general, the spin dependent amplitude depends on the total nuclear spin $F = J + I$

$$E_{\rm PNC}^{\rm sd} = \langle n's, F'M_{F'}|D|ns, FM_F\rangle. \tag{5.21}$$

Using sum over states method as before, the spin dependent amplitude is given by

$$\langle n's, F'M_{F'}|D|ns, FM_F\rangle = \sum_m \left\{ \frac{\langle n's, F'M_{F'}|D|m\rangle\langle m|H^{\rm sd}|ns, FM_F\rangle}{E_{ns} - E_m} + \frac{\langle n's, F'M_{F'}|H^{\rm sd}|m\rangle\langle m|D|ns, FM_F\rangle}{E_{n's} - E_m} \right\}. \tag{5.22}$$

In order to express this amplitude in reduced matrix element form we need to expand the hyperfine states $|FM\rangle$ and carry out the summation over the magnetic angular momentum. The hyperfine states can be expanded in term of electron angular state

$|sm_s\rangle$ and the the nuclear spin state $|I\mu\rangle$ using the angular momentum diagram (see appendix A)

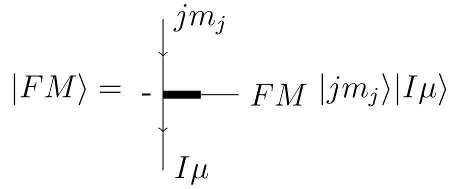

(5.23)

We first expand the spin dependent hamiltonian Eq. (5.14) in the spherical basis

$$H^{\text{sd}} = \sum_{\lambda} (-1)^{\lambda} I_{-\lambda} h^{\text{sd}}_{\lambda}, \tag{5.24}$$

so the amplitude can be reduced to

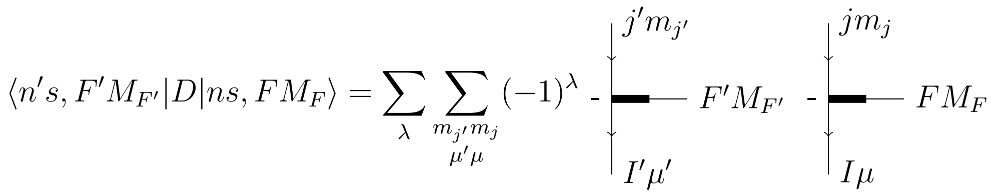

$$\times \sum_n \left\{ \frac{1}{E_{ns} - E_n} \langle j'm_{j'}|D|j_n m_n\rangle \langle j_n m_n|h^{\text{sd}}_{\lambda}|jm\rangle \langle I\mu_n|I_{-\lambda}|I\mu\rangle \delta(\mu', \mu_n) \right.$$
$$\left. + \frac{1}{E_{n's} - E_n} \langle j'm_{j'}|h^{\text{sd}}_{\lambda}|j_n m_n\rangle \langle j_n m_n|D|jm\rangle \langle I\mu'|I_{-\lambda}|I\mu_n\rangle \delta(\mu_n, \mu) \right\}$$

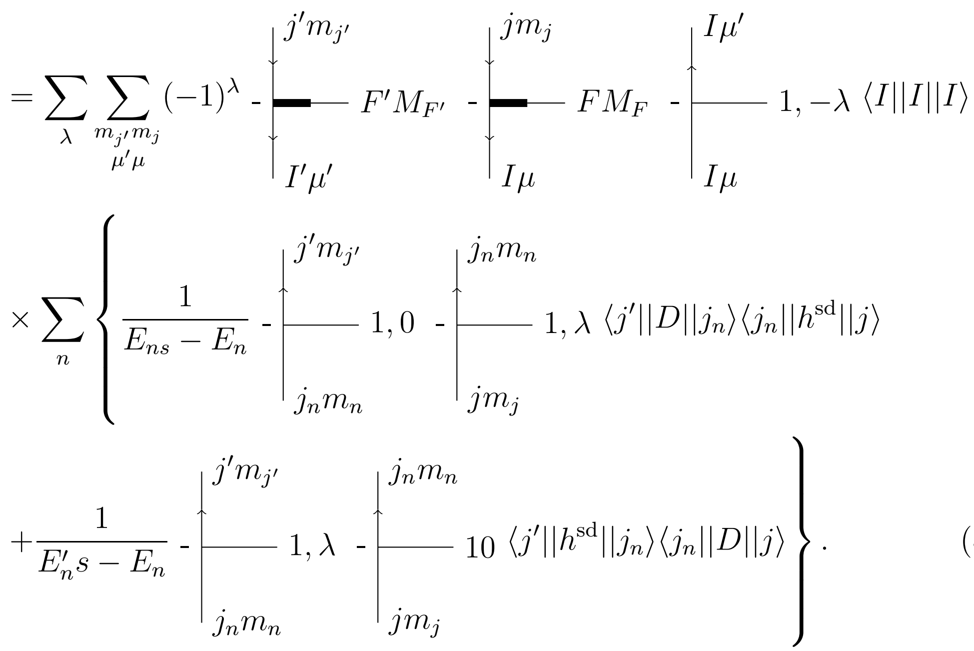

(5.25)

Now, since

$$\langle I||I||I\rangle = \sqrt{I(I+1)(2I+1)}, \tag{5.26}$$

and

$$(-1)^{\lambda}$$ 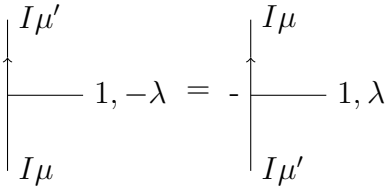 (5.27)

we obtain, after summing over the magnetic quantum number

$$\langle n's, F'M_{F'}|D|ns, FM_F\rangle = $$ 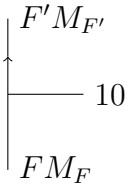

$$\times \sqrt{(2F+1)(2F+1)}\sqrt{I(I+1)(2I+1)}$$
$$\times \sum_n \left\{ (-1)^{j-j'+1} \begin{Bmatrix} F' & F & 1 \\ j_n & j' & I \end{Bmatrix} \begin{Bmatrix} I & j_n & F \\ j & I & 1 \end{Bmatrix} \frac{\langle j'||D||j_n\rangle\langle j_n||h^{\rm sd}||j\rangle}{E_{ns}-E_n} \right.$$
$$\left. +(-1)^{F-F'+1} \begin{Bmatrix} F' & F & 1 \\ j_n & j' & I \end{Bmatrix} \begin{Bmatrix} I & j_n & F \\ j' & I & 1 \end{Bmatrix} \frac{\langle j'||h^{\rm sd}||j_n\rangle\langle j_n||D||j\rangle}{E_{n's}-E_n} \right\}. \quad (5.28)$$

Note that the reduced matrix element $\langle n's, F'||D||ns, F\rangle$ is given by the second, third and fourth line of the previous equation.

The reduced matrix element $\langle a||h^{\rm sd}||b\rangle$ in Eq. (5.28) is given by

$$\langle a||h^{\rm sd}||b\rangle = i\frac{G_F}{\sqrt{2}}\kappa \int_0^\infty dr \rho_N(r)(f_a g_b \langle -\kappa_a||\sigma||\kappa_b\rangle - f_b g_a \langle \kappa_a||\sigma||-\kappa_b\rangle), \quad (5.29)$$

where

$$\langle -\kappa_a||\sigma||\kappa_b\rangle = (-1)^{j_a+l_b-1/2}\sqrt{6[j_a][j_b]} \begin{Bmatrix} j_a & j_b & 1 \\ 1/2 & 1/2 & l_b \end{Bmatrix} \delta(l_b\bar{l}_a) \quad (5.30)$$

$$\langle \kappa_a||\sigma||-\kappa_b\rangle = (-1)^{j_a+l_a-1/2}\sqrt{6[j_a][j_b]} \begin{Bmatrix} j_a & j_b & 1 \\ 1/2 & 1/2 & l_a \end{Bmatrix} \delta(l_a\bar{l}_b) \quad (5.31)$$

and

$$\bar{l} = l(-\kappa). \quad (5.32)$$

In our work, we calculate the spin independent, spin dependent amplitude and matrix elements using all order method.

Table 5.5: Absolute values of the spin-dependent PNC reduced matrix elements for $6s - 7s$ transition in Cs calculated using different approximations. DF-lowest order Dirac Fock, RPA and all-order

$F_F - F_I$	DF	RPA	all-order
3 - 4	5.481[-12]	7.299[-12]	7.798[-12]
4 - 3	4.746[-12]	6.432[-12]	7.080[-12]

In Table 5.5 we show the result of spin dependent reduced matrix element of Cs $6s - 7s$ transition with $F = 3$ ($F' = 4$) and $F = 4$ ($F' = 3$). We calculate the matrix elements using three different approximations, relativistic Dirac-Hartree-Fock (DHF), DHF plus RPA and all-order. Our value of anapole coupling constant is $\kappa_a = 0.88$ which is 5% lower than the value used in [64]. We find that with more inclusion of the correlation corrections, the individual PNC matrix elements significantly change, however the shift in the total spin-dependent PNC amplitude is relatively small.

In Table 5.6 we show the transition contribution to the total spin independent PNC amplitude and reduced matrix element spin dependent for $7s - 8s$ transition in ^{210}Fr calculated using various approximations. Depending on the electronic state n, we separate the contributions into three categories: from the main term ($n = 7 - 25$), core ($n = 2 - 6$), and the tail ($n = 26 - 70$). The core and tail contributions are calculated using DHF with RPA and the main contributions using the all order method. We use four different variants of the all order: SD, SDpT, SDsc, and SDpTsc. The SDsc/SDpTsc refer to the SD/SDpT methods with empirical energy scaling. For the main contributions, the final values and accuracies are taken by evaluating the four all order results. For the core and tail contributions, the RPA value is taken as the final value with the difference between DF and RPA values taken as the uncertainty. We find that the core and tail give less than 1% contribution to the total spin independent amplitude whereas they give slightly more contribution of about 12% to the total spin dependent amplitude.

Table 5.6: Spin-independent PNC amplitude $E1_{\rm PNC}$ (in $10^{-11}i|e|a_0(-Q_W/N)$ and reduced matrix elements $\langle 8sF_F||z||7sF_I\rangle$ of the spin-dependent PNC amplitude in a.u. divided by κ for $7s-8s$ transition in ^{210}Fr calculated using various approximations.

^{210}Fr	$E1_{\rm PNC}$	SD-PNC:$\langle 8sF_F\|\|z\|\|7sF_I\rangle$	
		$F_I=4$, $F_F=5$	$F_I=5$, $F_F=4$
Main term $n=7-25$			
DF	12.50	7.15	-8.00
RPA	14.62	9.83	-10.76
All-order SD	14.39	9.86	-10.80
All-order SDpT	14.47	9.66	-10.60
All-order SDsc	14.30	9.39	-10.32
All-order SDpTsc	14.39	9.47	-10.40
Final	14.39(9)	9.60(47)	-10.53(48)
Core $n=2-6$			
DF	-0.03	-0.23	0.30
RPA	-0.06	-0.93	0.93
Final	-0.06(2)	-0.93(35)	0.93(35)
Tail $n=26-70$			
DF	-0.03	0.06	-0.06
RPA	-0.04	0.29	-0.29
Final	-0.04(1)	0.29(23)	-0.29(23)
Total	14.29(10)	8.96(62)	-9.88(62)

Table 5.7: Comparison of the spin-independent PNC amplitude, in $10^{-11}i|a_0|a_0(-Q_W/N)$ for the $7s - 8s$ transition in ^{210}Fr with other results.

	Present	Ref. [122]	Ref. [124]	Ref. [123]
^{223}Fr	15.70(10)	15.90(16)	15.41(17)	15.72
^{210}Fr	14.29(10)		14.02(15)	14.34

Finally, we summarize our results of the ^{223}Fr and ^{210}Fr spin-independent amplitude and compare them with other theoretical results in Table 5.7. We found that our results agree within theoretical uncertainty with the results from [122] and [123].

Chapter 6

SPECIFIC MASS SHIFT CALCULATIONS OF Na, K, AND Rb

The atomic nucleus is far heavier than the electrons. Therefore it is a common approximation to assume an infinite nucleus mass to simplify the calculation of an atomic system. A finite nuclear mass will induce a small correction in the atom electronic spectrum. This correction is referred as the isotope shift.

Isotope shift consists of two main terms, mass shift and field shift. Mass shift arises from the nuclear recoil and field shift arises from the finite size of the nuclear charge distribution. Mass shift is further divided into 2 parts, normal mass shift (NMS) $-(1/2M)\sum_i p_i^2$ and specific mass shift (SMS) $(1/2M)\sum_{i\neq j}\mathbf{p}_i\cdot\mathbf{p}_j$. While the former can be evaluated accurately, it is hard to do the same with the latter. Field shift is obtained from the operator $\delta V/\delta\langle r^2\rangle$ where V is the nuclear potential and $\langle r^2\rangle$ is the mean-square radius of the nucleus.

6.1 Method

We will now derive the formulation for the NMS and SMS. The Hamiltonian for a single valence system with N electrons and atomic mass M_A is given by

$$H(\vec{r_0},\vec{r_i},\vec{p_0},\vec{p_i}) = \frac{p_0^2}{2M_A} + \sum_i \frac{p_i^2}{2m_e} + \sum_i V_{e-N}(\vec{r_i}-\vec{r_0}) + \frac{1}{2}\sum_{i\neq j} V_{e-e}(\vec{r_i}-\vec{r_j}), \quad (6.1)$$

Where $i = 1, ..., N$, the index i is for the electron and 0 for the nucleus. If we do the following coordinate transformation

$$\vec{\rho_i} = \vec{r_i} - \vec{r_0}, \quad (6.2)$$

$$\vec{R} = \frac{M_A\vec{r_0} + m_e\sum_i \vec{r_i}}{M_T}, \quad (6.3)$$

with $M_T = M_A + Nm_e$, Eq. (6.1) can be rewritten as

$$H(\vec{\rho}_i, \vec{\pi}_i) = \sum_i \frac{\pi_i^2}{2\mu} + \sum_i V_{e-N}(\vec{\rho}_i) + \frac{1}{2}\sum_{i\neq j} V_{e-e}(\vec{\rho}_i - \vec{\rho}_j) + \frac{1}{2M_A}\sum_{i\neq j} \vec{\pi}_i \cdot \vec{\pi}_j. \tag{6.4}$$

In the Eq. (6.4), $\vec{\pi}_i$ is the generalized conjugate momentum of $\vec{\rho}_i$ and μ is the reduced mass given by

$$\mu = \frac{M_A m_e}{M_A + m_e}. \tag{6.5}$$

The first and fourth terms in Eq. (6.4) are the corrections that arise from using finite nuclear mass as opposed to using infinite one.

The first term of Eq. (6.4) will create a *normal mass shift* (NMS), it scales the Rydberg constant by the ratio μ/m_e so the shift is given by

$$\delta E_{NMS} = E_\mu - E_{m_e} = \left(\frac{\mu}{m_e} - 1\right) E_{m_e} = -\frac{m_e}{M_A + m_e} E_{m_e} = -\frac{m_e}{M_A} E_\mu. \tag{6.6}$$

Here, E_{m_e} is the energy calculated using the infinite nuclear mass assumption and E_μ is the energy obtained without one. We may use Eq. (6.6) to evaluate the normal mass shift by replacing E_μ with experimental energy to obtain an accurate approximation to the normal mass shift.

The fourth term of Eq. (6.4) contributes to what is referred as *specific mass shift* (SMS)

$$\delta E_{SMS} = \frac{1}{2M_A} \left\langle \sum_{i\neq j} \vec{\pi}_i \cdot \vec{\pi_j} \right\rangle. \tag{6.7}$$

We commonly calculate the matrix element using the infite nuclear mass assumption, therefore we need to scale the above expression. Since momentum is directly proportional to mass so that $\vec{p}_i \propto m_e$ and $\vec{\pi}_i \propto \mu$ then we can relate both momentum by $\vec{p}_i = \mu\vec{\pi}_i/m_e$. Therefore Eq. (6.7) can be written as

$$\delta E_{SMS} = \frac{1}{2M_A}\left(\frac{\mu}{m_e}\right)^2 \left\langle \sum_{i\neq j} \vec{p}_i \cdot \vec{p}_j \right\rangle = \frac{M_A}{2(M_A + m_e)^2} \left\langle \sum_{i\neq j} \vec{p}_i \cdot \vec{p}_j \right\rangle. \tag{6.8}$$

Hence we can obtain the specific mass shift by multiplying the transition matrix element $\langle ij|\frac{1}{2}\sum_{i\neq j} \vec{p}_i \cdot \vec{p}_j|kl\rangle$ with $\frac{M_A}{(M_A + m_e)^2}$.

In the second quantization, the SMS operator $P = \frac{1}{2}\sum_{i\neq j}\vec{p}_i\cdot\vec{p}_j$ can be expressed as a sum of one-partice operator S and two-particle operator T

$$\begin{aligned} P &= S+T \\ &= \sum_{ij} t_{ij} : a_i^\dagger a_j : + \frac{1}{2}\sum_{ijkl} t_{ijkl} : a_i^\dagger a_j^\dagger a_l a_k :, \end{aligned} \tag{6.9}$$

where $t_{ijkl} = \langle ij|\mathbf{p}_1\cdot\mathbf{p}_2|kl\rangle$ and $t_{ij} = -\sum_a t_{iaaj}$. In the angular momentum basis, the operator t_{ijkl} can be decomposed as

$$t_{ijkl} = \sum_\lambda (-1)^\lambda \langle i|p_\lambda|k\rangle\langle j|p_{-\lambda}|l\rangle. \tag{6.10}$$

This can be expressed diagrammatically as

$\langle ij|\mathbf{p}_1\cdot\mathbf{p}_2|kl\rangle =$ 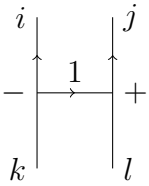 $+\, T_1(ijkl),$ (6.11)

where the term $T_1(ijkl)$ is given by

$$T_1(ijkl) = -\langle \kappa_i \parallel C_1 \parallel \kappa_k\rangle\langle \kappa_j \parallel C_1 \parallel \kappa_l\rangle P(ik)P(jl). \tag{6.12}$$

Here, κ is the relativistic total angular momentum, $\langle \kappa_i \parallel C_1 \parallel \kappa_j\rangle$ is the reduced matrix element of a normalized spherical harmonic operator given by

$$\langle \kappa_i||C_1||\kappa_j\rangle = (-1)^{j_i+1/2}\sqrt{(2j_i+1)(2j_j+1)}\begin{pmatrix} j_j & j_i & 1 \\ -1/2 & 1/2 & 0\end{pmatrix}\Pi(l_j+l_i+1), \tag{6.13}$$

$$\Pi(l) = \begin{cases} 1, \text{if } l \text{ is even} \\ 0, \text{if } l \text{ is odd}\end{cases}, \tag{6.14}$$

and $P(ij)$ is the radial matrix element of the momentum operator given by

$$P(ba) = -im_e c\int_0^\infty dr\left[(\kappa_b-\kappa_a-1)g_b(r)f_a(r) + (\kappa_b-\kappa_a+1)f_b(r)g_a(r)\right]. \tag{6.15}$$

In Eq. (6.15), $f_a(r)$ and $g_a(r)$ are the small and large radial components of the Dirac wavefunction respectively.

The calculation of the specific mass shift operators S and T in the third order MBPT formalism has been done in [71]. This was done by replacing the Coulomb matrix elements $(V_{HF} - U)_{ij}$ with $(V_{HF} - U)_{ij} + t_{ij}$ and g_{ijkl} with $g_{ijkl} + t_{ijkl}$ in the first-, second- and third-order energy [1]. Here, we calculate for the first time the SMS operator within the framework of all-order formalism. The complete one- and two-body matrix elements used to calculate this operator are given in chapter 2.

6.2 Results

Since the all-order two-body operator is being tested for the first time in this calculation, it is important to evaluate its performance by comparing them with the results obtained earlier using the third order MBPT.

First, we were checking the convergence behavior of the SD all-order two-body terms by calculating the terms from Eq. (2.86)-(2.109) for the $3s$ state of Na. In the calculation of Na, $3s$ energy level using SD all-order, eight iterations were required to reach convergence. We calculated the two-body terms for every iteration 1 to 8 to check their convergence. The results are shown in Table 6.1 where each column represents the values of each term after every iteration and the total T are given in the last row. We can see that most of the terms converge in 2 to 4 iterations except for $T^{(b)}, T^{(c)}, T^{(o)}, T^{(p)}, T^{(u)}, T^{(v)}$ and $T^{(w)}$ terms which require about 6 iteration to converge. We can also see that the final value of T are dominated by $T^{(b)}, T^{(c)}, T^{(p)}, T^{(v)}$ and $T^{(w)}$ terms. Thus the two-body terms converged within the energy convergence range.

It is worth noting that the combined terms $T^{(b)}$ and $T^{(c)}$ at zeroth iteration are equal to the second order two-particle SMS matrix element $T^{(2)}$ [71]. This is because at the zeroth iteration the double excitation coefficient recovers the Coulomb matrix elements which in turns give the exact formula of the two-particle SMS matrix element $T^{(2)}$. We can also see that term $T^{(p)}$ makes a significant jump from the zeroth to the first iteration. This term starts to pick up fourth order term in their first iteration, considering that they contribute to about 10% from the total SMS constant,

Table 6.1: Contributions to the SD all-order two particle operator SMS constant after every all-order iteration iteration in GHz amu for Na $3s$ state. The two body terms in the first column are given in Eqs. (2.86)-(2.109).

iteration	0	1	2	3	4	5	6	7	8
$T^{(a)}$	0.00	0.00	0.00	0.00	0.00	0.00	0.00	0.00	0.00
$T^{(b)}$	27.21	26.10	25.96	25.98	25.98	25.97	25.98	25.99	25.99
$T^{(c)}$	67.83	79.25	77.11	77.62	77.30	77.29	77.27	77.26	77.26
$T^{(d)}$	0.00	-0.01	-0.01	-0.01	-0.01	-0.01	-0.01	-0.01	-0.01
$T^{(e)}$	0.00	0.27	0.27	0.32	0.32	0.32	0.33	0.33	0.33
$T^{(f)}$	0.00	0.00	0.00	0.00	0.00	0.00	0.00	0.00	0.00
$T^{(g)}$	0.00	-0.05	-0.05	-0.05	-0.06	-0.06	-0.06	-0.06	-0.06
$T^{(h)}$	0.00	-0.01	-0.01	-0.01	-0.01	-0.01	-0.01	-0.01	-0.01
$T^{(i)}$	0.00	0.10	0.13	0.14	0.15	0.15	0.15	0.15	0.15
$T^{(j)}$	0.00	0.02	0.04	0.05	0.05	0.05	0.05	0.05	0.05
$T^{(k)}$	0.00	0.09	0.12	0.13	0.13	0.13	0.13	0.13	0.13
$T^{(l)}$	0.00	0.73	0.83	0.91	0.93	0.93	0.94	0.94	0.94
$T^{(m)}$	0.00	-0.02	-0.05	-0.06	-0.06	-0.06	-0.06	-0.06	-0.06
$T^{(n)}$	0.00	-0.15	-0.15	-0.15	-0.16	-0.16	-0.16	-0.16	-0.16
$T^{(o)}$	0.00	1.52	1.52	1.66	1.67	1.69	1.69	1.69	1.69
$T^{(p)}$	0.00	14.15	14.72	16.24	16.39	16.59	16.59	16.59	16.59
$T^{(q)}$	0.33	0.63	0.64	0.66	0.66	0.66	0.66	0.66	0.66
$T^{(r)}$	1.45	1.55	1.62	1.63	1.63	1.63	1.64	1.64	1.64
$T^{(s)}$	-0.16	-0.13	-0.14	-0.14	-0.14	-0.14	-0.14	-0.14	-0.14
$T^{(t)}$	4.96	5.61	6.18	6.30	6.36	6.38	6.39	6.39	6.39
$T^{(u)}$	0.72	0.41	-0.08	-0.14	-0.19	-0.21	-0.21	-0.21	-0.21
$T^{(v)}$	-33.84	-36.38	-39.34	-39.82	-40.12	-40.22	-40.23	-40.23	-40.23
$T^{(w)}$	43.71	48.09	53.40	54.18	54.70	54.87	54.87	54.87	54.87
$T^{(x)}$	1.64	1.62	1.66	1.66	1.66	1.66	1.66	1.66	1.66
total	113.85	143.39	144.37	147.10	147.18	147.45	147.47	147.47	147.47

this shows the importance of high order terms in the calculation of two particle SMS matrix element.

Next we make term by term comparisons between the SD all-order and MBPT two body terms. At the zeroth iteration, Eqs. (2.102-2.109) recover the third order two-particle SMS matrix elements. Furthermore at the first iteration, the core double and core valence excitation coefficients are given by

$$\begin{aligned}(\epsilon_{ab}-\epsilon_{mn})\rho_{mnab} &= g_{mnab}+\sum_{cd}\frac{g_{cdab}g_{mncd}}{\epsilon_{cd}-\epsilon_{mn}}+\sum_{rs}\frac{g_{mnrs}g_{rsab}}{\epsilon_{ab}-\epsilon_{rs}}+\left[\sum_{rc}\frac{\tilde{g}_{cnrb}\tilde{g}_{mrac}}{\epsilon_{ac}-\epsilon_{mr}}\right] \\ &\quad +\begin{bmatrix} a\leftrightarrow b \\ m\leftrightarrow n\end{bmatrix}, \qquad (6.16)\end{aligned}$$

$$\begin{aligned}(\epsilon_{vb}-\epsilon_{mn}+\delta E_v)\rho_{mnvb} &= g_{mnvb}+\sum_{cd}\frac{g_{cdvb}g_{mncd}}{\epsilon_{cd}-\epsilon_{mn}}+\sum_{rs}\frac{g_{mnrs}g_{rsvb}}{\epsilon_{vb}-\epsilon_{rs}}+\left[\sum_{rc}\frac{\tilde{g}_{cnrb}\tilde{g}_{mrvc}}{\epsilon_{vc}-\epsilon_{mr}}\right] \\ &\quad +\begin{bmatrix} v\leftrightarrow b \\ m\leftrightarrow n\end{bmatrix}. \qquad (6.17)\end{aligned}$$

Therefore, ignoring δE_v, the second, third, fourth and fifth terms in the previous equations will recover the third order two-particle SMS matrix elements when plugged to Eqs. (2.87) and (2.88).

We list the nonzero SD two particle SMS terms and their MBPT counterpart in Table 6.2. The first column is the valence two-particle SD matrix element and the second column is the corresponding terms from MBPT equation given in appendix B. By comparing with the total third order two-particle terms, we can see that the SD terms only cover 21 out of 36 total third order terms. Thus there are 15 missing terms in the SD equation in the third order.

We show the values of the third-order missing terms and compare them with $T^{(SD)}$ values for Na, K and Rb states in Table 6.3. The row labeled $T^{(SD)}$ shows the values of $T^{(SD)}$, the row labelled "missing terms" shows the values of third order missing terms and the row labeled (%) shows the percentage of the missing terms and the $T^{(SD)}$. We can see that the missing terms contribute to about 15-165% of the total

Table 6.2: List of equivalent two particle matrix elements between SD and third order MBPT [71]. The values in the second column refer to the terms from the second and third order MBPT approach given in appendix B.

SD	MBPT
	zeroth iteration
$T^{(q)}$	(B.70)
$T^{(r)}$	(B.79)
$T^{(s)}$	(B.76)
$T^{(t)}$	(B.58)
$T^{(u)}$	(B.64)
$T^{(v)}$	(B.61)
$T^{(w)}$	(B.67)+(B.73)
$T^{(x)}$	(B.52)+(B.82)
	first iteration
$T^{(b)}$	(B.49)+(B.71)+(B.72)+(B.74)+(B.80)+(B.81)+(B.83)
$T^{(c)}$	(B.50)+(B.65)+(B.66)+(B.68)+(B.77)+(B.84)+(B.86)

two-particle matrix element, these give significant errors to the SD calculation when excluded.

We give the breakdown on isotope shift contribution for Na, K and Rb in different approaches in Tables 6.4, 6.5 and 6.6 respectively. The one-particle SMS matrix elements obtained using SD and SDpT method are given in $S^{(\mathrm{SD})}$ and $S^{(\mathrm{SDpT})}$ respectively. $T^{(2)}$ and $T^{(3)}$ give the second and third order MBPT two-particle matrix elements; $T^{(\mathrm{SD})}$ and $T^{(\mathrm{SDpT})}$ give the SD and SDpT two-particle matrix elements; the values in row labelled "miss." gives the missing third order terms and the sum of $T^{(\mathrm{SD})}$ and the missing terms are given in "$T^{(\mathrm{SDpT})}$+miss.". The total SMS matrix elements constants in HF, MBPT, SD and SDpT are given in $P^{(1)}$, $P^{(\mathrm{MBPT})}$, $P^{(\mathrm{SD})}$ and $P^{(\mathrm{SDpT})}$ respectively. We also add the missing terms to the total SDpT isotope shift and put the results in the row labeled "$P^{(\mathrm{SDpT})}$+miss.".

We can see from comparing the results of SD and SDpT one- and two-body matrix elements that there is less than 5% difference for the lower states s and p. The

Table 6.3: Comparison between the $T^{(SD)}$ and the missing third order terms for Na and K states in GHz amu.

			Na		
	$3s$	$3p_{1/2}$	$3p_{3/2}$	$3d_{3/2}$	$3d_{5/2}$
$T^{(SD)}$	146.6	42.9	42.7	1.2	1.2
missing terms	-53.2	-16.0	-15.9	-1.9	-1.9
Δ (%)	36.3	37.3	37.2	162.6	162.7
			K		
	$4s$	$4p_{1/2}$	$4p_{3/2}$	$3d_{3/2}$	$3d_{5/2}$
$T^{(SD)}$	232.3	69.8	68.9	93.6	93.3
missing terms	-97.0	-35.1	-34.7	-15.8	-15.8
Δ (%)	41.8	50.2	50.4	16.9	16.9
			Rb		
	$5s$	$5p_{1/2}$	$5p_{3/2}$	$4d_{3/2}$	$4d_{5/2}$
$T^{(SD)}$	357.9	97.4	92.3	201.7	196.7
missing terms	-186.8	-62.8	-60.2	-39.2	-38.6
Δ (%)	52.2	64.5	65.2	19.4	19.6

higher d states show large difference, about 50-112% for the one-body and 9-20% for two-body matrix elements; these differences are more prominent in the heavier system K and Rb. The difference between the SD and SDpT total SMS matrix elements is less than 14%. A similar behavior can also be seen between the two-body SMS matrix elements of the third-order MBPT and SDpT+miss which differs by up to 20% for s and p states but up to 177% for the d states. The difference between the total SMS matrix elements of the third order MBPT and SDpT+miss. varies between 3-72%.

Experimental values of specific mass isotope shift constants has been extracted for Na in [125] and for K and Rb in [126]. In Table 6.7 we give the comparison between experiment and theoretical values. We list the values for the first order (HF), third order (MBPT) [71, 126], all-order (SD and SDpT) and the SD+missing MBPT terms. The transitional specific-mass isotope shift constants are obtained by substracting the values from the corresponding states which are $3p_{1/2} - 3s$ for Na, $4s - 4p_{1/2}$ for K and

Table 6.4: Contributions to specific-mass isotope-shift constants (GHz amu) for Na in different approaches.

	$3s$	$3p_{1/2}$	$3p_{3/2}$	$3d_{3/2}$	$3d_{5/2}$
$S^{(\mathrm{SD})}$	194.7	51.6	51.5	2.6	2.6
$S^{(\mathrm{SDpT})}$	205.2	51.6	51.5	2.8	2.8
$T^{(2)}$	95.0	28.2	28.1	-0.4	-0.4
$T^{(3)}$	-24.3	-7.5	-7.5	-0.5	-0.5
$T^{(2)} + T^{(3)}$	70.7	20.6	20.6	-0.9	-0.9
$T^{(\mathrm{SD})}$	146.9	43.2	43.1	1.1	1.1
$T^{(\mathrm{SDpT})}$	146.6	42.8	42.7	1.2	1.1
miss.	-53.2	-16.0	-15.9	-1.9	-1.9
$T^{(SDpT)}$ + miss.	93.4	26.8	27.2	-0.7	-0.8
$P^{(1)}$	-222.0	-115.6	-115.5	-4.8	-4.9
$P^{(\mathrm{MBPT})}$	53.9	-43.4	-43.4	-3.0	-3.0
$P^{(\mathrm{SD})}$	130.1	-20.8	-20.9	-1.0	-1.0
$P^{(\mathrm{SDpT})}$	119.3	-21.1	-21.3	-1.1	-1.1
$P^{(\mathrm{SDpT})}$+miss.	76.6	-37.2	-37.2	-2.7	-2.9

Table 6.5: Contributions to specific-mass isotope-shift constants (GHz amu) for K in different approaches.

	$4s$	$4p_{1/2}$	$4p_{3/2}$	$3d_{3/2}$	$3d_{5/2}$	$4d_{3/2}$	$4d_{5/2}$
$S^{(\mathrm{SD})}$	202.9	66.3	63.3	-47.9	-47.7	-32.1	-31.8
$S^{(\mathrm{SDpT})}$	202.9	66.3	66.0	-26.8	-26.7	-19.1	-18.9
$T^{(2)}$	143.2	35.8	35.5	19.0	19.1	14.4	14.4
$T^{(3)}$	-32.9	-8.2	-8.1	-13.3	-13.4	-8.9	-8.9
$T^{(2)} + T^{(3)}$	110.4	27.7	27.4	5.7	5.8	5.5	5.5
$T^{(\mathrm{SD})}$	232.2	69.8	68.9	93.6	93.3	60.6	60.3
$T^{(\mathrm{SDpT})}$	226.6	68.1	67.3	76.5	76.4	50.0	49.8
miss.	-97	-35.1	-34.7	-15.8	-15.8	-8.2	-8.2
$T^{(SDpT)}$ + miss.	129.6	33.0	32.6	60.7	60.6	41.8	41.6
$P^{(1)}$	-387.9	-118.7	-117.7	-113.8	-114.5	-74.8	-75.2
$P^{(\mathrm{MBPT})}$	-74.6	-24.8	-24.3	-134.8	-135.5	-88.4	-88.5
$P^{(\mathrm{SD})}$	47.2	17.4	14.5	-68.1	-68.9	-46.3	-46.6
$P^{(\mathrm{SDpT})}$	41.6	15.6	15.6	-64.0	-64.8	-43.9	-44.2
$P^{(\mathrm{SDpT})}$+miss.	-55.4	-19.4	-19.1	-79.9	-80.6	-52.1	-52.5

Table 6.6: Contributions to specific-mass isotope-shift constants (GHz amu) for Rb in different approaches.

	$5s$	$5p_{1/2}$	$5p_{3/2}$	$4d_{3/2}$	$4d_{5/2}$	$5d_{3/2}$	$5d_{5/2}$
$S^{(\mathrm{SD})}$	280.3	105.4	104.7	-42.6	-41.2	2.7	3.9
$S^{(\mathrm{SDpT})}$	289.4	107.4	106.3	-17.9	-17.1	9.6	10.5
$T^{(2)}$	220.1	46.6	44.2	42.0	42.5	28.6	28.7
$T^{(3)}$	-82.1	-18.8	-21.2	-34.2	-34.4	-21.2	-21.2
$T^{(2)} + T^{(3)}$	137.9	27.8	23.1	7.8	8.0	7.4	7.5
$T^{(\mathrm{SD})}$	357.9	97.4	92.3	201.7	196.7	85.3	82.3
$T^{(\mathrm{SDpT})}$	348.3	94.6	89.7	168.1	164.6	74.9	72.6
miss.	-186.8	-62.8	-60.2	-39.2	-38.6	-18.8	-18.4
$T^{(SDpT)}$ + miss.	161.5	31.8	29.5	128.9	126.0	56.1	54.2
$P^{(1)}$	-590.5	-150.7	-144.2	-218.5	-222.2	-132.7	-133.9
$P^{(\mathrm{MBPT})}$	-163.2	-15.6	-14.8	-228.6	-231.3	-115.7	-115.8
$P^{(\mathrm{SD})}$	47.7	52.1	52.7	-59.4	-66.7	-44.7	-47.6
$P^{(\mathrm{SDpT})}$	47.2	51.2	51.8	-68.3	-74.7	-48.1	-50.8
$P^{(\mathrm{SDpT})}$+miss.	-139.6	-11.5	-8.4	-107.5	-113.3	-67.0	-69.2

$5s - 5p_{3/2}$ for Rb. As can be seen, the final result of SDpT+miss total SMS isotope shift agrees by 3% for Na, but it disagrees for K and Rb. Our results differ with the previous third order MBPT result by 12-32%. We need to point out that the missing terms added to the SD results were calculated using HF energies instead of SD energies. A more accurate calculation can be made by improving the method that incorporate the missing terms inside the SD framework.

Table 6.7: Comparison of specific-mass isotope-shift constants for Na, K and Rb between experimental values and values from different approximation.

		Na	
	$3s$	$3p_{1/2}$	$3p_{1/2} - 3s$
HF	-222.0	-115.6	106.4
MBPT	53.9	-43.4	-97.3
SD	130.1	-20.8	-150.9
SDpT	119.3	-21.1	-140.4
SDpT+miss	76.6	-37.2	-113.8
expt.			-110.0
		K	
	$4s$	$4p_{1/2}$	$4s - 4p_{1/2}$
HF	-387.9	-118.7	-269.2
MBPT	-74.6	-24.8	-49.9
SD	47.2	17.4	29.9
SDpT	41.6	15.6	26.0
SDpT+miss	-55.4	-19.4	-36.0
expt.			-16.4
		Rb	
	$5s$	$5p_{1/2}$	$5s - 5p_{1/2}$
HF	-590.5	-144.2	-446.3
MBPT	-163.2	-14.8	-148.3
SD	47.7	52.7	-5.0
SDpT	47.2	51.8	-4.7
SDpT+miss	-139.6	-8.4	-131.2
expt.			-10.5

Chapter 7

CALCULATIONS OF ENERGIES, MATRIX ELEMENTS AND LIFETIMES OF HIGHLY CHARGED Mo AND Tc IONS

In this chapter, we calculate the properties of Mo and Tc ions. We determine the energies, transition matrix elements, and lifetimes of these ions. In order to determine the theoretical uncertainties we use multiple theoretical methods including the SD, SDpT, CI+MBPT and CI+all-order methods.

7.1 Results

We divide our calculations into two parts. In the first part, we show the results of Mo VI and Tc VII, which are monovalent systems. In the second part, we show the results of Mo VI and Tc VII, which are divalent systems. We provide the calculated results of the E1, M1 and E2 transition matrix elements. We obtain the transition rates for the corresponding transitions from the following formulas [6]

$$A_{ab}^{E1} = \frac{2.02613 \times 10^{18}}{\lambda^3} \frac{|Z_{E1}|^2}{[J_a]} \mathrm{s}^{-1}, \tag{7.1}$$

$$A_{ab}^{M1} = \frac{2.69735 \times 10^{13}}{\lambda^3} \frac{|Z_{M1}|^2}{[J_a]} \mathrm{s}^{-1}, \tag{7.2}$$

$$A_{ab}^{E2} = \frac{1.1198 \times 10^{18}}{\lambda^5} \frac{|Z_{E2}|^2}{[J_a]} \mathrm{s}^{-1}, \tag{7.3}$$

for transition from state $a \to b$. In the above formulas, Z is the reduced matrix element, J_a is the total angular momentum of state a and λ is the transition wavelength in Å. The lifetime τ in seconds can be obtained by taking the inverse sum of the transition rate to all possible final state

$$\tau_i = \frac{1}{\sum_j A_{ij}} \mathrm{s} \tag{7.4}$$

7.1.1 Mo VI and Tc VII

Mo VI and Tc VII have an equivalent electronic structure like Rb. Therefore, we can use SD and SDpT to calculate them by using the appropriate values for the nuclear parameters.

We show the theoretical results of the energies in Table 7.1 and the experimental values of Mo VI for comparison. We found for Mo VI, the SD values show agreed very well with the experiments with a difference of 0.0-0.7% excepts for $4d_{5/2}$ state which differ by 4.2%. The SDpT results of Mo VI give worse agreement with the experiments compared to the the SD results with a difference of 2.8-5.6%. If we take the SD results as the best estimate and using the difference between the SD and SDpT as the theoretical errors then the theoretical results agree within the uncertainty with the experimental results. For the Tc VII, we can use the SD results as the best estimate, and the 0.4-4.8% difference between the SD and SDpT results can be taken as the theoretical uncertainties.

We show the theoretical transition matrix elements and the lifetime of Mo VI in Table 7.2 and Tc VII in Table 7.3. We also show the resulting lifetimes calculated using the values of SD matrix elements. We calculated the transition matrix elements using both the SD and SDpT methods for comparison. We found for both case of Mo VI and Tc VII, that these transition matrix elements mostly agrees with 2-5% differences, except for the following transitions. First, the $M1$ transition of $5s_{1/2} - 4d_{3/2}$ which has about 10% difference between the SD and SDpT values. Second, the $E1$ transitions from $4d$ to $4f$ states which differ by 18-28% between the SD and SDpT values.

7.1.2 Mo V and Tc VI

Mo V and Tc VI have an equivalent electronic structure like Sr. Therefore, we can use CI+MBPT and CI+all-order to calculate them by using the appropriate values for the nuclear parameters.

We show the energies of several low lying states of Mo V in Table 7.4, and Tc VI in Table 7.5. For both Mo V and Tc VI, in general the calculated energies

Table 7.1: Energies of Mo VI and Tc VII ions in cm^{-1}. We give the values of the ground state energy in the first row of both Mo VI and Tc VII. We give the value of the energies of the other states relative to the ground state. The results of DHF, SD and SDpT methods are given in the columns as labeled. Experimental results are taken from [90].

Ion	Level	DHF	SD	SDpT	NIST
Mo VI	$4d_{3/2}$	542343	555043	564902	555127
	$4d_{5/2}$	2478	2700	2716	2584
	$5s_{1/2}$	115891	118920	126407	119726
	$5p_{1/2}$	176947	181770	189594	182404
	$5p_{3/2}$	181651	186792	194642	187331
	$4f_{5/2}$	272818	267135	274643	267047
	$4f_{7/2}$	272728	267449	275024	267457
	$5d_{3/2}$	275332	282565	290767	282826
	$5d_{5/2}$	276100	283380	291595	283611
Tc VII	$4d_{3/2}$	705148	718490	729100	
	$4d_{5/2}$	3326	3555	3569	
	$5s_{1/2}$	165429	168309	176368	
	$5p_{1/2}$	236031	240518	248892	
	$5p_{3/2}$	242272	247107	255510	
	$4f_{5/2}$	329554	314556	322739	
	$4f_{7/2}$	329461	315111	322739	
	$5d_{3/2}$	352662	359378	368149	
	$5d_{5/2}$	353715	360495	369282	

Table 7.2: Transition matrix elements of Mo VI and lifetimes calculated using SD and SDpT methods are given. The lifetimes correspond to the initial state of the transition. We calculated the lifetimes using the values of Z^{SD}.The numbers in brackets represent powers of 10.

Transition	Type	Z^{SD}	Z^{SDpT}	Lifetime
$4d_{5/2} - 4d_{3/2}$	E2	1.2886	1.2657	6.10 s
$4d_{5/2} - 4d_{3/2}$	M1	1.5489	1.5489	
$5s_{1/2} - 4d_{3/2}$	E2	2.3026	2.2363	6.27[-5] s
$5s_{1/2} - 4d_{3/2}$	M1	4.9534[-05]	5.5233[-05]	
$5s_{1/2} - 4d_{5/2}$	E2	2.8628	2.7823	
$5p_{1/2} - 4d_{3/2}$	E1	9.8934[-01]	9.4225[-01]	0.16 ns
$5p_{1/2} - 5s_{1/2}$	E1	1.7604	1.686	
$5p_{3/2} - 4d_{3/2}$	E1	4.3069[-01]	4.1086[-01]	0.14 ns
$5p_{3/2} - 4d_{5/2}$	E1	1.3157	1.2555	
$5p_{3/2} - 5s_{1/2}$	E1	2.4939	2.3899	
$4f_{5/2} - 4d_{3/2}$	E1	1.3207	1.0815	0.08 ns
$4f_{5/2} - 4d_{5/2}$	E1	3.5406[-01]	3.5406[-01]	
$4f_{7/2} - 4d_{5/2}$	E1	1.6395	1.3664	0.08 ns
$5d_{3/2} - 5p_{1/2}$	E1	2.7305	2.6586	0.22 ns
$5d_{3/2} - 5p_{3/2}$	E1	1.2499	1.2172	
$5d_{3/2} - 4f_{5/2}$	E1	2.8061	2.7315	
$5d_{5/2} - 5p_{3/2}$	E1	3.7424	3.6455	0.23 ns
$5d_{5/2} - 4f_{7/2}$	E1	3.3548	3.271	

Table 7.3: Transition matrix elements of Tc VII and lifetimes calculated using SD and SDpT methods are given. The lifetimes correspond to the initial state of the transition. The numbers in brackets represent powers of 10.

Transition	Type	Z^{SD}	Z^{SDpT}	Lifetime
$4d_{5/2} - 4d_{3/2}$	E2	1.0682	1.0539	2.06 s
$4d_{5/2} - 4d_{3/2}$	M1	1.5488	1.5488	
$5s_{1/2} - 4d_{3/2}$	E2	1.8505	1.8054	1.61[-5] s
$5s_{1/2} - 4d_{3/2}$	M1	5.0980[-05]	5.6155[-05]	
$5s_{1/2} - 4d_{5/2}$	E2	2.3033	2.2487	
$5p_{1/2} - 4d_{3/2}$	E1	8.5661[-01]	8.1950[-01]	0.09 ns
$5p_{1/2} - 5s_{1/2}$	E1	1.6132	1.5445	
$5p_{3/2} - 4d_{3/2}$	E1	3.7209[-01]	3.5680[-01]	0.08 ns
$5p_{3/2} - 4d_{5/2}$	E1	1.1383	1.0915	
$5p_{3/2} - 5s_{1/2}$	E1	2.2862	2.1902	
$4f_{5/2} - 4d_{3/2}$	E1	9.5650[-01]	7.1867[-01]	0.08 ns
$4f_{5/2} - 4d_{5/2}$	E1	2.5284[-01]	1.9086[-01]	
$4f_{7/2} - 4d_{5/2}$	E1	1.2136[+00]	9.4496[-01]	0.09 ns
$5d_{3/2} - 5p_{1/2}$	E1	2.4958	2.4245	0.16 ns
$5d_{3/2} - 5p_{3/2}$	E1	1.1422	1.11	
$5d_{3/2} - 4f_{5/2}$	E1	2.021	1.9769	
$5d_{5/2} - 5p_{3/2}$	E1	3.4211	3.3253	0.17 ns
$5d_{5/2} - 4f_{7/2}$	E1	2.4152	2.366	

of the $4d^2$ states are less accurate than the other states with 1-10% differences from the experimental values compared to the other states which differ by less than 1%. For Mo V, we found that the results of the CI+All order are slightly more accurate than the results of the CI+MBPT especially for $4d^2$ states which differ by 1-5% from the experimental values compared to the latter values which differ by 1-10% from the experimental values. For Tc VI, we found that less than 1% difference between the results of CI+All order and CI+MBPT for $4d5s$ and $4d5p$ states. However, similar to the results in Mo V we also found less agreements between the CI+All order and CI+MBPT for the $4d^2$ states where they differ by 3-34%.

We show the calculated translational matrix elements and the lifetime of Mo V in Tables 7.6, 7.7, and 7.8; and Tc VI in Tables 7.9, 7.10, and 7.11. We show the theoretical values of the translational matrix elements calculated using the CI+all-order method.

Table 7.4: Energies of Mo V ions relative to the ground state in cm^{-1}. The results of two different methods, CI+All-order and CI+MBPT, are given. Experimental energies [90] are given for comparisons.

Level	CI+All	CI+MBPT	NIST
$4d^2\ ^3F_2$	0	0	0
$4d^2\ ^3F_3$	1599.6	1600.9	1577.2
$4d^2\ ^3F_4$	3401.3	3428.7	3357.1
$4d^2\ ^1D_2$	10509.9	11300.1	10190.1
$4d^2\ ^3P_0$	11441.3	12109.9	11161.3
$4d^2\ ^3P_1$	12075.9	12758.5	11806.9
$4d^2\ ^3P_2$	13743.1	14459.1	13408.3
$4d^2\ ^1G_4$	17059.1	17357	16353.4
$4d^2\ ^1S_0$	39597.2	40657.8	37737.8
$4d5s\ ^3D_1$	92177.1	92790.8	92380.5
$4d5s\ ^3D_2$	92925.3	93544.8	93111.4
$4d5s\ ^3D_3$	94646.4	95287	94835.4
$4d5s\ ^1D_2$	99542.6	100159	99380.4
$4d5p\ ^1D^o_2$	147045.9	147935.1	146976.8
$4d5p\ ^3D^o_1$	148891.9	149710.5	148948.7
$4d5p\ ^3D^o_2$	150359.8	151219.7	150345.8
$4d5p\ ^3F^o_2$	151451.6	152297.6	151213.2
$4d5p\ ^3F^o_3$	151500.9	152345.1	151195.1
$4d5p\ ^3D^o_3$	153257.8	154099.2	153039.7
$4d5p\ ^3F^o_4$	155599.4	156463.5	155032.3
$4d5p\ ^3P^o_1$	156855.2	157896.4	156616.5
$4d5p\ ^3P^o_0$	157286.4	158343.7	157059.2
$4d5p\ ^3P^o_2$	158060.2	159133.8	157851.5
$4d5p\ ^1F^o_3$	160756.6	161469.3	159856.7
$4d5p\ ^1P^o_1$	162689.8	163691.2	162257.1

Table 7.5: Energies of Tc VI ions relative to the ground state in cm^{-1}. The results of two different methods, CI+All-order and CI+MBPT, are given. Experimental energies [90] are given for comparisons.

Level	CI+ALL	CI+MBPT
$4d^2\ ^3F_2$	0	0
$4d^2\ ^3F_3$	2246.0	2179.4
$4d^2\ ^3F_4$	4692.2	4605.5
$4d^2\ ^1D_2$	9738.8	12997.8
$4d^2\ ^3P_0$	12972.4	13606.7
$4d^2\ ^3P_1$	13832.8	14518.6
$4d^2\ ^3P_2$	15472.7	16958.6
$4d^2\ ^1G_4$	18436.3	19785.5
$4d^2\ ^1S_0$	45024.5	46388
$4d5s\ ^3D_1$	138543.4	139080.6
$4d5s\ ^3D_2$	139450.8	140002.3
$4d5s\ ^3D_3$	141806.9	142395.5
$4d5p\ ^1D^o_2$	202980.6	203806.6
$4d5p\ ^3D^o_1$	204860.5	205632.3
$4d5p\ ^3D^o_2$	206916.3	207767
$4d5p\ ^3F^o_2$	208350.2	209177.7
$4d5p\ ^3F^o_3$	208579.8	209380.3
$4d5p\ ^3D^o_3$	210815.9	211622.4
$4d5p\ ^3F^o_4$	213930.5	214792.4
$4d5p\ ^3P^o_1$	214602.3	215589.9
$4d5p\ ^3P^o_0$	215219.5	216222.2
$4d5p\ ^3P^o_2$	216267.2	217314.9
$4d5p\ ^1F^o_3$	219275.7	219743.6
$4d5p\ ^1P^o_1$	221892.2	222857

Table 7.6: Transition matrix elements of Mo V and lifetimes calculated using CI+All-order are given. The lifetimes correspond to the initial state of the transition. The numbers in brackets represent powers of 10.

Transition	Type	Z	Lifetime	Transition	Type	Z	Lifetime
$4d^2\ ^3F_3$-$4d^2\ ^3F_2$	M1	2.559	9.73 s	$4d^2\ ^1S_0$-$4d^2\ ^3F_2$	E2	0.2	0.05 s
$4d^2\ ^3F_3$-$4d^2\ ^3F_2$	E2	0.669		$4d^2\ ^1S_0$-$4d^2\ ^1D_2$	E2	2.204	
$4d^2\ ^3F_4$-$4d^2\ ^3F_2$	E2	0.073	8.53 s	$4d^2\ ^1S_0$-$4d^2\ ^3P_1$	M1	0.112	
$4d^2\ ^3F_4$-$4d^2\ ^3F_3$	M1	2.591		$4d^2\ ^1S_0$-$4d^2\ ^3P_2$	E2	1.369	
$4d^2\ ^3F_4$-$4d^2\ ^3F_3$	E2	0.655		$4d5s\ ^3D_1$-$4d^2\ ^3F_2$	M1	0	2.28[-04] s
$4d^2\ ^1D_2$-$4d^2\ ^3F_2$	M1	0.24	1.35 s	$4d5s\ ^3D_1$-$4d^2\ ^3F_2$	E2	3.129	
$4d^2\ ^1D_2$-$4d^2\ ^3F_2$	E2	0.643		$4d5s\ ^3D_1$-$4d^2\ ^3F_3$	E2	2.267	
$4d^2\ ^1D_2E1$-$4d^2\ ^3F_3$	M1	0.316		$4d5s\ ^3D_1$-$4d^2\ ^1D_2$	M1	0.001	
$4d^2\ ^1D_2$-$4d^2\ ^3F_3$	E2	0.746		$4d5s\ ^3D_1$-$4d^2\ ^1D_2$	E2	1.025	
$4d^2\ ^1D_2$-$4d^2\ ^3F_4$	E2	1.704		$4d5s\ ^3D_1$-$4d^2\ ^3P_0$	M1	0	
$4d^2\ ^3P_0$-$4d^2\ ^3F_2$	E2	1.691	16.0 s	$4d5s\ ^3D_1$-$4d^2\ ^3P_1$	M1	0	
$4d^2\ ^3P_0$-$4d^2\ ^1D_2$	E2	0.733		$4d5s\ ^3D_1$-$4d^2\ ^3P_1$	E2	2.214	
$4d^2\ ^3P_1$-$4d^2\ ^3F_2$	M1	0.022	12.0 s	$4d5s\ ^3D_1$-$4d^2\ ^3P_2$	M1	0	
$4d^2\ ^3P_1$-$4d^2\ ^3F_2$	E2	1.626		$4d5s\ ^3D_1$-$4d^2\ ^3P_2$	E2	0.955	
$4d^2\ ^3P_1$-$4d^2\ ^3F_3$	E2	2.355		$4d5s\ ^3D_1$-$4d^2\ ^1S_0$	M1	0	
$4d^2\ ^3P_1$-$4d^2\ ^1D_2$	M1	0.762		$4d5s\ ^3D_2$-$4d^2\ ^3F_2$	M1	0	2.26[-04] s
$4d^2\ ^3P_1$-$4d^2\ ^1D_2$	E2	1.357		$4d5s\ ^3D_2$-$4d^2\ ^3F_2$	E2	2.727	
$4d^2\ ^3P_1$-$4d^2\ ^3P_0$	M1	1.41		$4d5s\ ^3D_2$-$4d^2\ ^3F_3$	M1	0	
$4d^2\ ^3P_2$-$4d^2\ ^3F_2$	M1	0.059	1.82 s	$4d5s\ ^3D_2$-$4d^2\ ^3F_3$	E2	3.503	
$4d^2\ ^3P_2$-$4d^2\ ^3F_2$	E2	0.418		$4d5s\ ^3D_2$-$4d^2\ ^3F_4$	E2	2.386	
$4d^2\ ^3P_2$-$4d^2\ ^3F_3$	M1	0.133		$4d5s\ ^3D_2$-$4d^2\ ^1D_2$	M1	0.001	
$4d^2\ ^3P_2$-$4d^2\ ^3F_3$	E2	1.505		$4d5s\ ^3D_2$-$4d^2\ ^1D_2$	E2	1.525	
$4d^2\ ^3P_2$-$4d^2\ ^3F_4$	E2	2.81		$4d5s\ ^3D_2$-$4d^2\ ^3P_0$	E2	1.872	
$4d^2\ ^3P_2$-$4d^2\ ^1D_2$	M1	1.167		$4d5s\ ^3D_2$-$4d^2\ ^3P_1$	M1	0	
$4d^2\ ^3P_2$-$4d^2\ ^1D_2$	E2	0.082		$4d5s\ ^3D_2$-$4d^2\ ^3P_1$	E2	0.929	
$4d^2\ ^3P_2$-$4d^2\ ^3P_0$	E2	1.386		$4d5s\ ^3D_2$-$4d^2\ ^3P_2$	M1	0	
$4d^2\ ^3P_2$-$4d^2\ ^3P_1$	M1	1.385		$4d5s\ ^3D_2$-$4d^2\ ^3P_2$	E2	1.938	
$4d^2\ ^3P_2$-$4d^2\ ^3P_1$	E2	2.009		$4d5s\ ^3D_2$-$4d^2\ ^1G_4$	E2	0.98	
$4d^2\ ^1G_4$-$4d^2\ ^3F_2$	E2	0.267	1.31 s	$4d5s\ ^3D_2$-$4d^2\ ^1S_0$	E2	0	
$4d^2\ ^1G_4$-$4d^2\ ^3F_3$	M1	0.179		$4d5s\ ^3D_2$-$4d5s\ ^3D_1$	M1	2.082	
$4d^2\ ^1G_4$-$4d^2\ ^3F_3$	E2	0.072		$4d5s\ ^3D_2$-$4d5s\ ^3D_1$	E2	1.466	
$4d^2\ ^1G_4$-$4d^2\ ^3F_4$	M1	0.231		$4d5s\ ^3D_3$-$4d^2\ ^3F_2$	M1	0	2.23[-04] s
$4d^2\ ^1G_4$-$4d^2\ ^3F_4$	E2	0.312		$4d5s\ ^3D_3$-$4d^2\ ^3F_2$	E2	0.786	
$4d^2\ ^1G_4$-$4d^2\ ^1D_2$	E2	1.545		$4d5s\ ^3D_3$-$4d^2\ ^3F_3$	M1	0	
$4d^2\ ^1G_4$-$4d^2\ ^3P_2$	E2	1.117		$4d5s\ ^3D_3$-$4d^2\ ^3F_3$	E2	2.732	

Table 7.7: (Cont.) Transition matrix elements of Mo V and lifetimes calculated using CI+All-order are given. The lifetimes correspond to the initial state of the transition. The numbers in brackets represent powers of 10.

Transition	Type	Z	Lifetime	Transition	Type	Z	Lifetime
$4d5s\ ^3D_3$-$4d^2\ ^3F_4$	M1	0		$4d5p\ ^1D^o_2$-$4d^2\ ^3F_3$	E1	0.081	
$4d5s\ ^3D_3$-$4d^2\ ^3F_4$	E2	5.213		$4d5p\ ^1D^o_2$-$4d^2\ ^1D_2$	E1	1.132	
$4d5s\ ^3D_3$-$4d^2\ ^1D_2$	M1	0.001		$4d5p\ ^1D^o_2$-$4d^2\ ^3P_1$	E1	0.008	
$4d5s\ ^3D_3$-$4d^2\ ^1D_2$	E2	1.603		$4d5p\ ^1D^o_2$-$4d^2\ ^3P_2$	E1	0.385	
$4d5s\ ^3D_3$-$4d^2\ ^3P_1$	E2	2.217		$4d5p\ ^1D^o_2$-$4d5s\ ^3D_1$	E1	1.242	
$4d5s\ ^3D_3$-$4d^2\ ^3P_2$	M1	0		$4d5p\ ^1D^o_2$-$4d5s\ ^3D_2$	E1	1.628	
$4d5s\ ^3D_3$-$4d^2\ ^3P_2$	E2	2.73		$4d5p\ ^1D^o_2$-$4d5s\ ^3D_3$	E1	0.006	
$4d5s\ ^3D_3$-$4d^2\ ^1G_4$	M1	0		$4d5p\ ^1D^o_2$-$4d5s\ ^1D_2$	E1	2.163	
$4d5s\ ^3D_3$-$4d^2\ ^1G_4$	E2	0.392		$4d5p\ ^3D^o_1$-$4d^2\ ^3F_2$	E1	1.359	0.19 ns
$4d5s\ ^3D_3$-$4d5s\ ^3D_1$	E2	0.508		$4d5p\ ^3D^o_1$-$4d^2\ ^1D_2$	E1	0.006	
$4d5s\ ^3D_3$-$4d5s\ ^3D_2$	M1	2.12		$4d5p\ ^3D^o_1$-$4d^2\ ^3P_0$	E1	0.459	
$4d5s\ ^3D_3$-$4d5s\ ^3D_2$	E2	1.581		$4d5p\ ^3D^o_1$-$4d^2\ ^3P_1$	E1	0.226	
$4d5s\ ^1D_2$-$4d^2\ ^3F_2$	M1	0.002	2.08[-04] s	$4d5p\ ^3D^o_1$-$4d^2\ ^3P_2$	E1	0.004	
$4d5s\ ^1D_2$-$4d^2\ ^3F_2$	E2	0.005		$4d5p\ ^3D^o_1$-$4d^2\ ^1S_0$	E1	0.113	
$4d5s\ ^1D_2$-$4d^2\ ^3F_3$	M1	0.003		$4d5p\ ^3D^o_1$-$4d5s\ ^3D_1$	E1	1.828	
$4d5s\ ^1D_2$-$4d^2\ ^3F_3$	E2	0.648		$4d5p\ ^3D^o_1$-$4d5s\ ^3D_2$	E1	1.43	
$4d5s\ ^1D_2$-$4d^2\ ^3F_4$	E2	0.075		$4d5p\ ^3D^o_1$-$4d5s\ ^1D_2$	E1	0.134	
$4d5s\ ^1D_2$-$4d^2\ ^1D_2$	M1	0.001		$4d5p\ ^3D^o_2$-$4d^2\ ^3F_2$	E1	0.777	0.22 ns
$4d5s\ ^1D_2$-$4d^2\ ^1D_2$	E2	3.258		$4d5p\ ^3D^o_2$-$4d^2\ ^3F_3$	E1	1.269	
$4d5s\ ^1D_2$-$4d^2\ ^3P_0$	E2	0.22		$4d5p\ ^3D^o_2$-$4d^2\ ^1D_2$	E1	0.633	
$4d5s\ ^1D_2$-$4d^2\ ^3P_1$	M1	0.002		$4d5p\ ^3D^o_2$-$4d^2\ ^3P_1$	E1	0.619	
$4d5s\ ^1D_2$-$4d^2\ ^3P_1$	E2	0.172		$4d5p\ ^3D^o_2$-$4d^2\ ^3P_2$	E1	0.302	
$4d5s\ ^1D_2$-$4d^2\ ^3P_2$	M1	0.002		$4d5p\ ^3D^o_2$-$4d5s\ ^3D_1$	E1	0.043	
$4d5s\ ^1D_2$-$4d^2\ ^3P_2$	E2	2.73		$4d5p\ ^3D^o_2$-$4d5s\ ^3D_2$	E1	2.014	
$4d5s\ ^1D_2$-$4d^2\ ^1G_4$	E2	5.737		$4d5p\ ^3D^o_2$-$4d5s\ ^3D_3$	E1	1.588	
$4d5s\ ^1D_2$-$4d^2\ ^1S_0$	E2	1.931		$4d5p\ ^3D^o_2$-$4d5s\ ^1D_2$	E1	1.588	
$4d5s\ ^1D_2$-$4d5s\ ^3D_1$	M1	0.404		$4d5p\ ^3F^o_2$-$4d^2\ ^3F_2$	E1	0.407	0.30 ns
$4d5s\ ^1D_2$-$4d5s\ ^3D_1$	E2	0.286		$4d5p\ ^3F^o_2$-$4d^2\ ^3F_3$	E1	1.139	
$4d5s\ ^1D_2$-$4d5s\ ^3D_2$	M1	0.17		$4d5p\ ^3F^o_2$-$4d^2\ ^1D_2$	E1	0.691	
$4d5s\ ^1D_2$-$4d5s\ ^3D_2$	E2	0.279		$4d5p\ ^3F^o_2$-$4d^2\ ^3P_1$	E1	0.25	
$4d5s\ ^1D_2$-$4d5s\ ^3D_3$	M1	0.412		$4d5p\ ^3F^o_2$-$4d^2\ ^3P_2$	E1	0.142	
$4d5s\ ^1D_2$-$4d5s\ ^3D_3$	E2	0.308		$4d5p\ ^3F^o_2$-$4d5s\ ^3D_1$	E1	2.662	
$4d5p\ ^1D^o_2$-$4d^2\ ^3F_2$	E1	0.832	0.35 ns	$4d5p\ ^3F^o_2$-$4d5s\ ^3D_2$	E1	0.663	

Table 7.8: (Cont.) Transition matrix elements of Mo V and lifetimes calculated using CI+All-order are given. The lifetimes correspond to the initial state of the transition. The numbers in brackets represent powers of 10.

Transition	Type	Z	Lifetime	Transition	Type	Z	Lifetime
$4d5p\ ^3F^o_2$-$4d5s\ ^3D_3$	E1	0.376		$4d5p\ ^3P^o_2$-$4d^2\ ^3F_2$	E1	0.092	0.25 ns
$4d5p\ ^3F^o_2$-$4d5s\ ^1D_2$	E1	1.094		$4d5p\ ^3P^o_2$-$4d^2\ ^3F_3$	E1	0.212	
$4d5p\ ^3F^o_3$-$4d^2\ ^3F_2$	E1	0.313	0.26 ns	$4d5p\ ^3P^o_2$-$4d^2\ ^1D_2$	E1	0.389	
$4d5p\ ^3F^o_3$-$4d^2\ ^3F_3$	E1	1.251		$4d5p\ ^3P^o_2$-$4d^2\ ^3P_1$	E1	0.691	
$4d5p\ ^3F^o_3$-$4d^2\ ^3F_4$	E1	1.188		$4d5p\ ^3P^o_2$-$4d^2\ ^3P_2$	E1	1.36	
$4d5p\ ^3F^o_3$-$4d^2\ ^1D_2$	E1	0.299		$4d5p\ ^3P^o_2$-$4d5s\ ^3D_1$	E1	0.348	
$4d5p\ ^3F^o_3$-$4d^2\ ^3P_2$	E1	0.429		$4d5p\ ^3P^o_2$-$4d5s\ ^3D_2$	E1	1.31	
$4d5p\ ^3F^o_3$-$4d^2\ ^1G_4$	E1	0.294		$4d5p\ ^3P^o_2$-$4d5s\ ^3D_3$	E1	2.326	
$4d5p\ ^3F^o_3$-$4d5s\ ^3D_2$	E1	1.342		$4d5p\ ^3P^o_2$-$4d5s\ ^1D_2$	E1	0.853	
$4d5p\ ^3F^o_3$-$4d5s\ ^3D_3$	E1	3.166		$4d5p\ ^1F^o_3$-$4d^2\ ^3F_2$	E1	0.036	0.16 ns
$4d5p\ ^3F^o_3$-$4d5s\ ^1D_2$	E1	0.752		$4d5p\ ^1F^o_3$-$4d^2\ ^3F_3$	E1	0.131	
$4d5p\ ^3D^o_3$-$4d^2\ ^3F_2$	E1	0.199	0.25 ns	$4d5p\ ^1F^o_3$-$4d^2\ ^3F_4$	E1	0.171	
$4d5p\ ^3D^o_3$-$4d^2\ ^3F_3$	E1	0.45		$4d5p\ ^1F^o_3$-$4d^2\ ^1D_2$	E1	0.044	
$4d5p\ ^3D^o_3$-$4d^2\ ^3F_4$	E1	1.673		$4d5p\ ^1F^o_3$-$4d^2\ ^3P_2$	E1	0.167	
$4d5p\ ^3D^o_3$-$4d^2\ ^1D_2$	E1	0.229		$4d5p\ ^1F^o_3$-$4d^2\ ^1G_4$	E1	2.545	
$4d5p\ ^3D^o_3$-$4d^2\ ^3P_2$	E1	0.446		$4d5p\ ^1F^o_3$-$4d5s\ ^3D_2$	E1	0.511	
$4d5p\ ^3D^o_3$-$4d^2\ ^1G_4$	E1	0.168		$4d5p\ ^1F^o_3$-$4d5s\ ^3D_3$	E1	0.634	
$4d5p\ ^3D^o_3$-$4d5s\ ^3D_2$	E1	3.186		$4d5p\ ^1F^o_3$-$4d5s\ ^1D_2$	E1	3.295	
$4d5p\ ^3D^o_3$-$4d5s\ ^3D_3$	E1	1.491		$4d5p\ ^1P^o_1$-$4d^2\ ^3F_2$	E1	0.059	0.25 ns
$4d5p\ ^3D^o_3$-$4d5s\ ^1D_2$	E1	0.248		$4d5p\ ^1P^o_1$-$4d^2\ ^1D_2$	E1	0.716	
$4d5p\ ^3F^o_4$-$4d^2\ ^3F_3$	E1	0.363	0.40 ns	$4d5p\ ^1P^o_1$-$4d^2\ ^3P_0$	E1	0.227	
$4d5p\ ^3F^o_4$-$4d5s\ ^3F_4$	E1	1.417		$4d5p\ ^1P^o_1$-$4d^2\ ^3P_1$	E1	0.16	
$4d5p\ ^3F^o_4$-$4d5s\ ^1G_4$	E1	0.109		$4d5p\ ^1P^o_1$-$4d^2\ ^3P_2$	E1	0.682	
$4d5p\ ^3F^o_4$-$4d5s\ ^3D_3$	E1	3.952		$4d5p\ ^1P^o_1$-$4d^2\ ^1S_0$	E1	0.746	
$4d5p\ ^3P^o_1$-$4d^2\ ^3F_2$	E1	0.189	0.30 ns	$4d5p\ ^1P^o_1$-$4d5s\ ^3D_1$	E1	0.092	
$4d5p\ ^3P^o_1$-$4d^2\ ^1D_2$	E1	0.671		$4d5p\ ^1P^o_1$-$4d5s\ ^3D_2$	E1	0.4	
$4d5p\ ^3P^o_1$-$4d^2\ ^3P_0$	E1	0.611		$4d5p\ ^1P^o_1$-$4d5s\ ^1D_2$	E1	2.12	
$4d5p\ ^3P^o_1$-$4d^2\ ^3P_1$	E1	0.633					
$4d5p\ ^3P^o_1$-$4d^2\ ^3P_2$	E1	0.503					
$4d5p\ ^3P^o_1$-$4d^2\ ^1S_0$	E1	0.191					
$4d5p\ ^3P^0_1$-$4d5s\ ^3D_1$	E1	1.39					
$4d5p\ ^3P^0_1$-$4d5s\ ^3D_2$	E1	1.639					
$4d5p\ ^3P^0_1$-$4d5s\ ^1D_2$	E1	1.639					
$4d5p\ ^3P^o_0$-$4d^2\ ^3P_1$	E1	0.711	0.25 ns				
$4d5p\ ^3P^o_0$-$4d5s\ ^3D_1$	E1	1.257					

Table 7.9: Transition matrix elements of Tc VI and lifetimes calculated using CI+All-order are given. The lifetimes correspond to the initial state of the transition. The numbers in brackets represent powers of 10.

Transition	Type	$E1$	Lifetime	Transition	Type	$E1$	Lifetime
$4d^2\ ^3F_3$-$4d^2\ ^3F_2$	M1	2.562	3.51 s	$4d^2\ ^1S_0$-$4d^2\ ^3F_2$	E2	0.131	0.03 s
$4d^2\ ^3F_3$-$4d^2\ ^3F_2$	E2	0.543		$4d^2\ ^1S_0$-$4d^2\ ^1D_2$	E2	1.985	
$4d^2\ ^3F_4$-$4d^2\ ^3F_2$	E2	0.051	3.41 s	$4d^2\ ^1S_0$-$4d^2\ ^3P_1$	M1	0.131	
$4d^2\ ^3F_4$-$4d^2\ ^3F_3$	M1	2.589		$4d^2\ ^1S_0$-$4d^2\ ^3P_2$	E2	0.681	
$4d^2\ ^3F_4$-$4d^2\ ^3F_3$	E2	0.53		$4d5s\ ^3D_1$-$4d^2\ ^3F_2$	M1	0.001	4.61[-05] s
$4d^2\ ^1D_2$-$4d^2\ ^3F_2$	M1	0.228	2.11 s	$4d5s\ ^3D_1$-$4d^2\ ^3F_2$	E2	2.461	
$4d^2\ ^1D_2$-$4d^2\ ^3F_2$	E2	0.383		$4d5s\ ^3D_1$-$4d^2\ ^3F_3$	E2	1.788	
$4d^2\ ^1D_2$-$4d^2\ ^3F_3$	M1	0.308		$4d5s\ ^3D_1$-$4d^2\ ^1D_2$	M1	0.007	
$4d^2\ ^1D_2$-$4d^2\ ^3F_3$	E2	0.306		$4d5s\ ^3D_1$-$4d^2\ ^1D_2$	E2	0.584	
$4d^2\ ^1D_2$-$4d^2\ ^3F_4$	E2	0.853		$4d5s\ ^3D_1$-$4d^2\ ^3P_0$	M1	0.002	
$4d^2\ ^3P_0$-$4d^2\ ^3F_2$	E2	0.024	12.8 s	$4d5s\ ^3D_1$-$4d^2\ ^3P_1$	M1	0.003	
$4d^2\ ^3P_0$-$4d^2\ ^1D_2$	E2	0.369		$4d5s\ ^3D_1$-$4d^2\ ^3P_1$	E2	1.74	
$4d^2\ ^3P_1$-$4d^2\ ^3F_2$	M1	0.024	5.09 s	$4d5s\ ^3D_1$-$4d^2\ ^3P_2$	M1	0.002	
$4d^2\ ^3P_1$-$4d^2\ ^3F_2$	E2	1.325		$4d5s\ ^3D_1$-$4d^2\ ^3P_2$	E2	0.922	
$4d^2\ ^3P_1$-$4d^2\ ^3F_3$	E2	1.917		$4d5s\ ^3D_1$-$4d^2\ ^1S_0$	M1	0	
$4d^2\ ^3P_1$-$4d^2\ ^1D_2$	M1	0.424		$4d5s\ ^3D_2$-$4d^2\ ^3F_2$	M1	0.006	4.54[-05] s
$4d^2\ ^3P_1$-$4d^2\ ^1D_2$	E2	0.687		$4d5s\ ^3D_2$-$4d^2\ ^3F_2$	E2	2.145	
$4d^2\ ^3P_1$-$4d^2\ ^3P_0$	M1	1.408		$4d5s\ ^3D_2$-$4d^2\ ^3F_3$	M1	0.004	
$4d^2\ ^3P_2$-$4d^2\ ^3F_2$	M1	0.008	1.06 s	$4d5s\ ^3D_2$-$4d^2\ ^3F_3$	E2	2.734	
$4d^2\ ^3P_2$-$4d^2\ ^3F_2$	E2	0.466		$4d5s\ ^3D_2$-$4d^2\ ^3F_4$	E2	1.891	
$4d^2\ ^3P_2$-$4d^2\ ^3F_3$	M1	0.164		$4d5s\ ^3D_2$-$4d^2\ ^1D_2$	M1	0.002	
$4d^2\ ^3P_2$-$4d^2\ ^3F_3$	E2	1.333		$4d5s\ ^3D_2$-$4d^2\ ^1D_2$	E2	0.987	
$4d^2\ ^3P_2$-$4d^2\ ^3F_4$	E2	2.534		$4d5s\ ^3D_2$-$4d^2\ ^3P_0$	E2	1.46	
$4d^2\ ^3P_2$-$4d^2\ ^1D_2$	M1	0.711		$4d5s\ ^3D_2$-$4d^2\ ^3P_1$	M1	0.002	
$4d^2\ ^3P_2$-$4d^2\ ^1D_2$	E2	0.03		$4d5s\ ^3D_2$-$4d^2\ ^3P_1$	E2	0.73	
$4d^2\ ^3P_2$-$4d^2\ ^3P_0$	E2	1.215		$4d5s\ ^3D_2$-$4d^2\ ^3P_2$	M1	0	
$4d^2\ ^3P_2$-$4d^2\ ^3P_1$	M1	1.523		$4d5s\ ^3D_2$-$4d^2\ ^3P_2$	E2	1.687	
$4d^2\ ^3P_2$-$4d^2\ ^3P_1$	E2	1.523		$4d5s\ ^3D_2$-$4d^2\ ^1G_4$	E2	0.933	
$4d^2\ ^1G_4$-$4d^2\ ^3F_2$	E2	0.217	0.87 s	$4d5s\ ^3D_2$-$4d^2\ ^1S_0$	E2	0.206	
$4d^2\ ^1G_4$-$4d^2\ ^3F_3$	M1	0.211		$4d5s\ ^3D_2$-$4d5s\ ^3D_1$	M1	2.062	
$4d^2\ ^1G_4$-$4d^2\ ^3F_3$	E2	0.068		$4d5s\ ^3D_2$-$4d5s\ ^3D_1$	E2	1.194	
$4d^2\ ^1G_4$-$4d^2\ ^3F_4$	M1	0.272		$4d5s\ ^3D_3$-$4d^2\ ^3F_2$	M1	0.001	4.52[-05] s
$4d^2\ ^1G_4$-$4d^2\ ^3F_4$	E2	0.299		$4d5s\ ^3D_3$-$4d^2\ ^3F_2$	E2	0.62	
$4d^2\ ^1G_4$-$4d^2\ ^1D_2$	E2	1.508		$4d5s\ ^3D_3$-$4d^2\ ^3F_3$	M1	0.002	
$4d^2\ ^1G_4$-$4d^2\ ^3P_2$	E2	0.65		$4d5s\ ^3D_3$-$4d^2\ ^3F_3$	E2	2.154	

Table 7.10: (Cont.) Transition matrix elements of Tc VI and lifetimes calculated using CI+All-order are given. The lifetimes correspond to the initial state of the transition. The numbers in brackets represent powers of 10.

Transition	Type	$E1$	Lifetime	Transition	Type	$E1$	Lifetime
$4d5s\ ^3D_3$-$4d^2\ ^3F_4$	M1	0.003		$4d5p\ ^1D^o_2$-$4d^2\ ^3P_1$	E1	0	
$4d5s\ ^3D_3$-$4d^2\ ^3F_4$	E2	4.107		$4d5p\ ^1D^o_2$-$4d^2\ ^3P_2$	E1	0.054	
$4d5s\ ^3D_3$-$4d^2\ ^1D_2$	M1	0.006		$4d5p\ ^1D^o_2$-$4d5s\ ^3D_1$	E1	1.249	
$4d5s\ ^3D_3$-$4d^2\ ^1D_2$	E2	0.723		$4d5p\ ^1D^o_2$-$4d5s\ ^3D_2$	E1	1.66	
$4d5s\ ^3D_3$-$4d^2\ ^3P_1$	E2	1.739		$4d5p\ ^1D^o_2$-$4d5s\ ^3D_3$	E1	0.014	
$4d5s\ ^3D_3$-$4d^2\ ^3P_2$	M1	0.004		$4d5p\ ^1D^o_2$-$4d5s\ ^1D_2$	E1	1.77	
$4d5s\ ^3D_3$-$4d^2\ ^3P_2$	E2	2.383		$4d5p\ ^3D^o_1$-$4d^2\ ^3F_2$	E1	1.142	0.11 ns
$4d5s\ ^3D_3$-$4d^2\ ^1G_4$	M1	0		$4d5p\ ^3D^o_1$-$4d^2\ ^1D_2$	E1	0.045	
$4d5s\ ^3D_3$-$4d^2\ ^1G_4$	E2	0.36		$4d5p\ ^3D^o_1$-$4d^2\ ^3P_0$	E1	0.394	
$4d5s\ ^3D_3$-$4d5s\ ^3D_1$	E2	0.414		$4d5p\ ^3D^o_1$-$4d^2\ ^3P_1$	E1	0.172	
$4d5s\ ^3D_3$-$4d5s\ ^3D_2$	M1	2.099		$4d5p\ ^3D^o_1$-$4d^2\ ^3P_2$	E1	0.01	
$4d5s\ ^3D_3$-$4d5s\ ^3D_2$	E2	1.277		$4d5p\ ^3D^o_1$-$4d^2\ ^1S_0$	E1	0.104	
$4d5s\ ^1D_2$-$4d^2\ ^3F_2$	M1	0.007	3.78[-05] s	$4d5p\ ^3D^o_1$-$4d5s\ ^3D_1$	E1	1.626	
$4d5s\ ^1D_2$-$4d^2\ ^3F_2$	E2	0.121		$4d5p\ ^3D^o_1$-$4d5s\ ^3D_2$	E1	1.336	
$4d5s\ ^1D_2$-$4d^2\ ^3F_3$	M1	0.012		$4d5p\ ^3D^o_1$-$4d5s\ ^1D_2$	E1	0.097	
$4d5s\ ^1D_2$-$4d^2\ ^3F_3$	E2	0.632		$4d5p\ ^3D^o_2$-$4d^2\ ^3F_2$	E1	0.602	0.12 ns
$4d5s\ ^1D_2$-$4d^2\ ^3F_4$	E2	0.092		$4d5p\ ^3D^o_2$-$4d^2\ ^3F_3$	E1	1.116	
$4d5s\ ^1D_2$-$4d^2\ ^1D_2$	M1	0.003		$4d5p\ ^3D^o_2$-$4d^2\ ^1D_2$	E1	0.547	
$4d5s\ ^1D_2$-$4d^2\ ^1D_2$	E2	2.878		$4d5p\ ^3D^o_2$-$4d^2\ ^3P_1$	E1	0.54	
$4d5s\ ^1D_2$-$4d^2\ ^3P_0$	E2	0.228		$4d5p\ ^3D^o_2$-$4d^2\ ^3P_2$	E1	0.069	
$4d5s\ ^1D_2$-$4d^2\ ^3P_1$	M1	0.003		$4d5p\ ^3D^o_2$-$4d5s\ ^3D_1$	E1	0.159	
$4d5s\ ^1D_2$-$4d^2\ ^3P_1$	E2	0.167		$4d5p\ ^3D^o_2$-$4d5s\ ^3D_2$	E1	1.693	
$4d5s\ ^1D_2$-$4d^2\ ^3P_2$	M1	0.006		$4d5p\ ^3D^o_2$-$4d5s\ ^3D_3$	E1	1.532	
$4d5s\ ^1D_2$-$4d^2\ ^3P_2$	E2	1.278		$4d5p\ ^3D^o_2$-$4d5s\ ^1D_2$	E1	1.471	
$4d5s\ ^1D_2$-$4d^2\ ^1G_4$	E2	4.414		$4d5p\ ^3F^o_2$-$4d^2\ ^3F_2$	E1	0.264	0.10 ns
$4d5s\ ^1D_2$-$4d^2\ ^1S_0$	E2	1.51		$4d5p\ ^3F^o_2$-$4d^2\ ^3F_3$	E1	1.053	
$4d5s\ ^1D_2$-$4d5s\ ^3D_1$	M1	0.498		$4d5p\ ^3F^o_2$-$4d^2\ ^3F_4$	E1	1.018	
$4d5s\ ^1D_2$-$4d5s\ ^3D_1$	E2	0.277		$4d5p\ ^3F^o_2$-$4d^2\ ^1D_2$	E1	0.156	
$4d5s\ ^1D_2$-$4d5s\ ^3D_2$	M1	0.208		$4d5p\ ^3F^o_2$-$4d^2\ ^3P_2$	E1	0.401	
$4d5s\ ^1D_2$-$4d5s\ ^3D_2$	E2	0.229		$4d5p\ ^3F^o_2$-$4d^2\ ^1G_4$	E1	0.292	
$4d5s\ ^1D_2$-$4d5s\ ^3D_3$	M1	0.508		$4d5p\ ^3F^o_2$-$4d5s\ ^3D_2$	E1	1.162	
$4d5s\ ^1D_2$-$4d5s\ ^3D_3$	E2	0.308		$4d5p\ ^3F^o_2$-$4d5s\ ^3D_3$	E1	2.894	
$4d5p\ ^1D^o_2$-$4d^2\ ^3F_2$	E1	0.75	0.20 ns	$4d5p\ ^3F^o_2$-$4d5s\ ^1D_2$	E1	0.82	
$4d5p\ ^1D^o_2$-$4d^2\ ^3F_3$	E1	0.076		$4d5p\ ^3F^o_3$-$4d^2\ ^3F_2$	E1	0.362	0.24 ns
$4d5p\ ^1D^o_2$-$4d^2\ ^1D_2$	E1	0.906		$4d5p\ ^3F^o_3$-$4d^2\ ^3F_3$	E1	0.904	

Table 7.11: (Cont.) Transition matrix elements of Tc VI and lifetimes calculated using CI+All-order are given. The lifetimes correspond to the initial state of the transition. The numbers in brackets represent powers of 10.

Transition	Type	$E1$	Lifetime	Transition	Type	$E1$	Lifetime
$4d5p\ ^3F^o_3$-$4d^2\ ^1D_2$	E1	0.644		$4d5p\ ^3P^o_2$-$4d5s\ ^3D_1$	E1	0.308	
$4d5p\ ^3F^o_3$-$4d^2\ ^3P_1$	E1	0.159		$4d5p\ ^3P^o_2$-$4d5s\ ^3D_2$	E1	1.176	
$4d5p\ ^3F^o_3$-$4d^2\ ^3P_2$	E1	0.032		$4d5p\ ^3P^o_2$-$4d5s\ ^3D_3$	E1	2.079	
$4d5p\ ^3F^o_3$-$4d5s\ ^3D_1$	E1	2.384		$4d5p\ ^3P^o_2$-$4d5s\ ^1D_2$	E1	0.927	
$4d5p\ ^3F^o_3$-$4d5s\ ^3D_2$	E1	0.614		$4d5p\ ^1F^o_3$-$4d^2\ ^3F_2$	E1	0.039	0.08 ns
$4d5p\ ^3F^o_3$-$4d5s\ ^3D_3$	E1	0.209		$4d5p\ ^1F^o_3$-$4d^2\ ^3F_3$	E1	0.126	
$4d5p\ ^3F^o_3$-$4d5s\ ^1D_2$	E1	1.148		$4d5p\ ^1F^o_3$-$4d^2\ ^3F_4$	E1	0.17	
$4d5p\ ^3D^o_3$-$4d^2\ ^3F_2$	E1	0.179	0.14 ns	$4d5p\ ^1F^o_3$-$4d^2\ ^1D_2$	E1	0.092	
$4d5p\ ^3D^o_3$-$4d^2\ ^3F_3$	E1	0.405		$4d5p\ ^1F^o_3$-$4d^2\ ^3P_2$	E1	0.144	
$4d5p\ ^3D^o_3$-$4d^2\ ^3F_4$	E1	1.401		$4d5p\ ^1F^o_3$-$4d^2\ ^1G_4$	E1	2.209	
$4d5p\ ^3D^o_3$-$4d^2\ ^1D_2$	E1	0.107		$4d5p\ ^1F^o_3$-$4d5s\ ^3D_2$	E1	0.586	
$4d5p\ ^3D^o_3$-$4d^2\ ^3P_2$	E1	0.383		$4d5p\ ^1F^o_3$-$4d5s\ ^3D_3$	E1	0.666	
$4d5p\ ^3D^o_3$-$4d^2\ ^1G_4$	E1	0.157		$4d5p\ ^1F^o_3$-$4d5s\ ^1D_2$	E1	2.989	
$4d5p\ ^3D^o_3$-$4d5s\ ^3D_2$	E1	2.937		$4d5p\ ^1P^o_1$-$4d^2\ ^3F_2$	E1	0.078	0.12 ns
$4d5p\ ^3D^o_3$-$4d5s\ ^3D_3$	E1	1.293		$4d5p\ ^1P^o_1$-$4d^2\ ^1D_2$	E1	0.786	
$4d5p\ ^3D^o_3$-$4d5s\ ^1D_2$	E1	0.322		$4d5p\ ^1P^o_1$-$4d^2\ ^3P_0$	E1	0.199	
$4d5p\ ^3F^o_4$-$4d^2\ ^3F_3$	E1	0.311	0.23 ns	$4d5p\ ^1P^o_1$-$4d^2\ ^3P_1$	E1	0.141	
$4d5p\ ^3F^o_4$-$4d5s\ ^3F_4$	E1	1.205		$4d5p\ ^1P^o_1$-$4d^2\ ^3P_2$	E1	0.462	
$4d5p\ ^3F^o_4$-$4d5s\ ^1G_4$	E1	0.105		$4d5p\ ^1P^o_1$-$4d^2\ ^1S_0$	E1	0.623	
$4d5p\ ^3F^o_4$-$4d5s\ ^3D_3$	E1	3.651		$4d5p\ ^1P^o_1$-$4d5s\ ^3D_1$	E1	0.082	
$4d5p\ ^3P^o_1$-$4d^2\ ^3F_2$	E1	0.206	0.14 ns	$4d5p\ ^1P^o_1$-$4d5s\ ^3D_2$	E1	0.326	
$4d5p\ ^3P^o_1$-$4d^2\ ^1D_2$	E1	0.477		$4d5p\ ^1P^o_1$-$4d5s\ ^1D_2$	E1	1.956	
$4d5p\ ^3P^o_1$-$4d^2\ ^3P_0$	E1	0.507					
$4d5p\ ^3P^o_1$-$4d^2\ ^3P_1$	E1	0.534					
$4d5p\ ^3P^o_1$-$4d^2\ ^3P_2$	E1	0.538					
$4d5p\ ^3P^o_1$-$4d^2\ ^1S_0$	E1	0.162					
$4d5p\ ^3P^0_1$-$4d5s\ ^3D_1$	E1	1.311					
$4d5p\ ^3P^0_1$-$4d5s\ ^3D_2$	E1	1.473					
$4d5p\ ^3P^0_1$-$4d5s\ ^1D_2$	E1	0.295					
$4d5p\ ^3P^o_0$-$4d^2\ ^3P_1$	E1	0.609	0.14 ns				
$4d5p\ ^3P^o_0$-$4d5s\ ^3D_1$	E1	1.151					
$4d5p\ ^3P^o_2$-$4d^2\ ^3F_2$	E1	0.099	0.13 ns				
$4d5p\ ^3P^o_2$-$4d^2\ ^3F_3$	E1	0.205					
$4d5p\ ^3P^o_2$-$4d^2\ ^1D_2$	E1	0.048					
$4d5p\ ^3P^o_2$-$4d^2\ ^3P_1$	E1	0.571					
$4d5p\ ^3P^o_2$-$4d^2\ ^3P_2$	E1	1.183					

Chapter 8

CONCLUSION AND SUMMARY

We calculated the dynamic polarizability of Sr by using the transition matrix element recommended value previously evaluated in [26]. The dynamic polarizability of $5s^2\,{}^1S_0$ and $5s5p\,{}^3P_0$ state of Sr are plotted in the range $350 < \lambda < 460$ nm and $525 < \lambda < 825$ nm. From these plots, we determine the magic and magic zero wavelengths. We obtain the magic zero wavelengths at 355.92, 368.45, 378.81, 403.43, 433.85, 479.13, 632.83 and 1666.6 nm for the $5s5p\,{}^3P_0$ and at 689.20 nm for the $5s^2\,{}^1S_0$. We also obtain the magic wavelengths of $5s^2\,{}^1S_0 - 5s5p\,{}^3P_0$ transition at 354.9, 360.0 377.75, 389.9 and 497.0 nm apart from the 813.4 nm magic wavelength. Our result for the 355.92 nm magic zero wavelength of $5s5,{}^3P_0$ is in agreement with the other calculations [89, 94] and the 689.20 nm of $5s^2\,{}^1S_0$ is just 5 nm longer than the one calculated in [89]. We also proposed an alternative method to extract the transition matrix element from the measurement of the magic zero wavelength.

We calculated the BBR shift of Tl^+ $6s^2\,{}^1S_0 - 6s6p\,{}^3P_0$ clock transition and Hg $6s^2\,{}^1S_0 - 6s6p\,{}^3P_0$ clock transition. Our final BBR shift value is $\Delta\nu_{\rm BBR} = 0.0157(16)$ Hz for Tl^+ and $\Delta\nu_{\rm BBR} = 0.189(11)$ Hz for Hg. These values correspond to the BBR shift to clock transition ratio of $\nu_{\rm BBR}/\nu_0 = -1.06(9) \times 10^{-17}$ for Tl^+ and $\nu_{\rm BBR}/\nu_0 = -1.68(9) \times 10^{-16}$ for Hg. In the case of Tl^+, the values of the BBR shift agrees with our prediction of small BBR shift in the IIIB group ions. We showed that in these systems the BBR dynamic contribution to the total BBR shift almost cancels each other for the corresponding clock transition states. This cancellation makes it possible for the calculation of BBR shift by solely using the static polarizability.

We calculated the magic and magic zero wavelength of Hg $6s^2\,{}^1S_0 - 6s6p\,{}^3P_0$ clock transition. Our final value is $\lambda_{\rm magic} = 367.7(1.7)$ nm for the magic wavelength

and $\lambda_{\text{magic-zero}} = 383.9(5.1)$ nm for the magic zero wavelength. Our result of the magic wavelength differs by 4-8 nm compared to other works [101, 32]. We derived the hyperfine quenching rates formula for $ns^2\,{}^1S_0 - nsnp\,{}^3P_0$ transition and applied it to the ^{113}Cd clock transition. We calculated the hyperfine quenching rate of ^{25}Mg, ^{87}Sr and ^{113}Cd. Our final value of hyperfine transition rates are 4.30×10^{-4} s^{-1}, 9.70×10^{-3} s^{-1} and 7.70×10^{-2} s^{-1} respectively for ^{25}Mg, ^{87}Sr and ^{113}Cd. Our value for ^{25}Mg differs by 2-3% compared to results in [40, 42] and for ^{87}Sr differs by 24-43% compared to results in [40, 41]. Since our results of the hyperfine quenching rate of ^{87}Sr and ^{25}Mg agreed within an order of magnitude from other theoretical results, we expect our result for the hyperfine quenching rate of ^{113}Cd should be in close proximity with the experimental result. Our calculations are currently being tested and used in the ongoing Cd and Hg clock experiments at RIKEN.

We derived the formulas to evaluate the two-particle SMS matrix element in the framework of all-order method. We used the formulas to calculate the two-particle SMS constant and derived the isotope-shift constant for Na, K, and Rb. We compared our result with the result from the experiment and found out that except for Na the theoretical and experimental results are still in disagreement. These results show that corrections from the fourth and higher order of perturbations have significant effects in the calculations of the specific mass shift.

We calculated the energies and lifetimes of Mo V, Mo VI, Tc VI and Tc VII in the framework of SD and SDpT All-order, CI+MBPT and CI+All-order. We found, by comparing with the available experimental data, that our calculations for electronic spectrum of Mo VI and Mo VII agree with the experimental data for up to 10% accuracy. There are currently no available experimental data to compare with for Tc VI and Tc VII. We expect our predictions of Tc data will be useful in future studies and experiments of Tc atom.

Appendix A

ANGULAR REDUCTION

The general one- and two-body matrix element z_{ij} and z_{ijkl} can be further reduced by integrating over the angular part. After the angular reduction, we can express the matrix elements using only the radial wavefunction.

A.1 Angular momentum diagram

To ease the summation over the magnetic angular quantum number we are going to utilize the graphical rules following the work in [80]. In this formalism, the basic elements of the diagram are introduced. Afterward, the summation over the magnetic quantum number can be done by connecting these basic elements.

We are now going to cover the basic elements of the diagram. First, the straight line represents

$$j_1 m_1 \quad\text{———}\quad j_2 m_2 \;= \delta_{j_1 j_2}\delta_{m_1 m_2}. \tag{A.1}$$

Second, the straight line with arrow represents

$$j_1 m_1 \quad\text{———}\!\!\rightarrow\!\!\text{———}\quad j_2 m_2 \;=\; j_2 m_2 \quad\text{———}\!\!\leftarrow\!\!\text{———}\quad j_1 m_1 \;= (-1)^{j_2 - m_2}\delta_{j_1 j_2}\delta_{-m_1 m_2}. \tag{A.2}$$

Third, the 3-j symbol represents the 3-j coefficient

$$+\left|\begin{array}{l} j_3 m_3 \\ \text{———}\; j_2 m_2 \\ j_1 m_1 \end{array}\right. \;=\; -\left|\begin{array}{l} j_1 m_1 \\ \text{———}\; j_2 m_2 \\ j_3 m_3 \end{array}\right. \;= \begin{pmatrix} j_1 & j_2 & j_3 \\ m_1 & m_2 & m_3 \end{pmatrix}, \tag{A.3}$$

Here the sign in front of the symbol determines whether the quantum number is read clockwise (-) or counterclockwise (+).

The rule of summation in this diagram method is represented by connecting the vertex corresponds to the summed quantum number, thus

$$\sum_{m_3} \; j_1 m_1 \underline{\qquad\qquad} j_2 m_2 \;\; j_2 m_2 \underline{\qquad\qquad} j_3 m_3 \;\; = \delta_{j_2 j_3} \; j_1 m_1 \underline{\qquad\qquad} j_3 m_3 \; . \tag{A.4}$$

From these definitions and rules, the following identities can be derived

1. Two arrows in the same direction give a factor of $(-1)^{2j}$

$$j_1 m_1 \underline{\longrightarrow\!\!\!\!\!\!\rightarrow} j_2 m_2 \;\; = (-1)^{2j_2} \; j_1 m_1 \underline{\qquad\qquad} j_2 m_2 \tag{A.5}$$

2. Two arrows in the opposite directions cancel

$$j_1 m_1 \underline{\longrightarrow\!\!\!\!\!\!\leftarrow} j_2 m_2 \;\; = \;\; j_1 m_1 \underline{\qquad\qquad} j_2 m_2 \tag{A.6}$$

3. Flipping the direction of an arrow gives a factor of $(-1)^{2j}$

$$\begin{aligned} j_1 m_1 \underline{\longrightarrow} j_2 m_2 \;\; &= \;\; j_1 m_1 \underline{\longrightarrow\!\!\!\!\leftarrow\!\!\!\!\rightarrow} j_2 m_2 \;\; = \;\; j_1 m_1 \underline{\longrightarrow\!\!\!\!\rightarrow\!\!\!\!\leftarrow} j_2 m_2 \\ &= \;\; (-1)^{2j_1} \; j_1 m_1 \underline{\longleftarrow} j_2 m_2 \end{aligned} \tag{A.7}$$

4. Changing the sign of the 3-j symbol gives a factor of $(-1)^{j_1+j_2+j_3}$

$$\begin{aligned} -\left| \begin{array}{l} j_1 m_1 \\ \qquad\qquad j_2 m_2 \\ j_3 m_3 \end{array} \right. \;\; &= \;\; \begin{pmatrix} j_1 & j_2 & j_3 \\ m_1 & m_2 & m_3 \end{pmatrix} = (-1)^{j_1+j_2+j_3} \begin{pmatrix} j_1 & j_3 & j_2 \\ m_1 & m_3 & m_2 \end{pmatrix} \\ &= \;\; (-1)^{j_1+j_2+j_3} + \left| \begin{array}{l} j_1 m_1 \\ \qquad\qquad j_2 m_2 \\ j_3 m_3 \end{array} \right. \end{aligned} \tag{A.8}$$

5. Outward arrows from the 3-j symbol vertex cancel out

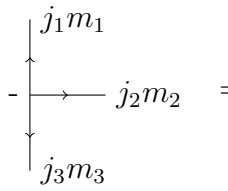

$$= (-1)^{j_1+j_2+j_3-(m_1+m_2+m_3)} \begin{pmatrix} j_1 & j_2 & j_3 \\ -m_1 & -m_2 & -m_3 \end{pmatrix}$$

$$= (-1)^{2(j_1+j_2+j_3)} \begin{pmatrix} j_1 & j_2 & j_3 \\ m_1 & m_2 & m_3 \end{pmatrix}$$

$$= \begin{pmatrix} j_1 & j_2 & j_3 \\ m_1 & m_2 & m_3 \end{pmatrix} =$$

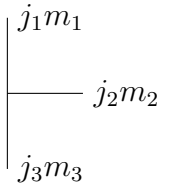

(A.9)

where we have used the 3-j symbol symmetry property

$$\begin{pmatrix} j_1 & j_2 & j_3 \\ -m_1 & -m_2 & -m_3 \end{pmatrix} = (-1)^{j_1+j_2+j_3} \begin{pmatrix} j_1 & j_2 & j_3 \\ m_1 & m_2 & m_3 \end{pmatrix} \tag{A.10}$$

and the selection rules $m_1 + m_2 + m_3 = 0$ and $(j_1 + j_2 + j_3)$ is integer.

6. Inward arrows from the 3-j symbol vertex cancel out

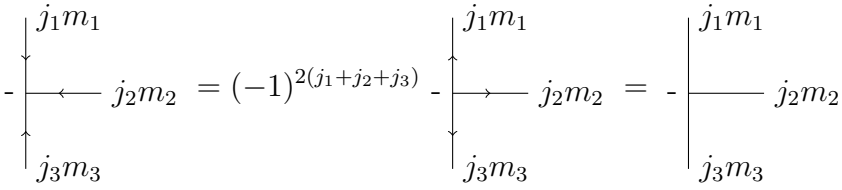

(A.11)

We can write the Coulomb matrix element g_{ijkl} in terms of its reduced matrix element using the angular momentum diagram as

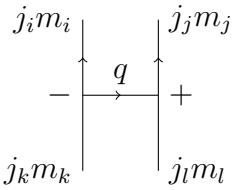

$$X_q(ijkl), \tag{A.12}$$

where $X_q(ijkl)$ is given by

$$X_q(ijkl) = (-1)^q \langle \kappa_i || C^q || \kappa_k \rangle \langle \kappa_j || C^q || \kappa_l \rangle R_q(ijkl). \tag{A.13}$$

$R_q(ijkl)$ is the Slater integral[6] and the reduced matrix element $\langle \kappa_i || C^q || \kappa_k \rangle$ is given by

$$\langle \kappa_i || C^q || \kappa_k \rangle = (-1)^{j_i + \frac{1}{2}} \sqrt{[j_i][j_k]} \begin{pmatrix} j_i & j_k & q \\ -\frac{1}{2} & \frac{1}{2} & 0 \end{pmatrix} \Pi(l_i + l_k + q), \tag{A.14}$$

where

$$\Pi(l) = \begin{cases} 1, \text{ if } l \text{ is even}, \\ 0, \text{ if } l \text{ is odd}. \end{cases} \tag{A.15}$$

Using similiar method we can also express the double excitation coefficient with its reduced coefficient

$$\rho_{ijkl} = \sum_q$$ 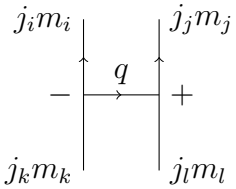 $$\rho_q(ijkl). \tag{A.16}$$

The single excitation coefficient is connected to its reduced coefficient by the following relation

$$\rho_{ij} = \delta_{\kappa_i \kappa_j} \delta_{m_i m_j} \rho(ij) \tag{A.17}$$

A.2 Commonly used identities

From the basic elements (A.1)-(A.3), we can derive the identities which are commonly used in the calculation. These identities are given as follow

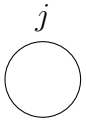

$$= [j] \tag{A.18}$$

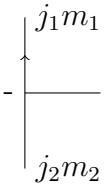

$$= \frac{1}{\sqrt{[j_1]}} \delta_{j_1 j_2} \delta_{m_1 m_2} \tag{A.19}$$

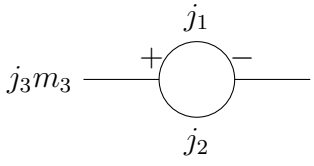

$$= \frac{1}{[j_3]} \delta_{j_3 j_3'} \delta_{m_3 m_3'} \tag{A.20}$$

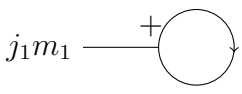

$$= \sqrt{[j_2]} \delta_{j_1 0} \delta_{m_1 0} \tag{A.21}$$

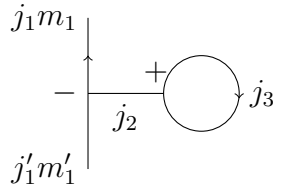

$$= \sqrt{\frac{[j_3]}{[j_1]}}\delta_{j_20}\delta_{j_1j'_1}\delta_{m_1m'_1} \tag{A.22}$$

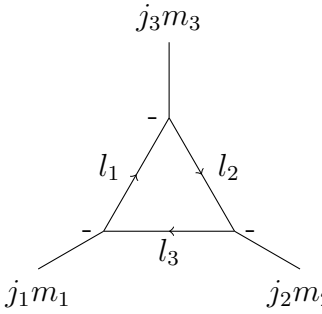

$$= \begin{Bmatrix} j_1 & j_2 & j_3 \\ l_1 & l_2 & l_3 \end{Bmatrix}$$

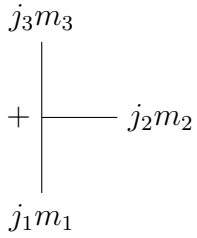

(A.23)

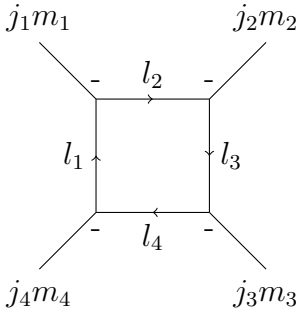

$$= \sum_k (-1)^{k+l_2-l_4}[k] \begin{Bmatrix} j_1 & j_4 & k \\ l_4 & l_2 & l_1 \end{Bmatrix} \times \tag{A.24}$$

$$\begin{Bmatrix} j_2 & j_3 & k \\ l_4 & l_2 & l_3 \end{Bmatrix}$$

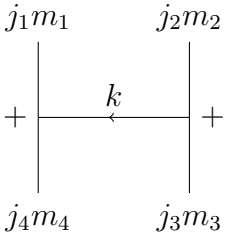

(A.25)

In the above equations we use $[j] = (2j + 1)$.

A.3 Example

We now given an example how to apply this technique for reducing one of the term in the SD two body matrix element

$$T^{(r)} = -2t_{vmnr}\rho^*_{vmab}\tilde{\rho}_{rnba} \tag{A.26}$$

In the reduced form, this term becomes

$$T^{(r)} = \sum_{\substack{mnrv \\ ab}}$$

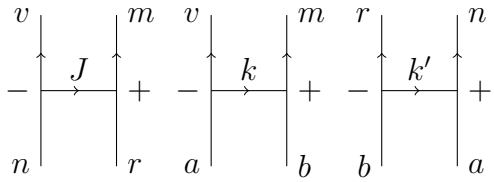

$$\times (-2) T_J(vmnr) \rho_k(vmab) \tilde{\rho}_{k'}(rnba), \tag{A.27}$$

where the indices refer to both the total angular and magnetic quantum number to simplify the notation. First, we connect the a and b legs in the second and third diagram of (A.27) then convert it to the form of (A.25).

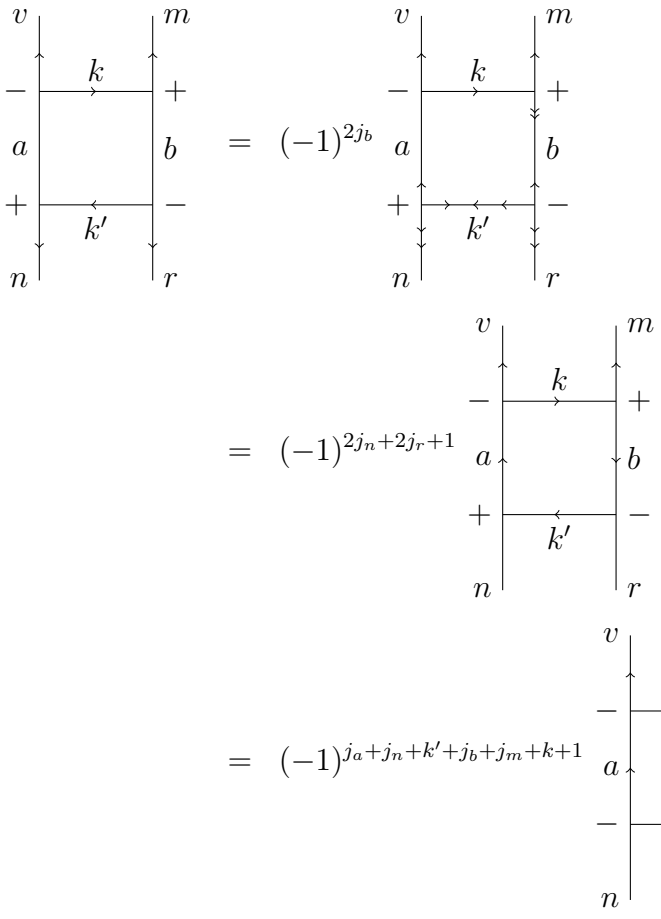

(A.28)

since the total angular momentum j is half integer. Applying (A.25) we obtain

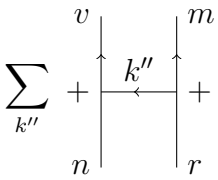

$$\sum_{k''} (-1)^{j_a+j_b+j_m+j_n+k''+1} [k''] \begin{Bmatrix} j_v & j_n & k'' \\ k' & k & j_a \end{Bmatrix} \begin{Bmatrix} j_m & j_r & k'' \\ k' & k & j_b \end{Bmatrix}. \tag{A.29}$$

It is easy to check that

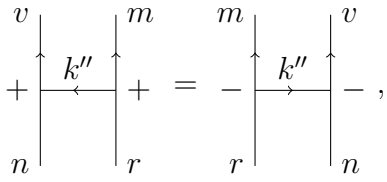

(A.30)

so we can combine this diagram with the first diagram of (A.27) by connecting the m and r legs

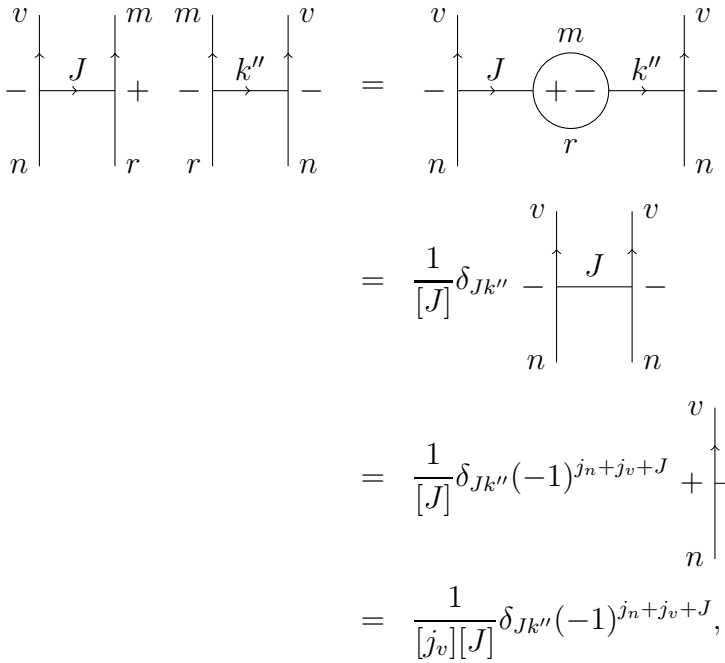

(A.31)

where we connect the n leg in the last step. Combining (A.29) and (A.31) and summing over the index k'' we arrived at the final result

$$T^{(r)} = -2 \sum_{\substack{abmnr \\ Jkk'}} \frac{1}{[j_v]} (-1)^{j_a+j_b+j_m+j_v} \begin{Bmatrix} j_v & j_n & J \\ k' & k & j_a \end{Bmatrix} \begin{Bmatrix} j_m & j_r & J \\ k' & k & j_b \end{Bmatrix} \tag{A.32}$$

Appendix B

MATRIX ELEMENT

Here we provide the one- and two- body matrix elements of the all-order formalism and the third order MBPT after angular reduction.

B.1 All-order terms

The one-body term consists of 20 terms given by

$$
\begin{aligned}
Z^{(a)} &= \sum_{ma} \frac{(-1)^{j_m - j_a + J}}{[J]} z(am)\tilde{\rho}_J(wmva) \\
&\quad + \sum_{ma} \frac{(-1)^{j_w - j_v + J}}{[J]} z(ma)\tilde{\rho}_J(vmwa) && \text{(B.1)} \\
Z^{(b)} &= -\sum_{a} \delta_{\kappa_w \kappa_a} z(av)\rho(wa) - \sum_{a} \delta_{\kappa_v \kappa_a} z(wa)\rho(va) && \text{(B.2)} \\
Z^{(c)} &= \sum_{m} \delta_{\kappa_m \kappa_v} z(wm)\rho(mv) + \sum_{m} \delta_{\kappa_m \kappa_v} z(mv)\rho(mw) && \text{(B.3)} \\
Z^{(d)} &= \sum_{mn} \delta_{\kappa_n \kappa_v} \delta_{\kappa_m \kappa_w} z(mn)\rho(mw)\rho(nv) && \text{(B.4)} \\
Z^{(e)} &= \sum_{ab} \delta_{\kappa_v \kappa_b} \delta\kappa_w \kappa_a z(ab)\rho(vb)\rho(wa) && \text{(B.5)} \\
Z^{(f)} &= -\sum_{ma} \delta_{\kappa_m \kappa_a} \rho(ma)\{\delta_{\kappa_m \kappa_w} z(av)\rho(mv) + \delta_{\kappa_m \kappa_v} z(wa)\rho(mv)\} && \text{(B.6)} \\
Z^{(g)} &= -\sum_{ma} \delta_{\kappa_m \kappa_a} \rho(ma)\{\delta_{\kappa_w \kappa_a} z(mv)\rho(wa) + \delta_{\kappa_v \kappa_a} z(wm)\rho(va)\} && \text{(B.7)} \\
Z^{(h)} &= \sum_{mna} \frac{(-1)^{j_a - j_m + J}}{[J]} \delta_{\kappa_n \kappa_w} z(am)\rho(nw)\tilde{\rho}_J(nmva) \\
&\quad + \sum_{mna} \frac{(-1)^{j_w - j_v + J}}{[J]} \delta\kappa_n \kappa_v z(ma)\tilde{\rho}_J(nmwa)\rho(nv) && \text{(B.8)} \\
Z^{(i)} &= \sum_{mna} \frac{(-1)^{j_a - j_n + J}}{[J]} \delta_{\kappa_m \kappa_a} z(mn)\rho(ma)\tilde{\rho}_J(wnva)
\end{aligned}
$$

$$+\sum_{mna}\frac{(-1)^{j_w-j_v+J}}{[J]}\delta_{\kappa_n\kappa_a}z(mn)\tilde{\rho}_J(vmwa)\rho(na) \tag{B.9}$$

$$\begin{aligned} Z^{(j)} &= -\sum_{mna}\frac{(-1)^{j_b-j_a+J}}{[J]}\delta_{\kappa_m\kappa_b}z(ab)\rho(mb)\tilde{\rho}_J(wmva) \\ &\quad -\sum_{mab}\frac{(-1)^{j_w-j_v+J}}{[J]}\delta_{\kappa_m\kappa_a}z(ab)\tilde{\rho}_J(vmwb)\rho(ma) \end{aligned} \tag{B.10}$$

$$\begin{aligned} Z^{(k)} &= -\sum_{mab}\frac{(-1)^{j_m-j_b+J}}{[J]}\delta_{\kappa_v\kappa_a}z(bm)\rho(va)\tilde{\rho}_J(wmab) \\ &\quad -\sum_{mab}\frac{(-1)^{j_w-j_v+J}}{[J]}\delta_{\kappa_w\kappa_a}z(mb)\tilde{\rho}_J(vmab)\rho(wa) \end{aligned} \tag{B.11}$$

$$\begin{aligned} Z^{(l)} &= -\sum_{mab}\delta_{\kappa_w\kappa_a}\delta_{\kappa_m\kappa_b}\sqrt{\frac{[j_m]}{[j_w]}}z(av)\rho(mb)\tilde{\rho}_0(wmab) \\ &\quad -\sum_{mab}\delta_{\kappa_v\kappa_a}\delta_{\kappa_m\kappa_b}\sqrt{\frac{[j_b]}{[j_v]}}z(wa)\tilde{\rho}_0(vmab)\rho(mb) \end{aligned} \tag{B.12}$$

$$\begin{aligned} Z^{(m)} &= \sum_{mna}\delta_{\kappa_w\kappa_m}\delta_{\kappa_n\kappa_a}\sqrt{\frac{[j_a]}{[j_w]}}z(mv)\tilde{\rho}_0(nmaw)\rho(na) \\ &\quad +\sum_{mna}\delta_{\kappa_v\kappa_m}\delta_{\kappa_n\kappa_a}\sqrt{\frac{[j_a]}{[j_v]}}z(wm)\rho(na)\tilde{\rho}_0(nmav) \end{aligned} \tag{B.13}$$

$$\begin{aligned} Z^{(n)} &= -\sum_{\substack{mnab\\kk'}}(-1)^{j_m+j_b+j_v+j_n+J}\begin{Bmatrix} j_w & J & j_v \\ k' & j_n & k \end{Bmatrix}\begin{Bmatrix} k & J & k' \\ j_a & j_m & j_b \end{Bmatrix} \\ &\qquad \times z(ab)\rho_k(nmwb)\tilde{\rho}_{k'}(nmva) \end{aligned} \tag{B.14}$$

$$\begin{aligned} Z^{(o)} &= -\sum_{\substack{mabc\\kk'}}(-1)^{j_c+j_m+j_b+j_w+k+k'}\begin{Bmatrix} j_v & j_w & J \\ k & k' & j_b \end{Bmatrix}\begin{Bmatrix} k' & J & k \\ j_a & j_m & j_c \end{Bmatrix} \\ &\qquad \times z(ab)\rho_k(nmwb)\tilde{\rho}_{k'}(nmva) \end{aligned} \tag{B.15}$$

$$Z^{(p)} = -\sum_{\substack{mnra\\k}}\frac{(-1)^{J+k+j_w+j_m}}{[k]}\begin{Bmatrix} j_w & j_v & J \\ j_m & j_r & k \end{Bmatrix}z(rm)\tilde{\rho}_k(rnwa)\tilde{\rho}_k(mnva) \tag{B.16}$$

$$\begin{aligned} Z^{(q)} &= -\sum_{\substack{mnab\\kk'}}(-1)^{j_m+j_a+j_w+j_b+J}\begin{Bmatrix} k & k' & J \\ j_n & j_m & j_a \end{Bmatrix}\begin{Bmatrix} j_v & j_w & J \\ k' & k & j_b \end{Bmatrix} \\ &\qquad \times z(mn)\rho_k(mvab)\tilde{\rho}_{k'}(nwab) \end{aligned} \tag{B.17}$$

$$
\begin{aligned}
Z^{(r)} &= \sum_{mnab} \frac{(-1)^{j_n+j_b+j_w+j_v}}{[J]^2} z(bn)\tilde{\rho}_J(vmwa)\tilde{\rho}_J(mnab) \\
&\quad + \sum_{mnab} \frac{1}{[J]^2} z(nb)\tilde{\rho}_J(mnab)\tilde{\rho}_J(wmva) \qquad \text{(B.18)} \\
Z^{(s)} &= -\sum_{\substack{mnab \\ k}} \frac{1}{[k][j_w]} \delta_{\kappa_w\kappa_b} z(bv)\rho_k(nmwa)\tilde{\rho}_k(mnab) \\
&\quad - \sum_{\substack{mnab \\ k}} \frac{1}{[k][j_v]} \delta_{\kappa_v\kappa_b} z(wb)\rho_k(mnab)\tilde{\rho}_k(nmva) \qquad \text{(B.19)} \\
Z^{(t)} &= -\sum_{\substack{mnab \\ k}} \delta_{\kappa_w\kappa_m} z(mv)\rho_k(nmab)\tilde{\rho}(nwab) \\
&\quad - \sum_{\substack{mnab \\ k}} \frac{1}{[k][j_v]} \delta_{\kappa_v\kappa_m} z(wm)\rho_k(nvab)\tilde{\rho}_k(nmab). \qquad \text{(B.20)}
\end{aligned}
$$

The two-body terms consist of 28 terms given by

$$
\begin{aligned}
T^{(a)} &= 2\sum_{ma} \sqrt{\frac{[j_a]}{[j_v]}} \delta_{\kappa_m\kappa_a} \tilde{T}_0(vavm)\rho(ma) \qquad \text{(B.21)} \\
T^{(b)} &= -2\sum_{abmJ} \frac{1}{[J][j_v]} (-1)^{j_a+j_b+j_m+j_v} T_J(abvm)\tilde{\rho}_J(mvba) \qquad \text{(B.22)} \\
T^{(c)} &= 2\sum_{amnJ} \frac{1}{[J][j_v]} (-1)^{j_a+j_m+j_n+j_v+J} T_J(avmn)\tilde{\rho}_J(nmva) \qquad \text{(B.23)} \\
T^{(d)} &= -2\sum_{amb} \sqrt{\frac{[j_a]}{[j_v]}} \delta_{\kappa_v\kappa_b}\delta_{\kappa_m\kappa_a} \tilde{T}_0(vabm)\rho(vb)\rho(ma) \qquad \text{(B.24)} \\
T^{(e)} &= 2\sum_{amn} \sqrt{\frac{[j_a]}{[j_v]}} \delta_{\kappa_m\kappa_a}\delta_{\kappa_n\kappa_v} \tilde{T}_0(vmna)\rho(ma)\rho(nv) \qquad \text{(B.25)} \\
T^{(f)} &= -\sum_{amb} \sqrt{\frac{[j_a]}{[j_v]}} \delta_{\kappa_m\kappa_b}\delta_{\kappa_m\kappa_a} \tilde{T}_0(vavb)\rho(mb)\rho(ma) \qquad \text{(B.26)} \\
&\quad + \sum_{amn} \sqrt{\frac{[j_m]}{[j_v]}} \delta_{\kappa_m\kappa_a}\delta_{\kappa_n\kappa_a} \tilde{T}_0(vmvn)\rho(ma)\rho(na) \qquad \text{(B.27)} \\
T^{(g)} &= -2\sum_{abmnJ} \frac{\delta_{\kappa_m\kappa_b}}{[J][j_v]} (-1)^{j_a+j_b+j_v+j_n} \tilde{T}_J(manv)\tilde{\rho}_J(vnab)\rho(mb) \qquad \text{(B.28)} \\
T^{(h)} &= 2\sum_{abcmJ} \frac{\delta_{\kappa_m\kappa_c}}{[J][j_v]} (-1)^{j_a+j_b+j_m+j_v} T_J(abvc)\tilde{\rho}_J(mvba)\rho(mc) \qquad \text{(B.29)}
\end{aligned}
$$

$$T^{(i)} = 2\sum_{abcmJ}\frac{\delta_{\kappa_v\kappa_c}}{[J][j_v]}(-1)^{j_a+j_b+j_m+j_v}T_J(abmc)\tilde{\rho}_J(vmba)\rho(vc) \quad \text{(B.30)}$$

$$T^{(j)} = 2\sum_{abmn}\sqrt{\frac{[j_b]}{[j_v]}}\delta_{\kappa_n\kappa_b}\tilde{T}_0(vavm)\tilde{\rho}_0(mnab)\rho(nb) \quad \text{(B.31)}$$

$$T^{(k)} = -2\sum_{abmnJ}\frac{\delta_{\kappa_v\kappa_b}}{[J][j_v]}(-1)^{j_a+j_b+j_m+j_n}T_J(vamn)\tilde{\rho}_J(nmab)\rho(vb) \quad \text{(B.32)}$$

$$T^{(l)} = -2\sum_{abmnJ}\frac{\delta_{\kappa_n\kappa_b}}{[J][j_v]}(-1)^{j_a+j_m+j_n+j_v}\tilde{T}_J(avmb)\tilde{\rho}_J(nmva)\rho(nb) \quad \text{(B.33)}$$

$$T^{(m)} = 2\sum_{abmn}\sqrt{\frac{[j_m]}{[j_v]}}\delta_{\kappa_m\kappa_b}\tilde{T}_0(amnb)\tilde{\rho}_0(vnva)\rho(mb) \quad \text{(B.34)}$$

$$T^{(n)} = 2\sum_{amnrJ}\frac{\delta_{\kappa_m\kappa_a}}{[J][j_v]}(-1)^{j_m+j_n+j_r+j_v}T_J(mvrn)\tilde{\rho}_J(nrva)\rho(ma) \quad \text{(B.35)}$$

$$T^{(o)} = -2\sum_{abmnJ}\frac{\delta_{\kappa_n\kappa_v}}{[J][j_v]}T_J(vmab)\tilde{\rho}_J(mnba)\rho(nv) \quad \text{(B.36)}$$

$$T^{(p)} = 2\sum_{amnrJ}\frac{\delta_{\kappa_m\kappa_v}}{[J][j_v]}(-1)^{j_a+j_m+j_n+j_r}T_J(amnr)\tilde{\rho}_J(rnva)\rho(mv) \quad \text{(B.37)}$$

$$T^{(q)} = 2\sum_{abcmnJ}\frac{1}{[J]^2[j_v]}(-1)^{j_a+j_m+J}\tilde{T}_J(avmb)\tilde{\rho}_J(vnbc)\tilde{\rho}_J(nmca) \quad \text{(B.38)}$$

$$T^{(r)} = -2\sum_{\substack{abmnr\\Jk k'}}\frac{1}{[j_v]}(-1)^{j_a+j_b+j_m+j_v}\begin{Bmatrix} j_v & j_n & J\\ k' & k & j_a\end{Bmatrix}\begin{Bmatrix} j_m & j_r & J\\ k' & k & j_b\end{Bmatrix}$$
$$\times T_J(vmnr)\rho_k(vmab)\tilde{\rho}_{k'}(rnba) \quad \text{(B.39)}$$

$$T^{(s)} = 2\sum_{\substack{abcmn\\Jk k'}}\frac{1}{[j_v]}(-1)^{j_b+j_c+j_m+j_n}\begin{Bmatrix} j_v & j_n & k'\\ k & J & j_b\end{Bmatrix}\begin{Bmatrix} j_a & j_m & k'\\ k & J & j_c\end{Bmatrix}$$
$$\times T_J(avcb)\rho_k(mncb)\tilde{\rho}_{k'}(nmva) \quad \text{(B.40)}$$

$$T^{(t)} = -2\sum_{\substack{abcmn\\J}}\frac{\delta_{\kappa_n\kappa_a}}{\sqrt{[j_v][j_a]}[J]}T_J(mabc)\tilde{\rho}_J(nmcb)\tilde{\rho}_0(vnva) \quad \text{(B.41)}$$

$$T^{(u)} = -2\sum_{abmnrJ}\frac{1}{[J]^2[j_v]}(-1)^{j_v+j_n+J}\tilde{T}_J(vmna)\tilde{\rho}_J(mrab)\tilde{\rho}_J(nrvb) \quad \text{(B.42)}$$

$$T^{v)} = 2\sum_{\substack{abmnr\\J}}\frac{\delta_{\kappa_b\kappa_r}}{\sqrt{[j_b][j_v]}[J]}T_J(mnra)\tilde{\rho}_J(nmab)\tilde{\rho}_0(vrvb) \quad \text{(B.43)}$$

$$T^{(w)} = \sum_{abcmnJ}\frac{1}{[J]^2[j_v]}(-1)^{j_a+j_n+J}\tilde{T}_J(mabn)\tilde{\rho}_J(vmcb)\tilde{\rho}_J(vnca) \quad \text{(B.44)}$$

$$
\begin{aligned}
& - \sum_{abmnrJ} \frac{1}{[J]^2[j_v]} (-1)^{j_a+j_n+J} \tilde{T}_J(mabn)\tilde{\rho}_J(rmvb)\tilde{\rho}_J(rnva) && \text{(B.45)} \\
T^{(x)} \;=\; & -\frac{1}{2} \sum_{\substack{abcdm \\ Jkk'}} \frac{1}{[j_v]} (-1)^{j_c+j_d+j_m+j_v} \begin{Bmatrix} j_v & j_b & k' \\ J & k & j_d \end{Bmatrix} \begin{Bmatrix} j_m & j_a & k' \\ J & k & j_c \end{Bmatrix} \\
& \times T_J(abcd)\tilde{\rho}_k(vmdc)\tilde{\rho}_{k'}(vmba) && \text{(B.46)} \\
& + \frac{1}{2} \sum_{\substack{amnrs \\ Jkk'}} \frac{1}{[j_v]} (-1)^{j_m+j_n+j_r+j_s} \begin{Bmatrix} j_a & j_r & k' \\ J & k & j_m \end{Bmatrix} \begin{Bmatrix} j_w & j_s & k' \\ J & k & j_n \end{Bmatrix} \\
& \times T_J(mnrs)\tilde{\rho}_k(nmva)\tilde{\rho}_{k'}(srva) && \text{(B.47)} \\
& - \sum_{\substack{abcmn \\ k}} \frac{\delta_{\kappa_a\kappa_b}}{[k]\sqrt{[j_v][j_a]}} \tilde{T}_0(vavb)\rho_k(mnbc)\tilde{\rho}_k(nmca) && \text{(B.48)}
\end{aligned}
$$

B.2 MBPT matrix element

The second order two-particle matrix element is given by[71]

$$
\begin{aligned}
T^{(2)} \;=\; & -2 \sum_{mab} \frac{1}{[j_v][J]} \frac{T_J(mvab)\tilde{g}_J(mvab)}{\epsilon_{ab} - \epsilon_{mv}}, && \text{(B.49)} \\
& +2 \sum_{amn} \frac{1}{[j_v][J]} \frac{T_J(mnva)\tilde{g}_J(mnva)}{\epsilon_{va} - \epsilon_{mn}}. && \text{(B.50)}
\end{aligned}
$$

The third order two-particle matrix element is given by

$$
\begin{aligned}
T^{(3)} \;=\; & \sum_{mnabc} \sum_{kk'} \delta_{\kappa_c\kappa_b} \frac{(-1)^{j_m+j_n+j_a+j_v+k'}}{[k][j_c][j_v]} \frac{T_k(abmn)\tilde{g}_{k'}(cvvb)\tilde{g}_k(mnac)}{(\epsilon_{ab} - \epsilon_{mn})(\epsilon_{ac} - \epsilon_{mn})} && \text{(B.51)} \\
+ \; & \sum_{mnabc} \sum_{kk'} \delta_{\kappa_c\kappa_b} \frac{(-1)^{j_m+j_n+j_a+j_v+k'}}{[k][j_c][j_v]} \frac{g_k(abmn)\tilde{T}_{k'}(cvvb)\tilde{g}_k(mnac)}{(\epsilon_{ab} - \epsilon_{mn})(\epsilon_{ac} - \epsilon_{mn})} && \text{(B.52)} \\
+ \; & \sum_{mnabc} \sum_{kk'} \delta_{\kappa_c\kappa_b} \frac{(-1)^{j_m+j_n+j_a+j_v+k'}}{[k][j_c][j_v]} \frac{g_k(abmn)\tilde{g}_{k'}(cvvb)\tilde{T}_k(mnac)}{(\epsilon_{ab} - \epsilon_{mn})(\epsilon_{ac} - \epsilon_{mn})} && \text{(B.53)} \\
- \; & \sum_{mnabs} \sum_{kk'} \delta_{\kappa_m\kappa_s} \frac{(-1)^{j_b+j_n+j_a+j_v+k'}}{[k][j_s][j_v]} \frac{T_k(abmn)\tilde{g}_{k'}(mvvs)\tilde{g}_k(nsba)}{(\epsilon_{ab} - \epsilon_{mn})(\epsilon_{ba} - \epsilon_{ns})} && \text{(B.54)} \\
- \; & \sum_{mnabs} \sum_{kk'} \delta_{\kappa_m\kappa_s} \frac{(-1)^{j_b+j_n+j_a+j_v+k'}}{[k][j_s][j_v]} \frac{g_k(abmn)\tilde{T}_{k'}(mvvs)\tilde{g}_k(nsba)}{(\epsilon_{ab} - \epsilon_{mn})(\epsilon_{ba} - \epsilon_{ns})} && \text{(B.55)} \\
- \; & \sum_{mnabs} \sum_{kk'} \delta_{\kappa_m\kappa_s} \frac{(-1)^{j_b+j_n+j_a+j_v+k'}}{[k][j_s][j_v]} \frac{g_k(abmn)\tilde{g}_{k'}(mvvs)\tilde{T}_k(nsba)}{(\epsilon_{ab} - \epsilon_{mn})(\epsilon_{ba} - \epsilon_{ns})} && \text{(B.56)}
\end{aligned}
$$

$$+2 \sum_{mnabc} \sum_{kk'} \delta_{\kappa_c \kappa_n} \frac{(-1)^{j_b+j_m+j_a+j_v+k'}}{[k][j_c][j_v]} \frac{\tilde{T}_k(abmn) g_k(cmba) \tilde{g}_{k'}(vncv)}{(\epsilon_{ab} - \epsilon_{mn})(\epsilon_{cv} - \epsilon_{nv})} \tag{B.57}$$

$$+2 \sum_{mnabc} \sum_{kk'} \delta_{\kappa_c \kappa_n} \frac{(-1)^{j_b+j_m+j_a+j_v+k'}}{[k][j_c][j_v]} \frac{\tilde{g}_k(abmn) T_k(cmba) \tilde{g}_{k'}(vncv)}{(\epsilon_{ab} - \epsilon_{mn})(\epsilon_{cv} - \epsilon_{nv})} \tag{B.58}$$

$$+2 \sum_{mnabc} \sum_{kk'} \delta_{\kappa_c \kappa_n} \frac{(-1)^{j_b+j_m+j_a+j_v+k'}}{[k][j_c][j_v]} \frac{\tilde{g}_k(abmn) g_k(cmba) \tilde{T}_{k'}(vncv)}{(\epsilon_{ab} - \epsilon_{mn})(\epsilon_{cv} - \epsilon_{nv})} \tag{B.59}$$

$$-2 \sum_{mnabs} \sum_{kk'} \delta_{\kappa_b \kappa_s} \frac{(-1)^{j_n+j_m+j_a+j_v+k'}}{[k][j_b][j_v]} \frac{\tilde{T}_k(abmn) g_k(mnas) \tilde{g}_{k'}(vsbv)}{(\epsilon_{ab} - \epsilon_{mn})(\epsilon_{bv} - \epsilon_{vs})} \tag{B.60}$$

$$-2 \sum_{mnabs} \sum_{kk'} \delta_{\kappa_b \kappa_s} \frac{(-1)^{j_n+j_m+j_a+j_v+k'}}{[k][j_b][j_v]} \frac{\tilde{g}_k(abmn) T_k(mnas) \tilde{g}_{k'}(vsbv)}{(\epsilon_{ab} - \epsilon_{mn})(\epsilon_{bv} - \epsilon_{vs})} \tag{B.61}$$

$$-2 \sum_{mnabs} \sum_{kk'} \delta_{\kappa_b \kappa_s} \frac{(-1)^{j_n+j_m+j_a+j_v+k'}}{[k][j_b][j_v]} \frac{\tilde{g}_k(abmn) g_k(mnas) \tilde{T}_{k'}(vsbv)}{(\epsilon_{ab} - \epsilon_{mn})(\epsilon_{bv} - \epsilon_{vs})} \tag{B.62}$$

$$-2 \sum_{mnabs} \sum_{k} \frac{(-1)^{j_m+j_n+j_a+j_b+j_v+j_s+k}}{[k]^2[j_v]} \frac{\tilde{T}_k(bamn) \tilde{g}_k(nvas) \tilde{g}_k(msbv)}{(\epsilon_{ab} - \epsilon_{mn})(\epsilon_{bv} - \epsilon_{ms})} \tag{B.63}$$

$$-2 \sum_{mnabs} \sum_{k} \frac{(-1)^{j_m+j_n+j_a+j_b+j_v+j_s+k}}{[k]^2[j_v]} \frac{\tilde{g}_k(bamn) \tilde{T}_k(nvas) \tilde{g}_k(msbv)}{(\epsilon_{ab} - \epsilon_{mn})(\epsilon_{bv} - \epsilon_{ms})} \tag{B.64}$$

$$-2 \sum_{mnabs} \sum_{k} \frac{(-1)^{j_m+j_n+j_a+j_b+j_v+j_s+k}}{[k]^2[j_v]} \frac{\tilde{g}_k(bamn) \tilde{g}_k(nvas) \tilde{T}_k(msbv)}{(\epsilon_{ab} - \epsilon_{mn})(\epsilon_{bv} - \epsilon_{ms})} \tag{B.65}$$

$$- \sum_{mnarc} \sum_{k} \frac{(-1)^{j_c+j_r+k}}{[k]^2[j_v]} \frac{\tilde{T}_k(mnva) \tilde{g}_k(cnra) \tilde{g}_k(mrvc)}{(\epsilon_{va} - \epsilon_{mn})(\epsilon_{vc} - \epsilon_{mr})} \tag{B.66}$$

$$- \sum_{mnarc} \sum_{k} \frac{(-1)^{j_c+j_r+k}}{[k]^2[j_v]} \frac{\tilde{g}_k(mnva) \tilde{T}_k(cnra) \tilde{g}_k(mrvc)}{(\epsilon_{va} - \epsilon_{mn})(\epsilon_{vc} - \epsilon_{mr})} \tag{B.67}$$

$$- \sum_{mnarc} \sum_{k} \frac{(-1)^{j_c+j_r+k}}{[k]^2[j_v]} \frac{\tilde{g}_k(mnva) \tilde{g}_k(cnra) \tilde{T}_k(mrvc)}{(\epsilon_{va} - \epsilon_{mn})(\epsilon_{vc} - \epsilon_{mr})} \tag{B.68}$$

$$+2 \sum_{mnabc} \sum_{k} \frac{(-1)^{j_m+j_n+j_a+j_b+j_v+j_c+k}}{[k]^2[j_v]} \frac{\tilde{T}_k(abmn) \tilde{g}_k(cmva) \tilde{g}_k(nvbc)}{(\epsilon_{ab} - \epsilon_{mn})(\epsilon_{bc} - \epsilon_{nv})} \tag{B.69}$$

$$+2 \sum_{mnabc} \sum_{k} \frac{(-1)^{j_m+j_n+j_a+j_b+j_v+j_c+k}}{[k]^2[j_v]} \frac{\tilde{g}_k(abmn) \tilde{T}_k(cmva) \tilde{g}_k(nvbc)}{(\epsilon_{ab} - \epsilon_{mn})(\epsilon_{bc} - \epsilon_{nv})} \tag{B.70}$$

$$+2 \sum_{mnabc} \sum_{k} \frac{(-1)^{j_m+j_n+j_a+j_b+j_v+j_c+k}}{[k]^2[j_v]} \frac{\tilde{g}_k(abmn) \tilde{g}_k(cmva) \tilde{T}_k(nvbc)}{(\epsilon_{ab} - \epsilon_{mn})(\epsilon_{bc} - \epsilon_{nv})} \tag{B.71}$$

$$+ \sum_{mabrc} \sum_{k} \frac{(-1)^{j_c+j_r+k}}{[k]^2[j_v]} \frac{\tilde{T}_k(mvab) \tilde{g}_k(cmra) \tilde{g}_k(vrbc)}{(\epsilon_{ab} - \epsilon_{mv})(\epsilon_{bc} - \epsilon_{vr})} \tag{B.72}$$

$$+ \quad \sum_{mabrc} \sum_{k} \frac{(-1)^{j_c+j_r+k}}{[k]^2[j_v]} \frac{\tilde{g}_k(mvab)\tilde{T}_k(cmra)\tilde{g}_k(vrbc)}{(\epsilon_{ab}-\epsilon_{mv})(\epsilon_{bc}-\epsilon_{vr})} \tag{B.73}$$

$$+ \quad \sum_{mabrc} \sum_{k} \frac{(-1)^{j_c+j_r+k}}{[k]^2[j_v]} \frac{\tilde{g}_k(mvab)\tilde{g}_k(cmra)\tilde{T}_k(vrbc)}{(\epsilon_{ab}-\epsilon_{mv})(\epsilon_{bc}-\epsilon_{vr})} \tag{B.74}$$

$$+2 \quad \sum_{mncab} \sum_{kk'k''} \frac{1}{[j_v]} \begin{Bmatrix} k & k' & k'' \\ j_c & j_n & j_b \end{Bmatrix} \begin{Bmatrix} k & k' & k'' \\ j_v & j_m & j_a \end{Bmatrix} \frac{\tilde{T}_k(abmn)g_{k'}(cvba)g_{k''}(mnvc)}{(\epsilon_{ab}-\epsilon_{mn})(\epsilon_{vc}-\epsilon_{mn})} \tag{B.75}$$

$$+2 \quad \sum_{mncab} \sum_{kk'k''} \frac{1}{[j_v]} \begin{Bmatrix} k & k' & k'' \\ j_c & j_n & j_b \end{Bmatrix} \begin{Bmatrix} k & k' & k'' \\ j_v & j_m & j_a \end{Bmatrix} \frac{\tilde{g}_k(abmn)T_{k'}(cvba)g_{k''}(mnvc)}{(\epsilon_{ab}-\epsilon_{mn})(\epsilon_{vc}-\epsilon_{mn})} \tag{B.76}$$

$$+2 \quad \sum_{mncab} \sum_{kk'k''} \frac{1}{[j_v]} \begin{Bmatrix} k & k' & k'' \\ j_c & j_n & j_b \end{Bmatrix} \begin{Bmatrix} k & k' & k'' \\ j_v & j_m & j_a \end{Bmatrix} \frac{\tilde{g}_k(abmn)g_{k'}(cvba)T_{k''}(mnvc)}{(\epsilon_{ab}-\epsilon_{mn})(\epsilon_{vc}-\epsilon_{mn})} \tag{B.77}$$

$$-2 \quad \sum_{mnsab} \sum_{kk'k''} \frac{1}{[j_v]} \begin{Bmatrix} k & k' & k'' \\ j_v & j_b & j_m \end{Bmatrix} \begin{Bmatrix} k & k' & k'' \\ j_s & j_a & j_n \end{Bmatrix} \frac{\tilde{T}_k(abnm)g_{k'}(mnvs)g_{k''}(vsba)}{(\epsilon_{ab}-\epsilon_{mn})(\epsilon_{ba}-\epsilon_{vs})} \tag{B.78}$$

$$-2 \quad \sum_{mnsab} \sum_{kk'k''} \frac{1}{[j_v]} \begin{Bmatrix} k & k' & k'' \\ j_v & j_b & j_m \end{Bmatrix} \begin{Bmatrix} k & k' & k'' \\ j_s & j_a & j_n \end{Bmatrix} \frac{\tilde{g}_k(abnm)T_{k'}(mnvs)g_{k''}(vsba)}{(\epsilon_{ab}-\epsilon_{mn})(\epsilon_{ba}-\epsilon_{vs})} \tag{B.79}$$

$$-2 \quad \sum_{mnsab} \sum_{kk'k''} \frac{1}{[j_v]} \begin{Bmatrix} k & k' & k'' \\ j_v & j_b & j_m \end{Bmatrix} \begin{Bmatrix} k & k' & k'' \\ j_s & j_a & j_n \end{Bmatrix} \frac{\tilde{g}_k(abnm)g_{k'}(mnvs)T_{k''}(vsba)}{(\epsilon_{ab}-\epsilon_{mn})(\epsilon_{ba}-\epsilon_{vs})} \tag{B.80}$$

$$- \quad \sum_{mabcd} \sum_{lkk'} \frac{(-1)^{j_m+j_v+j_a+j_b}}{[j_v]} \begin{Bmatrix} j_m & j_a & k \\ l & k' & j_c \end{Bmatrix} \begin{Bmatrix} j_v & j_b & k \\ l & k' & j_d \end{Bmatrix} \frac{\tilde{T}_k(mvab)g_l(cdab)g_{k'}(mvcd)}{(\epsilon_{ab}-\epsilon_{mv})(\epsilon_{cd}-\epsilon_{mv})} \tag{B.81}$$

$$- \quad \sum_{mabcd} \sum_{lkk'} \frac{(-1)^{j_m+j_v+j_a+j_b}}{[j_v]} \begin{Bmatrix} j_m & j_a & k \\ l & k' & j_c \end{Bmatrix} \begin{Bmatrix} j_v & j_b & k \\ l & k' & j_d \end{Bmatrix} \frac{\tilde{g}_k(mvab)T_l(cdab)g_{k'}(mvcd)}{(\epsilon_{ab}-\epsilon_{mv})(\epsilon_{cd}-\epsilon_{mv})} \tag{B.82}$$

$$- \quad \sum_{mabcd} \sum_{lkk'} \frac{(-1)^{j_m+j_v+j_a+j_b}}{[j_v]} \begin{Bmatrix} j_m & j_a & k \\ l & k' & j_c \end{Bmatrix} \begin{Bmatrix} j_v & j_b & k \\ l & k' & j_d \end{Bmatrix} \frac{\tilde{g}_k(mvab)g_l(cdab)T_{k'}(mvcd)}{(\epsilon_{ab}-\epsilon_{mv})(\epsilon_{cd}-\epsilon_{mv})} \tag{B.83}$$

$$- \quad \sum_{mnars} \sum_{lkk'} \frac{(-1)^{j_m+j_v+j_a+j_b}}{[j_v]} \begin{Bmatrix} j_m & j_v & k \\ k' & l & j_r \end{Bmatrix} \begin{Bmatrix} j_n & j_a & k \\ k' & l & j_s \end{Bmatrix} \frac{\tilde{T}_k(mnva)g_l(mnrs)g_{k'}(rsva)}{(\epsilon_{va}-\epsilon_{mn})(\epsilon_{va}-\epsilon_{rs})} \tag{B.84}$$

$$- \sum_{mnars} \sum_{lkk'} \frac{(-1)^{j_m+j_v+j_a+j_b}}{[j_v]} \begin{Bmatrix} j_m & j_v & k \\ k' & l & j_r \end{Bmatrix} \begin{Bmatrix} j_n & j_a & k \\ k' & l & j_s \end{Bmatrix} \frac{\tilde{g}_k(mnva) T_l(mnrs) g_{k'}(rsva)}{(\epsilon_{va} - \epsilon_{mn})(\epsilon_{va} - \epsilon_{rs})} \tag{B.85}$$

$$- \sum_{mnars} \sum_{lkk'} \frac{(-1)^{j_m+j_v+j_a+j_b}}{[j_v]} \begin{Bmatrix} j_m & j_v & k \\ k' & l & j_r \end{Bmatrix} \begin{Bmatrix} j_n & j_a & k \\ k' & l & j_s \end{Bmatrix} \frac{\tilde{g}_k(mnva) g_l(mnrs) T_{k'}(rsva)}{(\epsilon_{va} - \epsilon_{mn})(\epsilon_{va} - \epsilon_{rs})} \tag{B.86}$$

Appendix C

PERMISSIONS

1. Tables 3.1, 3.2, 3.3, and 3.4 adapted with permission from Ref. [87]. Copyrighted by the American Physical Society.

2. Tables 4.1, 4.2, 4.3, 4.4, 4.5, 4.6, and 4.7 adapted with permission from Ref. [38]. Copyrighted by the American Physical Society.

3. Figures 3.1 and 3.2 adapted with permission from Ref. [87]. Copyrighted by the American Physical Society.

BIBLIOGRAPHY

[1] S. A. Blundell, D. S. Guo, W. R. Johnson, and J. Sapirstein. Formulas from first-, second-, and third-order perturbation theory for atoms with one valence electron. *Atomic Data Nucl. Data Tables*, 37(1):103, 1987.

[2] S. A. Blundell, W. R. Johnson, Z. W. Liu, and J. Sapirstein. Relativistic all-order calculations of energies and matrix elements for Li and Be^+. *Phys. Rev. A*, 40(5):2233, 1989.

[3] I. Shavitt. The Method of Configuration Interaction. In H. F. Schaefer III, editor, *Methods of electronic structure theory*, volume 3. Springer, New York, 1977.

[4] V. A. Dzuba, V. V. Flambaum, and M. G. Kozlov. Combination of the many-body perturbation theory with the configuration-interaction method. *Phys. Rev. A*, 54(5):3948, 1996.

[5] M. S. Safronova, M. G. Kozlov, W. R. Johnson, and D. Jiang. Development of a configuration-interaction plus all-order method for atomic calculations. *Phys. Rev. A*, 80:012516, 2009.

[6] W. R. Johnson. *Atomic Structure Theory*. Springer-Verlag, Berlin, 2010.

[7] C. deBoor. *A Practical Guide to Splines*. Springer, New York, 1978.

[8] I Lindgren. Accurate many-body calculations on the lowest ^2S and $2P$ states of the lithium atom. *Phys. Rev. A*, 31:1273, 1985.

[9] I. Lindgren and J. Morrison. *Atomic Many-Body Theory*. Springer-Verlag, Berlin, 1986.

[10] S. A. Blundell, W. R. Johnson, Z. W. Liu, and J. Sapirstein. Relativistic all-order equations for helium. *Phys. Rev. A*, 39(8):3768, 1989.

[11] S. A. Blundell, W. R. Johnson, and J. Sapirstein. Relativistic all-order calculations of energies and matrix elements in cesium. *Phys. Rev. A*, 43:3407, 1991.

[12] M. S. Safronova, W. R. Johnson, and A. Derevianko. Relativistic many-body calculations of energy levels, hyperfine constants, electric-dipole matrix elements, and static polarizabilities for alkali-metal atoms. *Phys. Rev. A*, 60(6):4476, 1999.

[13] I. Shavitt. The history and evolution of configuration interaction. *Mol. Phys.*, 94:3, 1998.

[14] S. G. Porsev, K. Beloy, and A. Derevianko. Precision determination of electroweak coupling from atomic parity violation and implications for particle physics. *Phys. Rev. Lett.*, 102:181601, 2009.

[15] M. S. Safronova, V. A. Dzuba, V. V. Flambaum, U. I. Safronova, S. G. Porsev, and M. G. Kozlov. Highly charged ions for atomic clocks, quantum information, and search for α variation. *Phys. Rev. Lett.*, 113:030801, 2014.

[16] M. S. Safronova, S. G. Porsev, and C. W. Clark. Ytterbium in quantum gases and atomic clocks: Van der Waals interactions and blackbody shifts. *Phys. Rev. Lett.*, 109:230802, 2012.

[17] M. S. Safronova, M. G. Kozlov, and C. W. Clark. Precision Calculation of Blackbody Radiation Shifts for Optical Frequency Metrology. *Phys. Rev. Lett.*, 107:143006, 2011.

[18] L. J. LeBlanc and J. H. Thywissen. Species-specific optical lattices. *Phys. Rev. A*, 75:053612, 2007.

[19] C. D. Herold, V. D. Vaidya, X. Li, S. L. Rolston, J. V. Porto, and M. S. Safronova. Precision measurement of transition matrix elements via light shift cancellation. *Phys. Rev. Lett.*, 109:243003, 2012.

[20] R. H. Leonard, A. J. Fallon, C. A. Sackett, and M. S. Safronova. High-precision measurements of the ^{87}Rb D-line tune-out wavelength. *Phys. Rev. A*, 92:052501, 2015.

[21] W. F. Holmgren, R. Trubko, I. Hromada, and A. D. Cronin. Measurement of a wavelength of light for which the energy shift for an atom vanishes. *Phys. Rev. Lett.*, 109:243004, 2012.

[22] B. M. Henson, R. I. Khakimov, R. G. Dall, K. G. H. Baldwin, L. Y. Tang, and A. G. Truscott. Precision measurement for metastable helium atoms of the 413 nm tune-out wavelength at which the atomic polarizability vanishes. *Phys. Rev. Lett.*, 115:043004, 2015.

[23] T. L. Nicholson, S. L. Campbell, R. B. Hutson, G. E. Marti, B. J. Bloom, et al. Systematic evaluation of an atomic clock at 2×10^{-18} total uncertainty. *Nat. Commun.*, 6:6896, 2015.

[24] X. Zhang, M. Bishof, S. L. Bromley, C. V. Kraus, M. S. Safronova, P. Zoller, A. M. Rey, and J. Ye. Spectroscopic observation of SU(N) symmetric interactions in Sr orbital magnetism. *Science*, 345:1467, 2014.

[25] S. Stellmer, B. Pasquiou, R. Grimm, and F. Schreck. Laser cooling to quantum degeneracy. *Phys. Rev. Lett.*, 110:263003, 2013.

[26] M. S. Safronova, S. G. Porsev, U. I. Safronova, M. G. Kozlov, and C. W. Clark. Blackbody-radiation shift in the Sr optical atomic clock. *Phys. Rev. A*, 87:012509, 2013.

[27] D. W. Allan. Statistics of Atomic Frequency Standards. *Proc. IEEE*, 54:221, 1966.

[28] T. Rosenband, P. O. Schmidt, D. B. Hume, W. M. Itano, T. M. Fortier, et al. Observation of the $^1S_0 \rightarrow ^3 P_0$ clock transition in $^{27}Al^+$. *Phys. Rev. Lett.*, 98:220801, 2007.

[29] T. Rosenband, D. B. Hume, P. O. Schmidt, C. W. Chou, A. Brusch, et al. Frequency ratio of Al^+ and Hg^+ single-ion optical clocks; metrology at the 17th decimal place. *Science*, 319:1808, 2008.

[30] C. W. Chou, D. B. Hume, J. C. J. Koelemeij, D. J. Wineland, and T. Rosenband. Frequency comparison of two high-accuracy Al^+ optical clocks. *Phys. Rev. Lett.*, 104:070802, 2010.

[31] H. Katori, T. Ido, and M. Kuwata-Gonokami. Optimal design of dipole potentials for efficient loading of Sr atoms. *J. Phys. Soc. Jpn*, 68:2479, 1999.

[32] H. Hachisu, K. Miyagishi, S. G. Porsev, A. Derevianko, V. D. Ovsiannikov, et al. Trapping of neutral mercury atoms and prospects for optical lattice clocks. *Phys. Rev. Lett.*, 100:053001, 2008.

[33] M. Takamoto, I. Ushijima, M. Das, N. Nemitz, T. Ohkubo, et al. Frequency ratios of Sr, Yb and Hg based optical lattice clocks and their applications. *C. R. Phys.*, 16:489, 2015.

[34] M. Takamoto, F. L. Hong, R. Higashi, and H. Katori. An optical lattice clock. *Nature*, 2005:435, 2005.

[35] The International System of Units (SI), edited by B. N. Taylor (U.S. GPO, Gaithersburg, MD, 2001), http://physics.nist.gov/Pubs/SP330/sp330.pdf (see also http://www.bipm.org).

[36] T. P. Heavner. First accuracy evaluation of NIST-F2. *Metrologia*, 51:174, 2014.

[37] H. Dehmelt, N. Yu, and W. Nagourney. The $6^1S_0 - 6^3P_0$ transition in thallium isotope ion $^{204}Tl^+$: a superior atomic clock. *Proc. Natl. Acad. Sci. USA*, 86:3938, 1989.

[38] Z. Zuhrianda, M. S. Safronova, and M. G. Kozlov. Anomalously small blackbody radiation shift in Tl^+ frequency standard. *Phys. Rev. A.*, 85:022513, 2012.

[39] J. Mitroy, M. S. Safronova, and C. W. Clark. Theory and applications of atomic and ionic polarizabilities. *J. Phys. B*, 43:202001, 2010.

[40] S. G. Porsev and A. Derevianko. Hyperfine quenching of the metastable $^3P_{0,2}$ states in divalent atoms. *Phys. Rev. A*, 69:042506, 2004.

[41] H. Katori, M. Takamoto, V. G. Pal'chikov, and V. D. Ovsiannikov. Ultrastable optical clock with neutral atoms in an engineered light shift trap. *Phys. Rev. Lett.*, 91:173005, 2003.

[42] R. H. Garstang. Hyperfine structure and intercombination line intensities in the spectra of magnesium, zinc, cadmium, and mercury. *J. Opt. Soc. Am.*, 52:845, 1962.

[43] A. Pich. The standard model of electroweak interactions. 2005. arXiv:hep-ph/0502010.

[44] D. J. Gross and F. Wilczek. Ultraviolet behavior of non-abelian gauge theories. *Phys. Rev. Lett.*, 30:1343, 1973.

[45] H. D. Politzer. Reliable perturbative results for strong interactions? *Phys. Rev. Lett.*, 30:1346, 1973.

[46] S. L. Glashow. Partial symmetries of weak interactions. *Nuc. Phys.*, 22:579, 1961.

[47] S. Weinberg. A model of leptons. *Phys. Rev. Lett.*, 19:1264, 1967.

[48] A. Salam. Elementary particle physics: relativistic groups and analyticity. In N. Svartholm, editor, *Eight Nobel Symposium*, page 367. Almquvist and Wiksell, Stockholm, 1968.

[49] J. J. Aubert, U. Becker, P. J. Biggs, J. Burger, M. Chen, et al. Experimental observation of a heavy particle J. *Phys. Rev. Lett.*, 33:1404, 1974.

[50] J. E. Augustin, A. M. Boyarski, M. Breidenbach, F. Bulos, J. T. Dakin, et al. Discovery of a narrow resonance in e^+e^- annihiliation. *Phys. Rev. Lett.*, 33:1406, 1974.

[51] UA1 collaboration. Experimental observation of isolated large transverse energy electrons with associated missing energy at s=540 GeV. *Phys. Lett. B*, 122:103, 1983.

[52] UA2 collaboration. Observation of single isolated electrons of high transverse momentum in events with missing transverse energy at the CERN p collider. *Phys. Lett. B*, 122:476, 1983.

[53] CMS collaboration. Observation of a new boson at a mass of 125 GeV with the CMS experiment at the LHC. *Phys. Lett. B*, 716:30, 2012.

[54] CMS collaboration. Observation of a new boson with mass near 125 GeV in pp collisions at $\sqrt{s} = 7$ and 8 TeV. *J. High Energy Phys.*, 06:081, 2013.

[55] ATLAS collaboration. Observation of a new particle in the search for the standard model Higgs boson with the ATLAS detector at the LHC. *Phys. Lett. B*, 716:1, 2012.

[56] T. Mannel. Theory and Phenomenology of CP Violation. In *Proceedings of the 7th International Conference of Hyperons, Charm and Beauty Hadrons - HYPERONS, CHARM AND BEAUTY HADRONS*, May 2006.

[57] V. A. Dzuba, V. V. Flambaum, and J. S. M. Ginges. Calculation of parity and time invariance violation in the radium atom. *Phys. Rev. A*, 61:062509, 2000.

[58] R. J. Holt, I. Ahmad, K. Bailey, B. Graner, J. P. Greene, et al. Progress toward an EDM measurement in ^{225}Ra. *Nucl. Phys. A*, 844:53c, 2010.

[59] C. S. Wu, E. Ambler, W. Hayward, D. D. Hoppes, and R. P. Hudson. Experimental test of parity conservtion in beta decay. *Phys. Rev.*, 105:1413, 1957.

[60] C. S. Wood, S. C. Bennett, D. Cho, B. P. Masterson, J. L. Roberts, et al. Measurement of parity nonconservation and an anapole moment in cesium. *Science*, 275:1759, 1997.

[61] D. Sheng, L. A. Orozco, and E. Gomez. Preliminary studies for anapole moment measurements in rubidium and francium. *J. Phys. B: At. Mol. Opt. Phys.*, 43:074004, 2010.

[62] S. G. Porsev, K. Beloy, and A. Derevianko. Precision determination of weak charge of ^{133}Cs from atomic parity violation. *Phys. Rev. D*, 82:036008, 2010.

[63] V. A. Dzuba, J. C. Berengut, V. V. Flambaum, and B. Roberts. Revisiting parity nonconservation in cesium. *Phys. Rev. Lett.*, 109:203003, 2012.

[64] W. C. Haxton and C. E. Wieman. Atomic parity nonconservation and nuclear anapole moments. *Ann. Rev. Nucl. Part. Sci.*, 51:261, 2001.

[65] J. K. Webb, V. V. Flambaum, C. W. Churchill, M. J. Drinkwater, and J. D. Barrow. Search for time variation of the fine structure constant. *Phys. Rev. Lett.*, 82:884, 1999.

[66] J. P. Uzan. The fundamental constants and their variation: observational and theoretical status. *Rev. Mod. Phys.*, 75:403, 2003.

[67] M. T. Murphy, J. K. Webb, V. V. Flambaum, V. A. Dzuba, C. W. Churchill, J. X. Prochaska, J. D. Barrow, and A. M. Wolfe. Possible evidence for a variable fine-structure constant from QSO absoption lines: motivations, analysis and results. *Mon. Not. R. Astron. Soc.*, 327:1208, 2001.

[68] J. K. Webb, M. T. Murphy, V. V. Flambaum, and S. J. Curran. Does the fine structure constant vary? A third quasar absorption sample consistent with varying α. *Astrophys. Space Sci.*, 283:565, 2003.

[69] K. Heilig and A. Steudel. Changes in mean-square nuclear charge radii from optical isotope shifts. *Atomic Data Nucl. Data Tables*, 14:613, 1974.

[70] V. V. Flambaum and J. C. Berengut. Atom made from charged elementary black hole. *Phys. Rev. D*, 63:084010, 2001.

[71] M. S. Safronova and W. R. Johnson. Third-order isotope-shift constants for alkali-metal atoms and ions. *Phys. Rev. A*, 64:052501, 2001.

[72] V. A. Dzuba. V^{N-M} approximation for atomic calculations. *Phys. Rev. A*, 71:032512, 2005.

[73] A. Derevianko, V. A. Dzuba, and V. V. Flambaum. Highly Charged Ions as a Basis of Optical Atomic Clockwork of Exceptional Accuracy. *Phys. Rev. Lett.*, 109:180801, 2012.

[74] S. P. W. Merrill. Spectroscopic Observations of Stars of Class S. *The Astrophysical Journal*, 116:21, 1952.

[75] M. S. Safronova, A. Derevianko, and W. R. Johnson. Relativistic many-body calculations of energy levels, hyperfine constants, and transition rates for sodiumlike ions, Z=11-16. *Phys. Rev. A*, 58(2):1016, 1998.

[76] F. Coester and H. Kummel. Short-range correlations in nuclear wave functions. *Nucl. Phys.*, 17:477, 1960.

[77] G. E. Brown and D. G. Ravenhall. On the interaction of two electrons. *Proc. Roy. Soc. A*, 208:552, 1951.

[78] S. A. Blundell, W. R. Johnson, and J. Sapirstein. Third-order many-body perturbation theory calculations of the ground-state energies of cesium and thallium. *Phys. Rev. A*, 42(7):3751, 1990.

[79] G. C. Wick. The Evaluation of the Collision Matrix. *Phys. Rev.*, 80:268, 1950.

[80] A. M. Martensson and S. Salomonson. Calculation of the Specific Mass Shift in Li and K using many-body perturbation theory. *J. Phys. B*, 15:2115, 1982.

[81] V. A. Dzuba and W. R. Johnson. Calculation of the energy levels of barium using B splines and a combined configuration-interaction and many-body-perturbation-theory method. *Phys. Rev. A*, 57(4):2459, 1998.

[82] I Lindgren. The Rayleigh-Schrodinger perturbation and the linked-diagram theorem for a multi-configurational model space. *J. Phys. B*, 7:2441, 1974.

[83] V. A. Dzuba and J. S. M. Ginges. Calculations of energy levels and lifetimes of low-lying states of barium and radium. *Phys. Rev. A*, 73:032503, 2006.

[84] E. R. Davidson. The iterative calculation of a few of the lowest eigenvalues and corresponding eigenvectors of large real-symmetric matrices. *J. Comput. Phys.*, 17:87, 1975.

[85] A. Dalgarno and J. T. Lewis. The exact calculation of long-range forces between atoms by perturbation theory. *Proc. Roy. Soc.*, 233:70, 1955.

[86] M. G. Kozlov and S. G. Porsev. Polarizabilities and hyperfine structure constants of the low-lying levels of barium. *Eur. Phys. J. D*, 5:59, 1999.

[87] M. S. Safronova, Z. Zuhrianda, U. I. Safronova, and C. W. Clark. Extracting transition rates from zero-polarizability spectroscopy. *Phys. Rev. A*, 92:040501, 2015.

[88] R. Grimm, M. Weidemüller, and Y. B. Ovchinnikov. Optical dipole traps for neutral atoms. *Adv. At. Mol. Opt. Phys.*, 42:95, 2000.

[89] A. J. Daley, M. M. Boyd, J. Ye, and P. Zoller. Quantum computing with alkaline-earth-metal atoms. *Phys. Rev. Lett.*, 101:170504, 2008.

[90] A. Kramida, Y. Ralchenko, J. Reader, and NIST ASD Team (2012). NIST Atomic Spectra Database (ver. 5.0), [Online]. Available: http://physics.nist.gov/asd [2013, June 24]. National Institute of Standards and Technology, Gaithersburg, MD.

[91] M. Yasuda, T. Kishimoto, M. Takamoto, and H. Katori. Photoassociation spectroscopy of ^{88}Sr: reconstruction of the wave function near the last node. *Phys. Rev. A*, 78:014502, 2006.

[92] T. Middelmann, S. Falke, C. Lisdat, and U. Sterr. High accuracy correction of blackbody radiation shift in an optical lattice clock. *Phys. Rev. Lett.*, 109:263004, 2012.

[93] A. D. Ludlow, T. Zelevinsky, G. K. Campbell, S. Blatt, M. M. Boyd, et al. Sr lattice clock at 1×10^{-16} fractional uncertainty by remote optical evaluation with a Ca clock. *Science*, 319:1805, 2008.

[94] Y. Cheng, J. Jiang, and J. Mitroy. Tune-out wavelengths for the alkaline-earth-metal atoms. *Phys. Rev. A*, 88:022511, 2013.

[95] J. W. Farley and W. H. Wing. Accurate calculation of dynamic Stark shifts and depopulation rates of Rydberg energy levels induced by blackbody radiation. Hydrogen, helium and alkali-metal atoms. *Phys. Rev. A*, 23:2397, 1981.

[96] S. G. Porsev and A. Derevianko. Multipolar theory of blackbody radiation shift of atomic energy levels and its implications for optical lattice clocks. *Phys. Rev. A*, 74:020502, 2006.

[97] J. Mitroy, J. Y. Zhang, M. W. J. Bromley, and K. G. Rollin. Blackbody radiation shift of the Al+ clock transition. *Eur. Phys. J. D*, 53:15, 2009.

[98] T. Rosenband, W. M. Itano, P. Schmidt, J. Hume, D. Koelemeij, et al. Blackbody radiation shift of the $^{27}Al^{+}$ $^{1}S_0 - ^{3}P_0$ transition. *Proc. EFTF Conf.*, 20:289, 2006.

[99] G. Breit. Dirac's equation and the spin-spin interactions of two electrons. *Phys. Rev.*, 39:616, 1932.

[100] O. Zatsarinny and K. Bartschat. Fully relativistic B-spline R-matrix calculations for electron collisions with mercury. *Phys. Rev. A.*, 79:042713, 2009.

[101] A. Ye and G. Wang. Dipole polarizabilities of $ns^2\,^1S_0$ and $nsnp^3P_0$ states and relevant magic wavelengths of group-IIB atoms. *Phys. Rev. A*, 78:014502, 2008.

[102] D. Goebel and U. Hohm. Dipole polarizability, Cauchy moments, and related properties of Hg. *J. Phys. Chem.*, 100:7710, 1996.

[103] K. T. Tang and J. P. Toennies. The dynamical polarisability and Van der Waals dimer potential of mercury. *Mol. Phys.*, 106:1645, 2008.

[104] I. I. Sobelman. *Atomic Spectra and Radiative Transition*. Springer-Verlag, Berlin, 1979.

[105] A. Lurio. Hyperfine structure of the ^3P states of Zn^{67} and Mg^{25}. *Phys. Rev.*, 126:1768, 1962.

[106] S. M. Heider and G. O. Brink. Hyperfine structure of ^{87}Sr in the $^3P_2$ metastable state. *Phys. Rev. A*, 16:1371, 1977.

[107] P. Thaddeus and R. Novick. Optical detection of level crossing in the $(5s5p)^3P_1$ state of Cd^{111} and Cd^{113}. *Phys. Rev.*, 126:1774, 1962.

[108] A. Khadjavi, A. Lurio, and W. Happer. Stark effect in the excited states of Rb, Cs, Cd, and Hg. *Phys. Rev.*, 167:128, 1968.

[109] C. Schwartz. Theory of Hyperfine Structure. *Phys. Rev.*, 97:380, 1955.

[110] N. D. Scielzo, J. R. Guest, E. C. Schulte, I. Ahmad, K. Bailey, et al. Measurement of the lifetimes of the lowest $^3P_1$ state of neutral Ba and Ra. *Phys. Rev. A*, 73:010501(R), 2006.

[111] W. L. Trimble, I. A. Sulai, I. Ahmad, K. Bailey, B. Graner, et al. Lifetime of the $7s6d\,^1D_2$ atomic state of radium. *Phys. Rev. A*, 80:054501, 2009.

[112] K. Wendt, S. A. Ahmad, W. Klempt, R. Neugart, E. W. Otten, et al. On the hyperfine structure and isotope shift of radium. *Z. Phys. D*, 4:227, 1987.

[113] E. Arnold, W. Borchers, M. Carre, H. T. Duong, P. Juncar, et al. Direct measurement of nuclear magnetic moments of radium isotopes. *Phys. Rev. Lett.*, 59:771, 1987.

[114] S. A. Blundell, W. R. Johnson, and J. Sapirstein. High-accuracy calculation of the $6s_{1/2} \rightarrow 7s_{1/2}$ parity-nonconserving transition in atomic cesium and implications for the standard model. *Phys. Rev. Lett.*, 65:1411, 1990.

[115] S. A. Blundell, W. R. Johnson, and J. Sapirstein. High-accuracy calculation of parity nonconservation in cesium and implications for particle physics. *Phys. Rev. D*, 45:1602, 1992.

[116] W. C. Haxton, C. P. Liu, and M. J. Ramsey-Musolf. Anapole moment and other constraints on the strangeness conserving hadronic weak interaction. *Phys. Rev. Lett.*, 86:5247, 2001.

[117] Y. B. Zel'dovich. Electromagnetic interaction with parity violation. *J. Exptl. Theoret. Phys. (U.S.S.R.)*, 33:1531, 1957.

[118] Y. B. Zel'dovich. Parity noncovervation in the first order in the weak-interaction constant in electron scattering and other effects. *Sov. Phys. JETP*, 9:682, 1959.

[119] V. V. Flambaum, I. B. Khriplovich, and O. P. Sushkov. Nuclear anapole moments. *Phys. Lett. B*, 146:367, 1984.

[120] V. V. Flambaum and D. W. Murray. Anapole moment and nucleon weak interactions. *Phys. Rev. C*, 56:1641, 1997.

[121] C. Bouchiat and C. A. Piketty. Nuclear spin dependent parity violating electron-nucleus interaction in heavy atoms. The anapole moment and the perturbation of the hadronic vector neutral current by the hyperfine interaction. *Phys. Lett. B*, 269:195, 1991.

[122] V. A. Dzuba, V. V. Flambaum, and O. P. Sushkov. Calculation of energy levels, $E1$ transition aplitudes, and parity violation in francium. *Phys. Rev. A*, 51:3454, 1995.

[123] V. M. Shabaev, I. I. Tupitsyn, K. Pachucki, G. Plunien, and V. A. Yerokhin. Radiative and correlation effects on the parity-nonconserving transition amplitude in heavy alkali-metal atoms. *Phys. Rev. A*, 72:062105, 2005.

[124] M. S. Safronova and W. R. Johnson. High-precision calculation of the parity-nonconserving amplitude in francium. *Phys. Rev. A*, 72:062105, 2005.

[125] Y. P. Gangrsky, K. P. Karalvanov, B. N. Marinova, L. M. Markov, L. M. Melnikova, et al. Hyperfine splitting and isotope shift in the atomic D_2 line of ^{22,23}Na and the quadrupole moment of ^{22}Na. *Eur. Phys. J. A*, 3:313, 1998.

[126] V. A. Dzuba, W. R. Johnson, and M. S. Safronova. Calculation of isotope shifts for cesium and francium. *Phys. Rev. A*, 72:022503, 2005.